

We thank Dr. Nick Savage and the anonymous reviewer 2 for their review. Please find in this document the response to the reviews and a version of the manuscript with marked changes.

Johannes Flemming

## Response to the review from Dr. Nick Savage

We would like to thank Nick Savage for his review of our paper and respond in the following way. The reviewers comments are put in italics. Suggested changes to the text are given in quotation marks.

*Title Please include the version of the IFS used in the title of the paper as required by GMD (CY40r1)*

We would prefer not to the cycle number of the IFS in the title of the paper because the IFS cycles (of which there are about 2 - 3 per year) reflect the development of the NWP code but are not yet linked to the development of the chemistry modules. The current chemistry scheme has been used for a several IFS cycles. It is the plan to introduce a proper version naming convention for the chemistry modules in the Copernicus Atmosphere Monitoring Service.

*Section 2.2 How large an impact does the correction of negative MMRs have on the budget of transported species?*

Negative interim MMR can occur because of the chosen operator splitting and lack of implicitness in the parameterisations and numerical solvers. They occur more often when a large time step is chosen. Using the Quasi-monotonic option for the Semi-Lagrangian Advection scheme avoids negative concentrations after the advection but quasi-monotonic restricting of the interpolation result is equivalent to a negative fix.

To answer the questions of the magnitude of the fix to chemical zero, we compared the source because of the chemical zero fixer to the largest of the four global sink and source terms (emission, dry and wet deposition, chemistry). For the majority of the species the contribution was below 0.1% .

The negative fixer source was in the order of 1% for nitrogen species such as NO, N<sub>2</sub>O<sub>5</sub> as well as up to 3% for highly soluble species such HNO<sub>3</sub>, HO<sub>2</sub>, NO<sub>3</sub>\_A. We suspect that areas of large gradients such as the NO<sub>x</sub> chemistry at the terminator in the stratosphere as well as intensive wet deposition are the reasons for the need to apply the negative fixer under these circumstances.

*Section 2.3 Are the biogenic emissions calculated from MEGAN offline and read from a file or is MEGAN used online?*

The MEGAN biogenic emissions were calculated off-line and accumulated in monthly means. We plan to use on-line calculated values in the future. We will change the text as follows:

“The biogenic emissions were simulated off-line by the MEGAN2.1 model (Guenther et al., 2006). The anthropogenic and natural emissions were used as monthly means. Daily Biomass ...”

### Section 2.4.3

*Please note that Price and Rind (1994) derived a correction factor for cloud top height as the resolution of the model is decreased. They found that as resolution decreases the global lightning frequencies decrease exponentially and corrected for this with a calibration factor. Was this calibration factor used in this implementation?*

We are aware of the paper (as the factor is used in the MOZART CTM) but we did not use it. We suspect that the correction factor is also depends strongly on the parameterisation of convection in the model. Instead we scaled the emission to be 4.9 Tg yr<sup>-1</sup> at a T159 (110 km) resolution. Running the model at T255 (80km) resolution - as done for the paper - led to an increase (without changing coefficients in the parameterisation) to 5.7 Tg yr<sup>-1</sup>. Please note that the parameterisation of Meijer et al. 2001 based on convective precipitation was used.

*Section 2.5.1 Please give more details of the heterogeneous chemistry of SO<sub>2</sub> - what reactions are included, how is the pH calculated and how is the relationship of pH and reaction rate calculated? For the heterogeneous conversion of N<sub>2</sub>O<sub>5</sub> into nitric acid how is the surface area of aerosols calculated - does it account for hygroscopic growth? Which aerosols are used - the prognostic scheme in the IFS or a climatology? Is the surface area of water droplets based on a calculated size distribution or is there an assumed size distribution used in the cloud scheme?*

Then heterogeneous chemistry is treated in a simple way mostly and it follows the implementation of the TM5 model as describe in Huijnen et al. (2010). We will add the following rephrase the corresponding text as follows:

“For the loss of trace gases by heterogeneous oxidation processes, the model explicitly accounts for the oxidation of SO<sub>2</sub> in cloud through aqueous phase reactions with H<sub>2</sub>O<sub>2</sub> and O<sub>3</sub>, depending on the acidity of the solution. The pH is computed from the SO<sub>4</sub>, MSA, HNO<sub>3</sub>, NO<sub>3</sub>\_A, NH<sub>3</sub> and NH<sub>4</sub> concentrations, as well as from a climatological CO<sub>2</sub> value. The pH, in combination with the Henry coefficient, defines the factor of sulphate residing in the aqueous phase, compared to the gas phase concentration (Dentener and Crutzen, 1993). The heterogeneous conversion of N<sub>2</sub>O<sub>5</sub> into HNO<sub>3</sub> on cloud droplets and aerosol particles is applied with a reaction probability ( $\gamma$ ) set to 0.02 (Evans and Jacob, 2005). The surface area density is computed based on a climatological aerosol size distribution function, applied to the SO<sub>4</sub>, MSA and NO<sub>3</sub>\_A aerosol, as well as to clouds assuming a droplet size of 8  $\mu$ m.”

Dentener, F. J. and Crutzen, P. J.: Reaction of N<sub>2</sub>O<sub>5</sub> on tropospheric aerosols: Impact on the global distributions of NO<sub>x</sub>, O<sub>3</sub> and OH, J. Geophys. Res., 98(D4), 7149–7163, 1993.

*Section 2.5.4 Please explain in more detail what data is used to prescribe surface methane concentrations - are they based on observations or a model (and give a reference). Spatially is a single number used everywhere, is a zonal mean or a 2D fields? Temporally is there a seasonal cycle or is it the same all through the year? (I note that it is mentioned later that monthly zonal mean concentrations are prescribed, but still no reference, and it would be better to say that here)*

CH<sub>4</sub> is nudged towards zonal-mean monthly varying surface concentrations derived from a latitudinal interpolation of the monthly-mean observations at the stations South Pole, Cape Grim, Mauna Loa, Mace Head, Barrow, and Alert. These are the same CH<sub>4</sub> surface concentrations as used in the work of Bândă et al. (2014)

Bândă, N., M. Krol, T. van Noije, M. van Weele, J. E. Williams, P. Le Sager, U. Niemeier, L. Thomason, and T. Röckmann (2014), The effect of stratospheric sulfur from Mount Pinatubo on tropospheric oxidizing capacity and methane, J. Geophys. Res. Atmos., 119, doi:10.1002/2014JD022137.

We will add the following at line 509

“The CH<sub>4</sub> surface concentrations were derived from a latitudinal interpolation of observations from the stations South Pole, Cape Grim, Mauna Loa, Mace Head, Barrow and Alert, as discussed in Banda et al. (2015).”

*Section 3.1 One model resolution is given here a spectral truncation and the other in lat-lon spacing. It would be useful here if the approximate resolution of both is given in km to make it easier to compare the resolution of the two models.*

We will add the approximate resolution in km in brackets. It was 80x80 km for C-IFS CB05 and about 120 x 120 km for MOZ.

*Section 3.2.1 How is the model sampled for comparisons with MOZAIC data?*

The model column is obtained over the airport at the middle time between start and end of the profile observation. The columns are interpolated in time between to subsequent output time steps. This procedure does not take into account the horizontal movement of the plane, which could be about to 200 km during the ascent and descent.

“The model column for the comparison with the profile was obtained at the middle between start and end time of the profile observation. The model columns were interpolated in time between two subsequent output time steps.”

*"Only the rural Airbase O<sub>3</sub> observations have been selected for the evaluation of the diurnal cycle". Please clarify - two plots for surface ozone over Europe are shown - a seasonal and a diurnal cycle. I assume that both of these analyses were carried out using all EMEP data and the Airbase observations at rural sites. If this is correct, this would be better phrased as "For evaluation over Europe, the EMEP observations and the rural Airbase O<sub>3</sub> observations were used."*

The assumption is correct. We will change the text following your suggestions

*Section 3.3 Does the lower bias in C-IFS imply that the Cariolle scheme is performing better in the lower stratosphere than the MOZAIC chemistry? If so, please comment on this and implications for future choices of upper boundary conditions for ozone - if the Cariolle scheme is cheaper and better, why are you planning to add a detailed stratospheric chemistry scheme to CB05?*

Please note that the stratospheric ozone was nudged to the MACC re-analysis above the tropopause (see line 541). As shown in Flemming et al (2011), both the MOZART stratospheric chemistry and the Cariolle parameterisation have specific issues and strengths. We are planning to implement stratospheric chemistry schemes not only to provide boundary conditions for the troposphere and to assimilated total columns ozone observations but also to provide more specific information about stratospheric composition in CAMS.

*Section 3.4 I would say that the model reproduces well only the location of the global maxima (the manuscript correctly identifies the commonly observed underestimation*

of CO in the NH later on).

We will correct the text as follows:

“ .... reproduced well the location of the observed ...”

*Section 3.5 The low bias in the outflow regions may also be related to insufficient production of NO<sub>x</sub> reservoir species such as PAN and alkyl nitrates.*

We agree that limitations of the chemical mechanism CB05 and not only the emissions are the reason for the underestimation. For example, Alkyl nitrates are not considered. We will add the following line:

“Further, an insufficient simulation of NO<sub>x</sub> reservoir species such as PAN and the lack of alkyl nitrates in CB05 might be the reason for the underestimation.”

*The overestimation of NO<sub>2</sub> in the biomass burning region coupled with the underestimation at this time suggest that the emissions modelling may be the issue here rather than the fire count.*

As pointed out by the reviewer, emission factor for NO may need to be re-considered. We will add:

“The overestimation during biomass burning events could be related to the assumed NO emission factor.”

*Section 3.6 Is the underestimation of winter HCHO in Eastern US possibly linked to the ozone bias here as well? Is there some important winter time chemistry missing in both CB05 and MOZAIC?*

Without further investigation we find it difficult to give a good explanation of the underestimation over the Easter US in January and February. Emissions of VOC as well as limitations of the chemical scheme are a possible explanation. The good match in the rest of the years is however encouraging. Uncertainties in the satellite retrievals could also play a role here. The observed values in December are much lower (and the model shows better agreement) than in January, when the model underestimates.

*Section 3.8 I found the following sentence confusing. "The additional resources allocated to the IFS are however mostly latent as the coupled MOZART model and the coupler software could not be made faster by using more resources." I think what is implied here is that in order to get enough memory, the coupled MOZART model needed to be run using a large number of CPUs. However, this is inefficient because there is insufficient parallelism in the coupled model to exploit this large CPU count. Please clarify.*

The assumption is correct. We will re-phrase the text as follows.

“However, there is insufficient parallelism in MOZART to exploit the larger number of CPU for speeding up the simulation of the coupled system”

*The more complex chemistry schemes presumably require more resources to run because of both the costs of tracer transport and the extra chemistry. It would be helpful to indicate how the additional costs are spread between these two aspects.*



Most of the increase in cost between C-IFS CB05, C-IFS MOZART and C-IFS MOCAGE are because of the demands of the chemistry. The overhead because of the advection of more tracers (CB05 56 tracers, MOZART 108, MOCAGE 112) is in the range of 10%. The SL advection is very efficient to simulate a larger number of tracers as the departure point is the same for all tracers.

We will add:

“The overhead because of the doubled number of advected species in C-IFS RACMOBUS and MOZART is small because of the efficiency of the SL advection scheme. “

*Section 4 If a consistent chemistry scheme were used in the C-IFS to that of the coupled framework, this would help resolve whether the improvements in SO<sub>2</sub> for example are due to difference in the diffusion schemes as suggested in the paper.*

We agree that a scientifically sound comparison of the MOZART and CB05 chemistry is only possible if the two schemes are implemented in C-IFS. This is now the case and work on this has started.

## Response to reviewer #2

We thank reviewer #2 for his or her insightful comments on the paper, in particular on improving the evaluation section. We were very impressed by the reviewer's attention to detail in spotting inconsistencies in the listing of the chemical mechanism in the supplement.

We would like to respond to the review as follows. The reviewer's comments are put in italics. Our suggestions for changes to the text are given in quotation marks.

*p.7736, l.26: WRF-Chem is a regional model, but it is implied to be global in this sentence.*

We agree with reviewer #2 that WRF-Chem is mainly a regional model but there are also global applications of the model, e.g. Zhang et al. (2012).

We will replace in the manuscript "WRF/chem (Grell et al. 2005)" with "GU-WRF/chem (Zhang et al., 2012)"

Zhang, Y., P. Karamchandani, T. Glotfelty, D. G. Streets, G. Grell, A. Nenes, F. Yu, and R. Bennartz (2012), Development and initial application of the global-through-urban weather research and forecasting model with chemistry (GU-WRF/Chem), J. Geophys. Res., 117, D20206, doi:10.1029/2012JD017966.

*p. 7755 and Table 2: North America ozone average of MOZAIC profiles and ozonesondes – It does not seem valid to average together all the stations of US and Canada. I would not consider Atlanta and Vancouver as having similar conditions at all.*

We agree with reviewer #2 that spatially averaging the observations and model results over a larger area needs to be done with caution. For the sake of generalisation of the global results we choose rather large areas. As we show monthly mean values averaged over layers of 200-300 hPa, we concluded that our approach is scientifically sound. The averages are calculated in such a way that stations/airports with more observations get a greater weight in the regional average.

The varying data availability was a major motivation to average the MOZAIC profiles over North America. For example Vancouver and Toronto had no observation from April to September whereas Dallas had most of the observation in this period. We therefore averaged over a larger number of airports to obtain a more complete monthly time series for 2008. Because of the airport location and the number of available profiles, the plots are dominated by observation in the Eastern US. Please find for your information below the time series plots separately for the eastern and western North-America and for the whole sub-continent (Fig R1). We argue that the differences in the CO bias of different regions compared to the North-American biases is not worth including the region-specific plots in the paper.

We will add in section 3.2.1

"Because of the varying data availability the North-American mean is dominated by the airports in the Eastern United States. "

*Tilmes et al. (ACP,2012, doi:10.5194/acp-12-7475-2012) shows significant differences among 4 ozonesonde sites spread across N. America, recommending against averaging them together for model evaluation. Please explain in more detail how this comparison was done. Was the model extracted for each site and then averaged? It seems it would be better to determine a model-measurement bias for each site, and then perhaps it is ok to average the biases.*

We were happy to follow the reviewer suggestion to consider sub-region in North-America for the evaluation with ozone sondes as suggested by Tilmes et al. (2012). We also divided the Tropics in three sub-regions as suggested by Tilmes et al. (2012). We found that more detailed information can be gained but also that the smaller averaging regions were more susceptible to data gaps and distortion by outlier observations. (The Tilmes et al. (2012) data set is probably less affected by these problems since they consider a 17 year period whereas we only study one year.) The structure of the biases in the sub-regions did confirm the conclusions drawn from the larger averaging area. We therefore suggest to discuss the biases for three sub-region in North-America as well as for three sub-region in the Tropics but to include the corresponding pictures in the supplement (see below Fig R2 and R3).

We will add in section 3.2.1

“Tilmes et al. (2012) suggest a further refinement of the North-America region into Canada, Eastern and Western United States as well of the Tropics into Atlantic/Africa, equatorial Americas and Eastern Indian Ocean/Western Pacific based on the inter-comparison of ozone sonde observation for the 1994-2010 period. The results will be discussed also for these sub-regions and corresponding figures will be presented in the supplement. “

in section 3.3

“A more detailed breakdown of North America (Canada, Eastern and Western United States) and the Tropics (Atlantic/Africa, equatorial Americas and Eastern Indian Ocean/Western Pacific) following Tilmes et al. (2012) is presented in the supplement.”

in section 3.3

“The LT underestimation occurred in all regions but was largest in early spring over Canada. C-IFS also underestimated over North America in MT. LT summer time ozone is overestimated in North-America by all models, in particular over the Eastern United States. The bias of C-IFS was the smallest in LT but in contrast to MOZ and REAN C-IFS underestimates summer time ozone in MT over the Eastern United States. The overestimation of UT ozone by MOZ was most pronounced in Canada.”

in section 3.3

“A more detailed analysis for different tropical regions shows that the seasonality is mostly well captured by all models over Atlantic-Africa, equatorial America and eastern Indian Ocean/Western Pacific in all three levels. Only the maxima occurring in equatorial America in September were underestimated by up to 15 ppb in MT and UT.”

*p. 7757: The description of the MOPITT data set is not written very clearly. Was the Level 3 product used, or did the authors perform their own gridding to 1x1 degree? Presumably the model profiles were transformed, taking into account the a priori profile as well as the averaging kernel (this should be stated more clearly -*

*l.21-23 seems a little confused - it is 2 operations).*

*l.20: The increased sensitivity at the surface of the joint (NIR+TIR) retrieval is due to the inclusion of the NIR channel.*

*l.24-26: I don't understand the point of this sentence.*

We used level 2 data and individual MOPITT pixels were binned onto a common 1x1 degree grid. The averaging kernels in combination with the a-priori profile were applied to the model profiles of CO.

The respective section (section 3.2.2) has been re-written as follows:

“MOPITT is a multispectral thermal infrared (TIR) / near infrared (NIR) instrument onboard the TERRA satellite with a pixel resolution of 22 km. TERRA’s local equatorial crossing time is approximately 10:30 a.m. The MOPITT CO level 2 pixels were binned within 1x1° within each month. Deeter et al. (2013a) report a bias of about +0.08e18 molec/cm2 and a standard deviation (SD) of the error of 0.19e18 molec/cm2 for the TIR/NIR product version 5. This is equivalent to a bias of about 4 % and a SD of 10% respectively assuming typical observations of 2.0 e18 molec/cm2. For the calculation of the simulated CO total column the a-priori profile in combination with the averaging kernels (AK) of the retrievals were applied. They have the largest values between 300 and 800 hPa. The AK have been applied to ensure that the difference between retrieval and AK-weighted model column is independent of the a-priori CO profiles used in the retrieval. One should note however, that the AK-weighted column is not equivalent to the modelled atmospheric CO burden anymore.”

*p.7758: As with the MOPITT description, it is not clear if the authors performed some of the processing of the GOME-2 retrievals or if they are describing the product they used. Please clarify. Was any transformation of model profiles performed to account for the sensitivity of the GOME-2 columns to the true profile (i.e., averaging kernels or airmass factors)?*

The modelled tropospheric columns have only been interpolated to the times and location of the observations. As the uncertainty in the NO<sub>2</sub> and HCHO retrievals are considerable, AK have not been applied to the modelled tropospheric columns. The retrieved and modelled tropospheric columns have been compared at time of and location of the satellite observations. Air mass factors were used for the retrievals.

We will in section 3.2.2

“ For comparison to GOME-2 data, model data are vertically integrated without applying AK to ...”

We also added a reference for the HCHO retrievals  
“(Vrekoussis et al., 2010).”

Vrekoussis, M., Wittrock, F., Richter, A., and Burrows, J. P.: GOME-2 observations of oxygenated VOCs: what can we learn from the ratio glyoxal to formaldehyde on a global scale?, Atmos. Chem. Phys., 10, 10145-10160, doi:10.5194/acp-10-10145-2010, 2010.

*p. 7760: The bias in surface ozone in MOZART could be at least partially due to a recently documented error in the dry deposition calculation for all versions of MOZART, which led to reduced deposition velocities than intended, and thus over-estimate of surface ozone, as described in Val Martin et al. (GRL, 2014, doi:10.1002/2014GL059651).*

We agree that differences in dry deposition velocities are also an important factor and will add in section 3.3:

“The recently reported (ValMartin et al. 2014) missing coupling of the leaf area index to the leaf and stomatal vegetation resistance in the calculation of dry deposition velocities could be an explanation for the MOZ bias.”

Val Martin, M., Heald, C. L. and Arnold, S. R.: Coupling dry deposition to vegetation phenology in the Community Earth System Model: Implications for the simulation of surface O<sub>3</sub>, *Geophys. Res. Lett.*, 41, 2988–2996, doi:10.1002/2014GL059651., 2014.

*p. 7761: It would be much easier to follow the arguments about the size of biases if the actual bias were plotted for each model. For example, the argument that "the bias of MOZ seems stronger over land" is hard to verify from these plots.*

We decided to show the simulated TC (AK applied) rather than the biases because they give a better impression of the actual fields. Please find below (Fig R4 and Fig R5) the biases corresponding to Fig 6 and Fig 7. We find that the bias in MOZ follows the land-sea patterns more than in the other models. However, it is difficult to exclude the possibility that the contrast is caused by satellite data retrieval rather than the model. The retrieval is sensitive to changes surface temperature and albedo

.

*Fig. 10 is only mentioned in passing in between discussion of Figs 8 and 9. It should be put in order and discussed more completely.*

We will describe Fig. 10 in more detail:

“The outcome of the comparison with LT CO from MOZAIC is consistent with the model bias with respect to the GAW surface observations in Europe (Figure 10). The winter biases were larger than summer biases and MOZ showed the largest underestimation. The GAW stations measuring CO are mostly located on mountains in the Alpine region and typical annual biases were about -15, -20 and -35 ppb for REAN, C-IFS and MOZ respectively. Biases of stations in flatter terrain such as Kollumerwaard tended to be larger.”

*p. 7762, l.18-19: The altitude levels that have the highest sensitivity for MOPITT should not have any bearing on the performance of the model, if the averaging kernels and a priori have been taken into account. I would remove this sentence.*

In this sentence we refer to REAN, which assimilated CO from MOPITT. We think it is a valid statement.

All technical errors have been corrected.

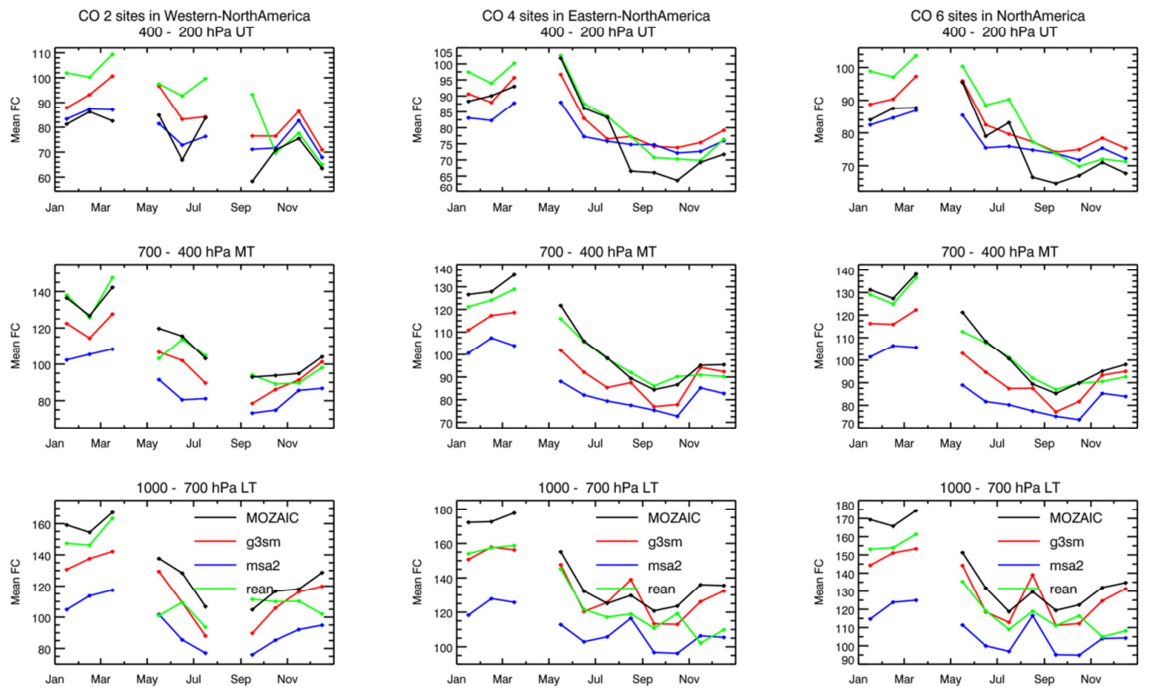
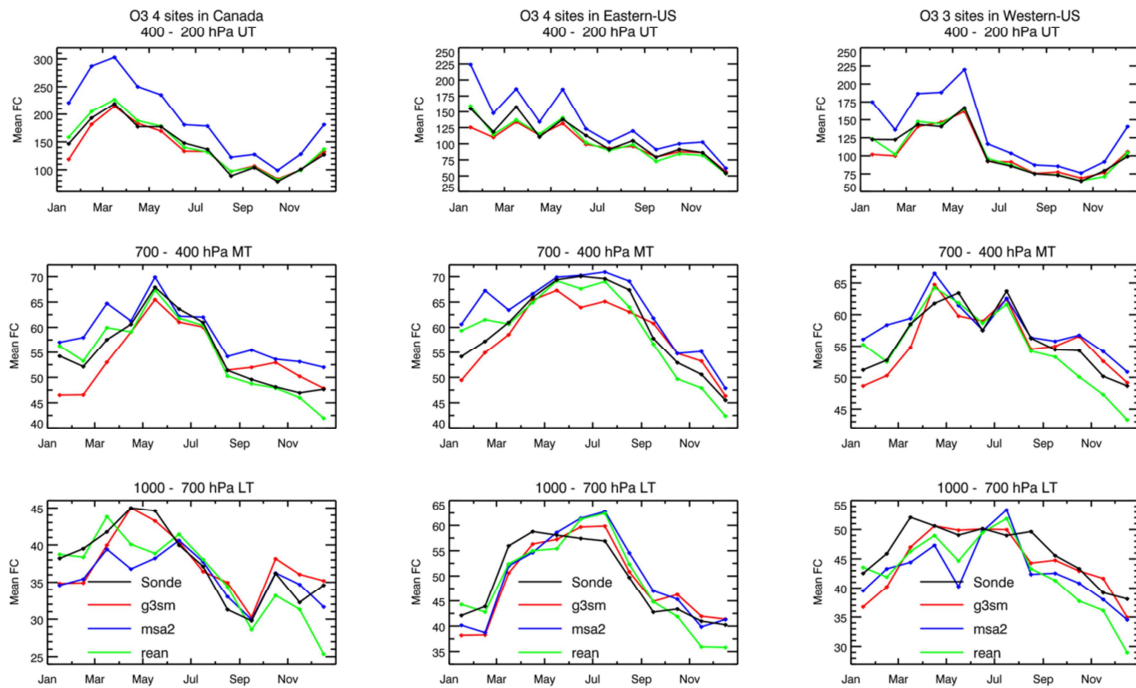
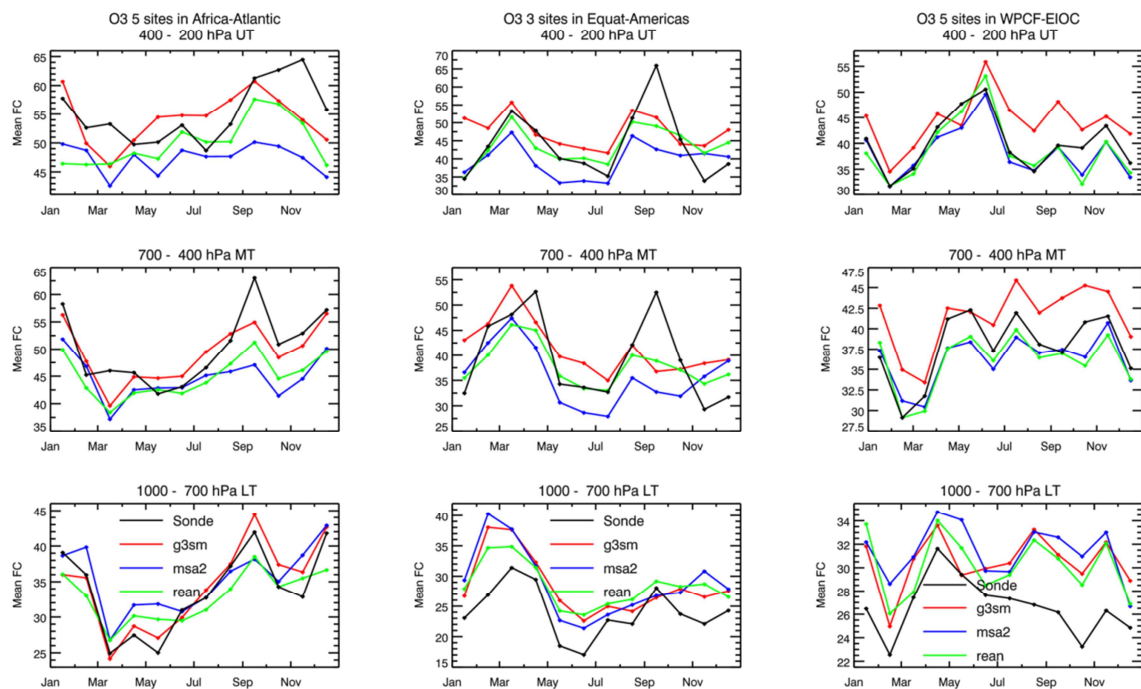


Figure R1 CO volume mixing ratios (ppb) over Western North America (left, 2 sites), Eastern North America (middle, 4 sites) and whole North America (right, 6 sites) averaged in the pressure bands 1000-700 hPa (bottom), 700-400 hPa (middle) and 400-200 hPa (top) observed by MOZAIC and simulated by C-IFS (red), MOZ (blue) and REAN (green) in 2008.



**Figure R2 Tropospheric ozone volume mixing ratios (ppb) over the Western-US (right) and Eastern-US (middle) and Canada (left) averaged in the pressure range 1000-700 hPa (bottom), 700-400 hPa (middle) and 400-200 hPa (top) observed by ozonesondes (black) and simulated by C-IFS (red), MOZ (blue) and REAN (green) in 2008**



**Figure R3** Tropospheric ozone volume mixing ratios (ppb) in the Tropics over Atlantic-Africa region (left) and Eastern Pacific and Indian Ocean (right) and equatorial Americas (middle) averaged in the pressure range 1000-700 hPa (bottom), 700-400 hPa (middle) and 400-200 hPa (top) observed by ozonesondes (black) and simulated by C-IFS (red), MOZ (blue) and REAN (green) in 2008

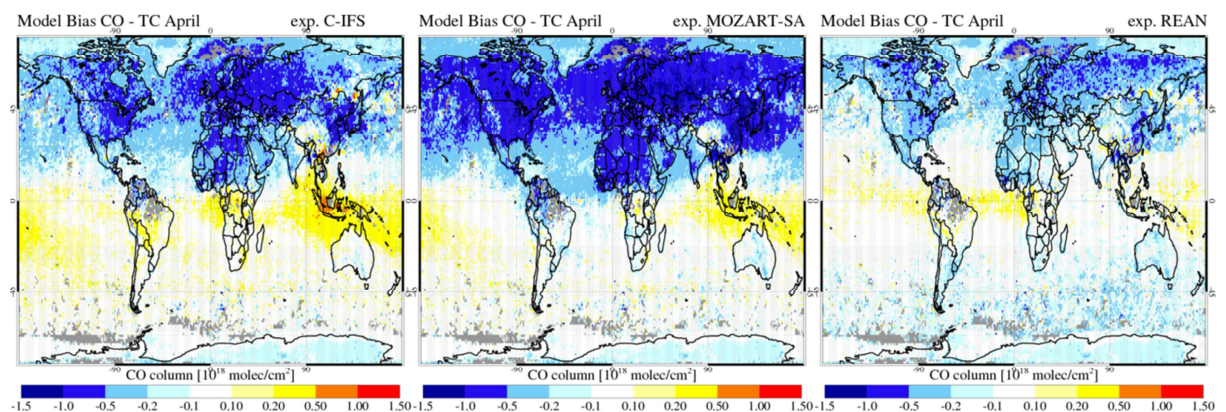


**Figure R4** Bias of CO total column with respect to retrieval MOPITT V6 for April 2008 of C-IFS (left), MOZ (middle) and REAN (right).



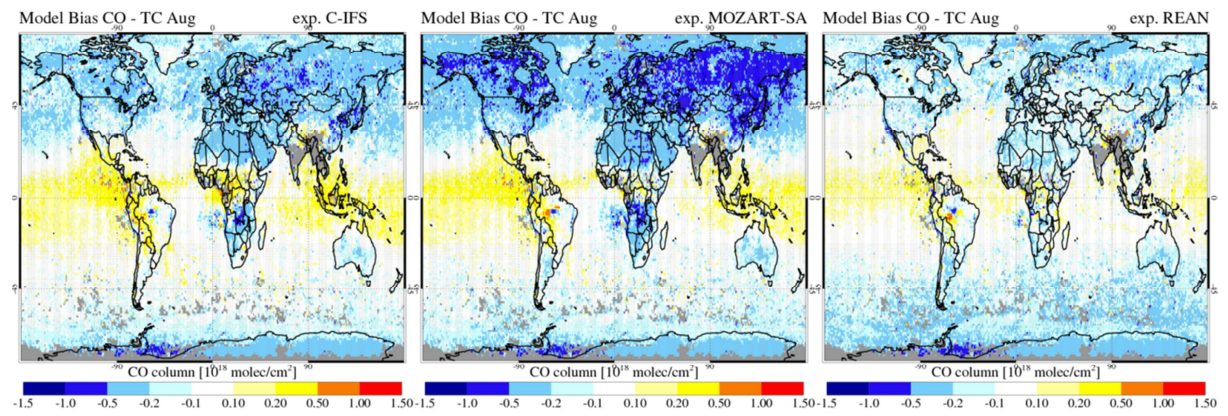


**Figure R5 Bias of CO total column with respect to retrieval MOPITT V6 for August 2008 of C-IFS (left), MOZ (middle) and REAN (right)**

# Tropospheric Chemistry in the Integrated Forecasting System of ECMWF

J. Flemming<sup>1</sup>, V. Huijnen<sup>2</sup>, J. Arteta<sup>3</sup>, P. Bechtold<sup>1</sup>, A. Beljaars<sup>1</sup>, A.-M.  
Blechschmidt<sup>4</sup>, B. Josse<sup>3</sup>, M. Diamantakis<sup>1</sup>, R. J. Engelen<sup>1</sup>, A. Gaudel<sup>5</sup>, A.  
Inness<sup>1</sup>, L. Jones<sup>1</sup>, E. Katragkou<sup>6</sup>, V. Marecal<sup>3</sup>, V.-H. Peuch<sup>1</sup>, A. Richter<sup>4</sup>, M.G.  
Schultz<sup>7</sup>, O. Stein<sup>7</sup> and A. Tsikerdekis<sup>6</sup>

[1] European Centre for Medium-Range Weather Forecasts, Reading, UK

[2] Royal Netherlands Meteorological Institute, De Bilt, The Netherlands

[3] Météo-France, Toulouse, France

[4] Universität Bremen, Germany

[5] CNRS, Laboratoire d'Aérodynamique, UMR 5560, Toulouse, France

[6] Department of Meteorology and Climatology, School of Geology, Aristotle University of  
Thessaloniki, Greece

[7] Institute for Energy and Climate Research, Forschungszentrum Jülich, Germany

Correspondence to: J. Flemming (Johannes.Flemming@ecmwf.int)

## Abstract

A representation of atmospheric chemistry has been included in the Integrated Forecasting System (IFS) of the European Centre for Medium-range Weather Forecasts (ECMWF). The new chemistry modules complement the aerosol modules of the IFS for atmospheric composition, which is named C-IFS. C-IFS for chemistry supersedes a coupled system, in which the Chemical Transport Model (CTM) Model for Ozone and Related chemical Tracers 3 was two-way coupled to the IFS (IFS-MOZART). This paper contains a description of the new on-line implementation, an evaluation with observations and a comparison of the performance of C-IFS with MOZART and with a re-analysis of atmospheric composition produced by IFS-MOZART within the Monitoring Atmospheric Composition and Climate (MACC) project. The chemical mechanism of C-IFS is an extended version of the Carbon Bond 2005 (CB05) chemical mechanism as implemented in the CTM Transport Model 5 (TM5). CB05 describes tropospheric chemistry with 54 species and 126 reactions. Wet deposition and lightning nitrogen monoxide (NO) emissions are modelled in C-IFS using the detailed input of the IFS physics package. A one-year simulation by C-IFS, MOZART and the MACC re-analysis is evaluated against ozonesondes, carbon monoxide (CO) aircraft profiles, European surface observations of ozone (O<sub>3</sub>), CO, sulphur dioxide (SO<sub>2</sub>) and nitrogen dioxide (NO<sub>2</sub>) as well as satellite retrievals of CO, tropospheric NO<sub>2</sub> and formaldehyde. Anthropogenic emissions from the MACC/CityZen (MACCity) inventory and biomass burning emissions from the Global Fire Assimilation System (GFAS) data set were used in the simulations by both C-IFS and MOZART. C-IFS (CB05) showed an improved performance with respect to MOZART for CO, upper tropospheric O<sub>3</sub>, winter time SO<sub>2</sub> and was of a similar accuracy for other evaluated species. C-IFS (CB05) is about ten times more computationally efficient than IFS-MOZART.

## 1 Introduction

Monitoring and forecasting of global atmospheric composition are key objectives of the atmosphere service of the European Copernicus Programme. The Copernicus Atmosphere Monitoring Service (CAMS) is based on combining satellite observations of atmospheric composition with state-of-the-art atmospheric modelling (Flemming et al., 2013 and Hollingsworth et al., 2008). For that purpose, the integrated forecasting system (IFS) of the European Centre for Medium-Range Weather Forecasts (ECMWF) was extended for forecast and assimilation of atmospheric composition. Modules for aerosols (Morcrette et al., 2009,

57 Benedetti et al., 2009) and greenhouse gases (Engelen et al., 2009) were integrated on-line in  
58 the IFS. Because of the complexity of the chemical mechanisms for reactive gases, modules  
59 for atmospheric chemistry were not initially included in the IFS. Instead a coupled system  
60 (Flemming et al., 2009a) was developed, which couples the IFS to the Chemical Transport  
61 Model (CTM) Model for OZone and Related chemical Tracers 3 (MOZART, Kinnison et al.,  
62 2007) or Transport Model 5 (TM5, Huijnen et al., 2010) by means of the Ocean Atmosphere  
63 Sea Ice Soil coupling software (OASIS4) coupler software (Redler et al., 2010). Van Noije et  
64 al. (2014) coupled TM5 to IFS for climate applications in a similar approach. The coupled  
65 system made it possible to assimilate satellite retrievals of reactive gases with the assimilation  
66 algorithm of the IFS, which is also used for the assimilation of meteorological observations as  
67 well as for aerosol and greenhouse gases.

68 The coupled system IFS-MOZART has been successfully used for a re-analysis of  
69 atmospheric composition (Inness et al., 2013), pre-operational atmospheric composition  
70 forecasts (Stein et al., 2012), forecast and assimilation of the stratospheric ozone (O<sub>3</sub>)  
71 (Flemming et al., 2011a, Lefever et al., 2014) and tropospheric carbon monoxide (CO)  
72 (Eligundi et al., 2010) and O<sub>3</sub> (Ordonez et al., 2010). The coupled system IFS-TM5 has been  
73 used in a case study on a period with intense biomass burning in Russia in 2010 (Huijnen et  
74 al., 2012). Nevertheless, the coupled approach has limitations such as the need for  
75 interpolation between the IFS and CTM model grids and the duplicate simulation of transport  
76 processes. Further, its computational performance is often not optimal as it can suffer from  
77 load imbalances between the coupled components.

78 Consequently, modules for atmospheric chemistry and related physical processes have now  
79 been integrated on-line in the IFS, thereby complementing the on-line integration strategy  
80 already pursued for aerosol and greenhouse gases in IFS. The IFS including modules for  
81 atmospheric composition is named Composition-IFS (C-IFS). C-IFS makes it possible (i) to  
82 use the detailed meteorological simulation of the IFS for the simulation of the fate of  
83 constituents (ii) to use the IFS data assimilation system to assimilate observations of  
84 atmospheric composition and (iii) to simulate feedback processes between atmospheric  
85 composition and weather. A further advantage of C-IFS is the possibility of model runs at a  
86 high horizontal and vertical resolution because of the high computational efficiency of C-IFS.  
87 C-IFS is the global model system run in pre-operational mode as part of the Monitoring

Atmospheric Composition and Climate - Interim Implementation project (MACC II and MACC III) in preparation of CAMS.

Including chemistry modules in general circulation models (GCM) to simulate interaction of stratospheric O<sub>3</sub> (e.g. Steil et al., 1998) and aerosols (e.g. Haywood et al., 1997) in the climate system started in the mid-1990s. Later, more comprehensive schemes for tropospheric chemistry were included in climate GCM such as ECHAM5-HAMMOZ (Pozzoli et al., 2008; Rast et al., 2014) and CAM-chem (Lamarque et al., 2012) to study short-lived greenhouse gases and the influence of climate change on air pollution (e.g. Fiore et al., 2010). In the UK Met Office's Unified Model (UM) stratospheric chemistry (Morgenstern et al., 2009) and tropospheric chemistry (O'Connor et al., 2014) can be simulated together with the GLOMAP mode aerosol scheme (Mann et al., 2010). Examples of the on-line integration of chemistry modules in global circulation models with focus on NWP are GEM-AQ (Kaminski et al., 2008), GEMS-BACH (Menard et al., 2007) and [GU-WRF/Chem \(Grell et al., 2005; Zhang et al., 2012\)](#). Savage et al. (2013) evaluate the performance of air quality forecast with the UM at the regional scale. Baklanov et al. (2014) give a comprehensive overview of on-line coupled chemistry-meteorological models for regional applications.

C-IFS is intended to run with several chemistry schemes for both the troposphere and the stratosphere in the future. Currently, only the tropospheric chemical mechanism CB05 originating from the TM5 CTM (Huijnen et al., 2010) has been thoroughly tested. For example, C-IFS (CB05) has been applied to study the HO<sub>2</sub> uptake on clouds and aerosols (Huijnen et al., 2014) and pollution in the Arctic (Emmons et al., 2014). The tropospheric and stratospheric scheme RACMOBUS of the MOCAGE model (Bousserez et al., 2007) and the MOZART 3 chemical scheme as well as an extension of the CB05 scheme with the stratospheric chemical mechanism of the BASCOE model (Errera et al., 2008) have been technically implemented and are being scientifically tested. Only C-IFS (CB05) is the subject of this paper.

Each chemistry scheme in C-IFS consists of the specific gas phase chemical mechanism, multi-phase chemistry, the calculation of photolysis rates and upper chemical boundary conditions. Dry and wet deposition, emission injection and parameterization of lightning NO emissions as well as transport and diffusion are simulated by the same approach for all chemistry schemes. Likewise, emissions and dry deposition input data are kept the same for all configurations.

The purpose of this paper is to document C-IFS and to present its model performance with respect to observations. Since C-IFS (CB05) replaced the current operational MACC model system for reactive gases (IFS-MOZART) both in data assimilation and forecast mode, the evaluation in this paper is carried out predominately with observations that are used for the routine evaluation of the MACC II system. The model results are compared (i) with a MOZART stand-alone simulation, which is equivalent to a IFS-MOZART simulation and (ii) with the MACC re-analysis (Inness et al., 2013), which is an application of IFS-MOZART in data assimilation mode. All model configurations used the same emission data. The comparison demonstrates that C-IFS is ready to be used operationally.

The paper is structured as follows. Section 2 is a description of the C-IFS, with focus on the newly implemented physical parameterizations and the chemical mechanism CB05. Section 3 contains the evaluation with observations of a one year simulation with C-IFS (CB05) and a comparison with the results from the MOZART run and the MACC re-analysis. The paper is concluded with a summary and an outlook in section 4.

## 2 Description of C-IFS

### 2.1 Overview of C-IFS

The IFS consists of a spectral NWP model that applies the semi-Lagrangian (SL) semi-implicit method to solve the governing dynamical equations. The simulation of the hydrological cycle includes prognostic representations of cloud fraction, cloud liquid water, cloud ice, rain and snow (Forbes et al., 2011). The simulations presented in this paper used the IFS release CY40r1. The technical and scientific documentation of this IFS release can be found at <http://www.ecmwf.int/research/ifsdocs/CY40r1/index.html>. Changes of the operational model are documented on <https://software.ecmwf.int/wiki/display/IFS/Operational+changes>.

At the start of the time step, the three-dimensional advection of the tracers mass mixing ratios is simulated by the ~~SL semi-Lagrangian~~ method as described in Temperton et al. (2001) and Hortal (2002). Next, the tracers are vertically distributed by the diffusion scheme (Beljaars et al., 1998) and by convective mass fluxes (Bechtold et al., 2014). The diffusion scheme also simulates the injection of emissions and the loss by dry deposition (see section 2.4.1). The output of the convection scheme is used to calculate NO production by lightning (see section 2.4.3). Finally, the sink and source terms due to chemical conversion (see section 2.5), wet

deposition (see section 2.4.2) and prescribed surface and stratospheric boundary conditions are calculated (see section 2.5.2).

The chemical species and the related processes are represented only in grid-point space. The horizontal grid is a reduced Gaussian grid (Hortal and Simmons, 1991). C-IFS can be run at varying vertical and horizontal resolutions. The simulations presented in this paper were carried out at a T255 spectral resolution (i.e. truncation at wavenumber 255), which corresponds to a grid box size of about 80 km. The vertical discretization uses 60 levels up to the model top at 0.1 hPa (65 km) in a hybrid sigma-pressure coordinate. The vertical extent of the lowest level is about 17 m; it is 100 m at about 300m above ground, 400-600 m in the middle troposphere and about 800 m at about 10 km height.

The modus operandi of C-IFS is one of a forecast model in a NWP framework. The simulations of C-IFS are a sequence of daily forecasts over a period of several days. Each forecast is initialised by the ECMWF's operational analysis for the meteorological fields and by the 3D chemistry fields from the previous forecast ("forecast mode"). Continuous simulations over longer periods are carried out in "relaxation mode". In relaxation mode the meteorological fields are relaxed to the fields of a meteorological re-analysis, such as ERA-Interim, during the run (Jung et al., 2008) to ensure realistic and consistent meteorological fields.

## **2.2 Transport**

The transport by advection, convection and turbulent diffusion of the chemical tracers uses the same algorithms as developed for the transport of water vapour in the NWP applications of IFS. The advection is simulated with a three-dimensional semi-Lagrangian advection scheme, which applies a quasi-monotonic cubic interpolation of the departure values. Since the semi-Lagrangian advection does not formally conserve mass a global mass fixer is applied. The effect of different global mass fixers is discussed in Diamantakis and Flemming (2014) and Flemming and Huijnen (2011b). A proportional mass was used for the runs presented in this paper because of the overall best balance between the results and computational cost.

The vertical turbulent transport in the boundary layer is represented by a first order K-diffusion closure. The surface emissions are injected as lower boundary flux in the diffusion scheme. The lower boundary flux condition also accounts for the dry deposition flux based on the projected surface mass mixing ratio in an implicit way. The vertical transport by

convection is simulated as part of the cumulus convection. It applies a bulk mass flux scheme which was originally described in Tiedtke (1989). The scheme considers deep, shallow and mid-level convection. Clouds are represented by a single pair of entraining/detraining plumes which determine the updraught and downdraught mass fluxes. (<http://old.ecmwf.int/research/ifsdocs/CY40r1/> in Physical Processes, Chapter 6, pp 73-90). Highly soluble species such as nitric acid (HNO<sub>3</sub>), hydrogen peroxide (H<sub>2</sub>O<sub>2</sub>) and aerosol precursors are assumed to be scavenged in the convective rain droplets and are therefore excluded from the convective mass transfer.

The operator splitting between the transport and the sink and source terms follows the implementation for water vapour (Beljaars et al., 2004). Advection, diffusion and convection are simulated sequentially. The sink and source processes are simulated in parallel using an intermediate update of the mass mixing ratios with all transport tendencies. At the end of the time step tendencies from transport and sink and source terms are added together for the final update the concentration fields. Resulting negative mass mixing ratios are corrected at this point by setting the updated mass mixing ratio to a “chemical zero” of 1.0e-25 kg/kg.

## 2.3 Emissions for 2008

The anthropogenic surface emissions were given by the MACCity inventory (Granier et al., 2011) and aircraft NO emissions of a total of ~0.8 Tg N/yr were applied (Lamarque et al., 2010). Natural emissions from soils and oceans were taken from the Precursors of Ozone and their Effects in the Troposphere (POET) database for 2000 (Granier et al., 2005; Olivier et al., 2003). The biogenic emissions were simulated off-line by the MEGAN2.1 model (Guenther et al., 2006). The anthropogenic and natural emissions were used as monthly means. Daily Biomass burning emissions were produced by the Global Fire Assimilation System (GFAS) version 1, which is based on satellite retrievals of fire radiative power (Kaiser et al., 2012). The actual emission totals used in the T255 simulation for 2008 from anthropogenic, biogenic sources and biomass burning as well as lightning NO are given in Table 1~~Table 1~~.

## 2.4 Physical parameterizations of sources and sinks

### 2.4.1 Dry deposition

Dry deposition is an important removal mechanism at the surface in the absence of precipitation. It depends on the diffusion close to the earth surface, the properties of the constituent and on the characteristics of the surface, in particular the type and state of the



213 vegetation and the presence of intercepted rain water. Dry deposition plays an important role  
214 in the biogeochemical cycles of nitrogen and sulphur, and it is a major loss process of  
215 tropospheric O<sub>3</sub>. Modelling the dry deposition fluxes in C-IFS is based on a resistance model  
216 (Wesely et al., 1989), which differentiates the aerodynamic, the quasi-laminar and the canopy  
217 or surface resistance. The inverse of the total resistance is equivalent to a dry deposition  
218 velocity  $V_D$ .

219 The dry deposition flux  $F_D$  at the model surface is calculated based on the dry deposition  
220 velocity  $V_D$ , the mass mixing ratio  $X_s$  and air density  $\rho_s$  at the lowest model level  $s$ , in the  
221 following way:

$$F_D = V_D X_s \rho_s$$

222 The calculation of the loss by dry deposition has to account for the implicit character of the  
223 dry deposition flux since it depends on the mass mixing ratio  $X_s$ . ~~itself~~

224 The dry deposition velocities were calculated as monthly mean values from a one-year  
225 simulation using the approach described in Michou et al. (2004). It used meteorological and  
226 surface input data such as wind speed, temperature, surface roughness and soil wetness from  
227 the ERA-interim data set. At the surface the scheme makes a distinction between uptake  
228 resistances for vegetation, bare soil, water, snow and ice. The surface and vegetation  
229 resistances for the different species are calculated using the stomatal resistance of water  
230 vapour. The stomatal resistance for water vapour is calculated depending on the leaf area  
231 index, radiation and the soil wetness at the uppermost surface layer. Together with the  
232 cuticular and mesophyllic resistances this is combined into the leaf resistance according to  
233 Wesely et al. (1989) using season and surface type specific parameters as referenced in  
234 Seinfeld and Pandis (1998).

235 Dry deposition velocities have higher values during the day because of lower aerodynamic  
236 resistance and canopy resistance. Zhang et al. (2003) reported that averaged observed O<sub>3</sub> and  
237 sulphur dioxide (SO<sub>2</sub>) dry deposition velocities can be up to 4 times higher at day time than at  
238 night time. As this important variation is not captured with the monthly-mean dry deposition  
239 values, a +/- 50% variation is imposed on all dry deposition values based on the cosine of the  
240 solar zenith angle. This modulation tends to decrease dry deposition for species with a night  
241 time maximum at the lowest model level and it increases dry deposition of O<sub>3</sub>.

242 Table A4 (supplement) contains annual total loss by dry deposition and expressed as a life-  
243 time estimate by dividing by tropospheric burden for a simulation using monthly dry  
244 deposition values for 2008. Dry deposition was most effective for many species in particular  
245 SO<sub>2</sub> and ammonia (NH<sub>3</sub>) as the respective lifetimes were one day to one week. For  
246 tropospheric O<sub>3</sub> the respective globally averaged time scale is about 3 months. Because dry  
247 deposition occurs mainly over ice-free land surfaces the corresponding time scale is at least  
248 three times shorter in these areas.

#### 249 2.4.2 Wet Deposition

250 Wet deposition is the transport and removal of soluble or scavenged constituents by  
251 precipitation. It includes the following processes:

- 252 • In-cloud scavenging and removal by rain and snow (rain out)
- 253 • Release by evaporation of rain and snow
- 254 • Below cloud scavenging by precipitation falling through without formation of  
255 precipitation (wash out)

256 It is important to take the sub-grid scale of cloud and precipitation-formation into account for  
257 the simulation of wet deposition. The IFS cloud scheme provides information on the cloud  
258 and the precipitation fraction for each grid box. It uses a random overlap assumption (Jakob  
259 and Klein, 2000) to derive cloud and precipitation area fraction. The same method has been  
260 used by Neu and Prather (2012), who demonstrated the importance of the overlap assumption  
261 for the simulation of the wet deposition. The precipitation fluxes for the simulation of wet  
262 removal in C-IFS were scaled to be valid over the precipitation fraction of the respective grid-  
263 box. The loss of tracer by rain-out and wash-out was limited to the area of the grid box  
264 covered by precipitation. Likewise, the cloud water and ice content is scaled to the respective  
265 cloud area fraction. If the sub-grid scale distribution was not considered in this way, wet  
266 deposition was lower for highly soluble species such as HNO<sub>3</sub> because the species is only  
267 removed from the cloudy or rainy grid box fraction. For species with low solubility the wet  
268 deposition loss was slightly decreased because of the decrease in effective cloud and rain  
269 water.

270 Even if wet deposition removes tracer mass only in the precipitation area, the mass mixing  
271 ratio representing the entire grid box is changed accordingly after each model time step. This  
272 is equivalent with the assumption that there is instantaneous mixing within the grid-box at the

time scale of the model time step. As discussed in Huijnen et al. (2014), this assumption may lead to an overestimation of the simulated tracer loss.

The module for wet deposition in C-IFS is based on the Harvard wet deposition scheme (Jacob et al., 2000 and Liu et al., 2001). In contrast to Jacob et al. (2000), tracers scavenged in wet convective updrafts are not removed as part of the convection scheme. Nevertheless, the fraction of highly soluble tracers in cloud condensate is simulated to limit the amount of tracers lifted upwards as only the gas phase fraction is transported by the mass flux. The removal by convective precipitation is simulated in the same way as for large-scale precipitation in the wet deposition routine.

The input fields to the wet deposition routine are the following prognostic variables, calculated by the IFS cloud scheme (Forbes et al., 2011): total cloud and ice water content, grid-scale rain- and snow water content and cloud and grid-scale precipitation fraction as well as the derived fluxes for convective and grid-scale precipitation fluxes at the grid cell interfaces. For convective precipitation a precipitation fraction of 0.05 is assumed and the convective rain and snow water content is calculated assuming a droplet fall speed of 5 m/s.

Wash-out, evaporation and rain-out are calculated after each other for large-scale and convective precipitation. The amount of trace gas dissolved in cloud droplets is calculated using Henry's-law-equilibrium or assuming that 70% of aerosol precursors such as sulphate ( $\text{SO}_4$ ),  $\text{NH}_3$  and nitrate ( $\text{NO}_3$ ) is dissolved in the droplet. The effective Henry coefficient for  $\text{SO}_2$ , which accounts for the dissociation of  $\text{SO}_2$ , is calculated following Seinfeld and Pandis (1998, p. 350). The other Henry's law coefficients are taken from the compilation by Sander (1999) ([www.henrys-law.org](http://www.henrys-law.org), Table A1 in the supplement).

The loss by rain out is determined by the precipitation formation rate. The retention coefficient  $R$ , which accounts for the retention of dissolved gas in the liquid cloud condensate as it is converted to precipitation, is one for all species in warm clouds ( $T > 268 \text{ K}$ ). For mixed clouds ( $T < 268 \text{ K}$ )  $R$  is 0.02 for all species but 1.0 for  $\text{HNO}_3$  and 0.6 for  $\text{H}_2\text{O}_2$  (von Blohn, 2011). In ice clouds only  $\text{H}_2\text{O}_2$  (Lawrence and Crutzen, 1998) and  $\text{HNO}_3$  are scavenged.

Partial evaporation of the precipitation fluxes leads to the release of 50% of the resolved tracer and 100% in the case of total evaporation (Jacobs et al., 2000). Wash-out is either mass-transfer or Henry-equilibrium limited.  $\text{HNO}_3$ , aerosol precursors and other highly soluble gases are washed out using a first order wash-out rate of  $0.1 \text{ mm}^{-1}$  (Levine and

Schwartz, 1982 ) to account for the mass transfer . For less soluble gases the resolved fraction in the rain water is calculated assuming Henry equilibrium in the evaporated precipitation.

Table A5 (supplement) contains total loss by wet deposition and expressed as time scale in days based on the tropospheric burden. For aerosol precursors nitrate, sulphate and ammonium,  $\text{HNO}_3$  and  $\text{H}_2\text{O}_2$  wet deposition is the most important loss process with respective timescales of 2–4 days.

### 2.4.3 NO emissions from lightning

NO emissions from lightning are a considerable contribution to the global atmospheric  $\text{NO}_x$  budget. Estimates of the global annual source vary between 2–8 TgN/yr (Schumann and Huntrieser, 2007). 5 TgN/yr (10.7 TgNO/yr) is the most commonly assumed value for global CTMs which is about 6-7 times the value of NO emissions from aircraft (Gauss et al., 2006) or 17% of the total anthropogenic emissions. NO emissions from lightning play an important role in the chemistry of the atmosphere because they are released in the rather clean air of the free troposphere, where they can influence the  $\text{O}_3$  budget and hence the OH- $\text{HO}_2$  partitioning (DeCaria et al., 2005) .

The parameterization of the lightning NO production in C-IFS consist of estimates of (i) the flash rate density, (ii) the flash energy release and (iii) the vertical emission profile for each model grid column. The estimate of the flash-rate density is based on parameters of the convection scheme. The C-IFS has two options to simulate the flash-rate densities using the following input parameters: (i) convective cloud height (Price and Rind, 1992) or (ii) convective precipitation (Meijer et al., 2001).

The parameterizations distinguish between land and ocean points by assuming about 5-10 times higher flash rates over land. Additional checks on cloud base height, cloud extent and temperature are implemented to select only clouds that are likely to generate lightning strokes. The coefficients of the two parameterizations were derived from field studies and depend on the model resolution. With the current implementation of C-IFS (T255L60), the global flash rates were 26 and 43 flashes per seconds for the schemes by Price and Rind (1992) and Meijer et al. (2001), respectively. It seemed therefore necessary to scale the coefficients to get a flash rate in the range of the observed values of about 40-50 flashes per second derived from observations of the Optical Transient Detector (OTD) and the Lightning Imaging Sensor

(LIS) (Cecil et al., 2012).

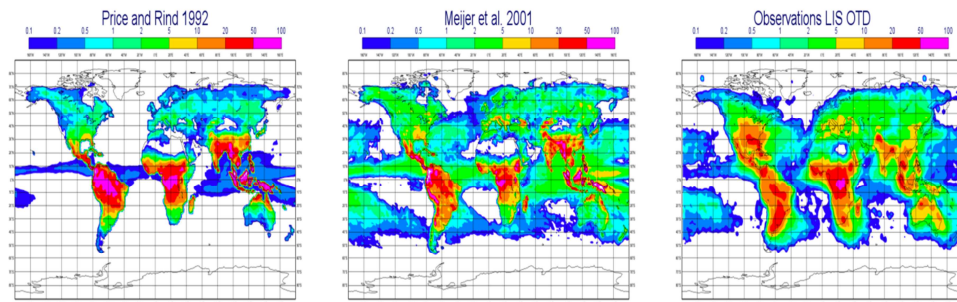


Figure 1 shows the annual flash rate density simulated by the two parameterisations together with observations from the LIS/OTD data set. The two approaches show the main flash activity in the tropics but there were differences in the distributions over land and sea. The smaller land-sea differences of Meijer et al. (2001) agreed better with the observations. The observed maximum over Central Africa was well reproduced by both parameterizations but the schemes produce an exaggerated maximum over tropical South America. The lightning activity over the United States was underestimated by both parameterisations. The parameterization by Meijer et al. (2001) has been used for the C-IFS runs presented in this paper.

Cloud to ground (CG) and cloud to cloud (CC) flashes are assumed to release a different amount of energy, which is proportional to the NO release. Price et al. (1997) suggest that the energy release of CG is 10 times higher. However, more recent studies suggest a similar value for CG and CC energy release based on aircraft observations and model studies (Ott et al., 2010), which is followed in C-IFS. In C-IFS, CG and CC fractions are calculated using the approach by Price and Rind (1993), which is based on a 4th order function of cloud height above freezing level.

The vertical distribution of the NO release is of importance for its impact on atmospheric chemistry. Many CTMs use the suggestion of Pickering et al. (1998) of a C-shape profile, which peaks at the surface and in the upper troposphere. Ott et al. (2010) suggest a “backward C-shape” profile which locates most of the emission in the middle of the troposphere. The vertical distribution can be simulated by C-IFS (i) according to Ott et al. (2010) or (ii) as a C-shape profile following Huijnen et al. (2010). The approach by Ott et al. (2010) is used in the

simulation presented here. As lightning NO emissions occur mostly in situations with strong convective transport, differences in the injection profile had little impact.

As the lightning emissions depend on the convective activity they change at different resolutions or after changes to the convection scheme. The C-IFS lightning emissions were 4.9 TgN/yr at T159 resolution and 5.7 Tg N/yr at T255 resolution.

## **2.5 CB05 chemistry scheme**

### *2.5.1 Gas-phase chemistry*

The chemical mechanism is a modified version of the Carbon Bond mechanism 5 (CB05, Yarwood et al., 2005), which is originally based on the work of Gery et al. (1989) with added reactions from Zaveri and Peters (1999) and from Houweling et al. (1998) for isoprene. The CB05 scheme adopts a lumping approach for organic species by defining a separate tracer species for specific types of functional groups. The speciation of the explicit species into lumped species follows the recommendations given in Yarwood et al. (2005). The CB05 scheme used in C-IFS has been further extended in the following way: An explicit treatment of methanol ( $\text{CH}_3\text{OH}$ ), ethane ( $\text{C}_2\text{H}_6$ ), propane ( $\text{C}_3\text{H}_8$ ), propene ( $\text{C}_3\text{H}_6$ ) and acetone ( $\text{CH}_3\text{COCH}_3$ ) has been introduced as described in Williams et al., (2013). The isoprene oxidation has been modified motivated by Archibald et al. (2010). Higher C3 peroxy-radicals formed during the oxidation of  $\text{C}_3\text{H}_6$  and  $\text{C}_3\text{H}_8$  were included following Emmons et al. (2010).

The CB05 scheme is supplemented with chemical reactions for the oxidation of  $\text{SO}_2$ , dimethyl sulphide (DMS), methyl sulphonic acid (MSA) and  $\text{NH}_3$ , as outlined in Huijnen et al. (2014). For the oxidation of DMS, the approach of Chin et al. (1996) is adopted. Table A1 (supplement) gives a comprehensive list of the trace gases included in the chemical scheme.

The reaction rates have been updated according to the recommendations given in either Sander et al. (2011) or Atkinson et al. (2004, 2006). The oxidation of CO by the hydroxyl radical (OH) implicitly accounts for the formation and subsequent decomposition of the intermediate species HOCO as outlined in Sander et al. (2006). For lumped species, e.g. ALD2, the reaction rate is determined by an average of the rates of reaction for the most abundant species, e.g. C2 and C3 aldehydes, in that group. An overview of all gas-phase reactions and reaction rates as applied in this version of C-IFS can be found in Table A2 (supplement).

For the loss of trace gases by heterogeneous oxidation processes, the model explicitly accounts for the oxidation of SO<sub>2</sub> in cloud through aqueous phase reactions with H<sub>2</sub>O<sub>2</sub> and O<sub>3</sub>, depending on the acidity of the solution. The pH is computed from the SO<sub>4</sub>, MSA, HNO<sub>3</sub>, NO<sub>3</sub> A, NH<sub>3</sub> and NH<sub>4</sub> concentrations, as well as from a climatological CO<sub>2</sub> value. The pH, in combination with the Henry coefficient, defines the factor of sulphate residing in the aqueous phase, compared to the gas phase concentration (Dentener and Crutzen, 1993) ~~In this version of C-IFS, The~~ heterogeneous conversion of N<sub>2</sub>O<sub>5</sub> into HNO<sub>3</sub> on cloud droplets and aerosol particles is applied with a reaction probability ( $\gamma$ ) set to 0.02 (Evans and Jacob, 2005). The surface area density is computed based on a climatological aerosol size distribution function, applied to the SO<sub>4</sub>, MSA and NO<sub>3</sub> A aerosol, as well as to clouds assuming a droplet size of 8  $\mu$ m.

Formatted: Subscript

#### 2.5.2 Photolysis rates

For the calculation of photo-dissociation rates an on-line parameterization for the derivation of actinic fluxes is used (Williams et al., 2012, 2006). It applies a Modified Band Approach (MBA) which is an updated version of the work by Landgraf and Crutzen (1998), tailored and optimized for use in tropospheric CTMs. The approach uses 7 absorption bands across the spectral range 202 – 695 nm. At instances of large solar zenith angles (71-85°) a different set of band intervals is used. In the MBA the radiative transfer calculation using the absorption and scattering components introduced by gases, aerosols and clouds is computed on-line for each of 7 pre-defined band intervals based on the 2-stream solver of Zdunkowski et al. (1980).

The optical depth of clouds is calculated based on a parameterization available in IFS (Slingo, 1989 and Fu et al., 1996) for the cloud optical thickness at 550 nm. For the simulation of the impact of aerosols on the photolysis rates a climatological field for aerosols is used, as detailed in Williams et al. (2012). There is also an option to use the MACC aerosol fields.

In total 20 photolysis rates are included in the scheme, as given in Table A3 (supplement). The explicit nature of the MBA implies a good flexibility in terms of updating molecular absorption properties (cross sections and quantum yields) and the addition of new photolysis rates into the model.

419 2.5.3 *The chemical solver*

420 The chemical solver used in C-IFS (CB05) is an Euler Backward Iterative (EBI) solver  
421 (Hertel et al., 1996). This solver has been originally designed for use with the CBM4  
422 mechanism of Gery et al. (1989). The chemical time step is 22.5 min, which is half of the  
423 dynamical model time step of 45 min at T255 resolution. Eight, four or one iterations are  
424 carried out for fast-, medium- and slow-reacting chemical species to obtain a solution. The  
425 number of iterations is doubled in the lowest four models levels, where the perturbations due  
426 to emissions can be large.

427 2.5.4 *Stratospheric boundary conditions*

428 The modified CB05 chemical mechanism includes no halogenated species and no photolytic  
429 destruction below 202 nm and is therefore not suited for the description of stratospheric  
430 chemistry. Thus realistic upper boundary conditions for the longer-lived gases such as O<sub>3</sub>,  
431 methane (CH<sub>4</sub>), and HNO<sub>3</sub> are needed to capture the influence of stratospheric intrusions on  
432 the composition of the upper troposphere.

433 | Stratospheric O<sub>3</sub> chemistry in C-IFS (CB05) is parameterized by the Cariolle scheme  
434 (Cariolle and Teyssèdre, 2007). Chemical tendencies for stratospheric and tropospheric O<sub>3</sub> are  
435 merged at an empirical interface of the diagnosed tropopause height in IFS. Additionally,  
436 stratospheric O<sub>3</sub> in C-IFS can be nudged to O<sub>3</sub> analyses of either the MACC re-analysis  
437 (Inness et al., 2013) or ERA interim (Dee et al., 2011). The tropopause height in IFS is  
438 diagnosed either from the gradient in humidity or the vertical temperature gradient.

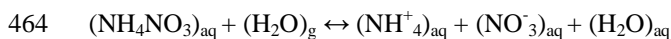
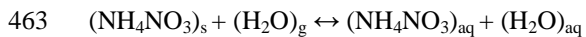
439 Stratospheric HNO<sub>3</sub> at 10 hPa is controlled by a climatology of HNO<sub>3</sub> and O<sub>3</sub> observations  
440 from the Microwave Limb Sounder (MLS) aboard the Upper Atmosphere Research satellite  
441 (UARS). HNO<sub>3</sub> is set to according to the observed HNO<sub>3</sub> - O<sub>3</sub> ratio and the simulated O<sub>3</sub>  
442 concentrations. Further, stratospheric CH<sub>4</sub> is constrained by a climatology based on  
443 observations of the Halogen Occultation Experiment instrument (Grooß and Russel, 2005), at  
444 45hPa and at 90 hPa in the extra-tropics, which implicitly accounts for the stratospheric  
445 chemical loss of CH<sub>4</sub> by OH, chlorine (Cl) and oxygen (O<sup>1</sup>D) radicals. It should be noted that  
446 also the surface concentrations of CH<sub>4</sub> are fixed in this configuration of the model.

447 2.5.5 *Gas-aerosol partitioning*

448 Gas-aerosol partitioning is calculated using the Equilibrium Simplified Aerosol Model  
449 (EQSAM, Metzger et al., 2002a, 2002b). The scheme has been simplified so that only the



partitioning between  $\text{HNO}_3$  and the nitrate aerosol ( $\text{NO}_3^-$ ) and between  $\text{NH}_3$  and the ammonium aerosol ( $\text{NH}_4^+$ ) is calculated.  $\text{SO}_4^{2-}$  is assumed to remain completely in the aerosol phase because of its very low vapour pressure. The assumptions of the equilibrium model are that (i) aerosols are internally mixed and obey thermodynamic gas/aerosol equilibrium and that (ii) the water activity of an aqueous aerosol particle is equal to the ambient relative humidity (RH). Furthermore, the aerosol water mainly depends on the aerosol mass and the type of the solute, so that parameterizations of single solute molalities and activity coefficients can be defined, depending only on the type of the solute and RH. The advantage of using such parameterizations is that the entire aerosol equilibrium composition can be solved analytically. For atmospheric aerosols in thermodynamic equilibrium with the ambient RH, the following reactions are considered in C-IFS. The subscripts g, s and aq denote gas, solid and aqueous phase, respectively:



## 2.6 Model budget diagnostics

C-IFS computes global diagnostics for every time step to study the contribution of different processes on the global budget. The basic outputs are the total and tropospheric tracer mass, the global integral of the total surface emissions, integrated wet and dry deposition fluxes, chemical conversion as well as elevated atmospheric emissions and the contributions of prescribed upper and lower vertical boundary conditions for  $\text{CH}_4$  and  $\text{HNO}_3$ . A time-invariant pressure-based tropopause definition, which varies with latitude, is used to calculate the tropospheric mass. To monitor the numerical integrity of the scheme, the contributions of the corrections to ensure positiveness and global mass conservation are calculated. Optionally, more detailed diagnostics can be requested that includes photolytic loss and the loss by OH for the tropics and extra-tropics.

A detailed analysis of the global chemistry budget is beyond the scope of this paper. Only a number of key terms for  $\text{CO}$ ,  $\text{O}_3$  and  $\text{CH}_4$  is summarized here. They are compared with values from the “Atmospheric Composition Change: the European Network of Excellence” (ACCENT) model inter-comparisons of chemistry models by Stevenson et al. (2006) for tropospheric  $\text{O}_3$  and by Shindell et al. (2006) for  $\text{CO}$ . A more recent inter-comparison was

481 carried out within the Atmospheric Chemistry and Climate Model Intercomparison Project  
482 (ACCMIP) (Lamarque et al., 2013). The ACCMIP values have been taken from Young et al.  
483 (2013) for tropospheric O<sub>3</sub> and from Voulgarakis et al. (2013) for CH<sub>4</sub>. It should be noted that  
484 the values from these inter-comparison are valid for present-day conditions but not  
485 specifically for 2008. A further source of the differences is the height of the tropopause  
486 assumed in the calculations. Overall, the comparison showed that the C-IFS (CB05) is well  
487 within the range of the multi model ensemble.

488 The annual mean of C-IFS tropospheric O<sub>3</sub> burden was 390 Tg. The values are at the upper  
489 end of the range simulated by the ACCENT ( $344 \pm 39$  Tg) and the ACCMIP ( $337 \pm 23$  Tg)  
490 models. The same holds for the loss by dry deposition, which was 1155 Tg/yr for C-IFS,  $1003 \pm 200$   
491 Tg/yr for ACCENT and in the range 687-1350 Tg/yr for ACCMIP. The tropospheric  
492 chemical O<sub>3</sub> production of C-IFS was 4608 Tg/yr and loss 4144 Tg/yr, which is for both  
493 values at the lower end of the range reported for the production ( $5110 \pm 606$  Tg/yr) and loss  
494 ( $4668 \pm 727$  Tg/yr) for the ACCENT models. The comparatively simple treatment of volatile  
495 organic compounds in CB05 could be an explanation for the low O<sub>3</sub> production and loss  
496 terms. Stratospheric inflow in C-IFS, estimated as the residue from the remaining terms was  
497 691 Tg and the corresponding value from the ACCENT multi-model mean is  $552 \pm 168$  Tg.

498 The annual mean total CO burden in C-IFS was 361 Tg, which is slightly larger than the  
499 ACCENT mean (345 Tg, 248-427 Tg). The total CO emissions in 2008 were 1008 Tg which  
500 is in-line with the number used in ACCENT (1077 Tg/yr) but lower than the estimate (1550  
501 Tg/yr ) of the Third Assessment Report (Prather et al. 2001) of the Intergovernmental Panel  
502 on Climate Change (IPCC), which also takes into account results from inverse modelling  
503 studies. The tropospheric chemical CO production was 1434 Tg/yr, which is very close to the  
504 ACCENT multi-mean of  $1505 \pm 236$  Tg/yr. The chemical CO loss in C-IFS was 2423 Tg  
505 and the loss by dry deposition 24 Tg.

506 The annual mean CH<sub>4</sub> total and tropospheric burdens of C-IFS (CB05) are 4874 and 4271  
507 Tg/yr, respectively. The global chemical CH<sub>4</sub> loss by OH was 467 Tg/yr. Following  
508 Stevenson et al. (2006), this leads to a global CH<sub>4</sub> lifetime estimate of 9.1 yr. This value is  
509 within the ACCMIP range of  $9.8 \pm 1.6$  yr but lower than an observation-based  $11.2 \pm 1.3$  yr  
510 estimate by Prather et al., 2012. CH<sub>4</sub> emissions were substituted by prescribed monthly zonal-  
511 mean surface concentrations to avoid the long-spin up needed by a direct modeling of the CH<sub>4</sub>  
512 surface fluxes. The CH<sub>4</sub> surface concentrations were derived from a latitudinal interpolation

Formatted: Subscript

of observations from the stations South Pole, Cape Grim, Mauna Loa, Mace Head, Barrow and Alert. The resulting CH<sub>4</sub> flux was 488 Tg/yr, which is of similar size as the sum of current estimates of the total CH<sub>4</sub> emissions of 500 - 580 Tg/yr and the loss by soils of 30-40 Tg/yr (Forth Assessment Report by IPCC<  
[http://www.ipcc.ch/publications\\_and\\_data/ar4/wg1/en/ch7s7-4-1.html#ar4top](http://www.ipcc.ch/publications_and_data/ar4/wg1/en/ch7s7-4-1.html#ar4top)).

### **3 Evaluation with observations and comparison with the coupled system IFS-MOZART**

The main motivation for the development of C-IFS is forecasting and assimilation of atmospheric composition as part of the CAMS. Hence, the purpose of this evaluation is to show how C-IFS (CB05) performs relative to the coupled CTM MOZART-3 (Kinnison et al., 2007), which has been running in the coupled system IFS-MOZART in pre-operational mode since 2007. C-IFS will replace the coupled system in the next update of the CAMS system. The evaluation focuses on species which are relevant to global air pollution such as tropospheric O<sub>3</sub>, CO, nitrogen dioxide (NO<sub>2</sub>), SO<sub>2</sub> and formaldehyde (HCHO). The MACC re-analysis (Inness et al., 2013), which is an application of IFS-MOZART with assimilation of observations of atmospheric composition, has been included in the evaluation as a benchmark.

The MACC re-analysis (REAN) and the corresponding MOZART (MOZ) stand-alone run have already been evaluated with observations by Inness et al. (2013). Further, the MACC-II sub-project on validation has compiled a comprehensive report assessing REAN (MACC, 2013). REAN has been further evaluated with surface observations in Europe and North-America for O<sub>3</sub> by Im et al. (2014). C-IFS (CB05) has been already evaluated with a special focus on hydroperoxyl (HO<sub>2</sub>) in relation to CO in Huijnen et al. (2014). The performance of an earlier version of C-IFS (CB05) in the Arctic was evaluated and inter-compared with CTMs of the POLARCAT model intercomparison Project (POLMIP) by Monks et al. (2014) for CO and Arnold et al. (2014) for reactive nitrogen. The POLMIP inter-comparisons show that C-IFS (CB05) performs within the range of state-of-the-art CTMs.

#### **3.1 Summary of model runs setup**

C-IFS (CB05) was run from 1 January to 31 December 2008 with a spin up starting 1 July 2007 at a T255 resolution (80 km x 80 km) with 60 model levels in monthly chunks. The meteorological simulation was relaxed to dynamical fields of the MACC re-analysis (see

section 2.1). Likewise stratospheric O<sub>3</sub> above the tropopause was nudged to the MACC re-analysis.

MOZ is a run with the MOZART CTM at 1.1°×1.1° (120 x 120 km) horizontal resolution using the 60 vertical levels of C-IFS. The setup of the MOZART model and the applied emissions and dry deposition velocities were the same in MOZ and REAN. The most important difference between MOZ and REAN is the assimilation of satellite retrieval of atmospheric composition in REAN. Further, REAN was produced with the coupled system IFS-MOZART whereas MOZ is a stand-alone driven by the meteorological fields of REAN. The latter is equivalent ~~to~~with a simulation of IFS-MOZART without data assimilation of atmospheric composition. The assimilated retrievals were CO and O<sub>3</sub> total columns, stratospheric O<sub>3</sub> profiles and tropospheric NO<sub>2</sub> columns. No observations of atmospheric composition have been feed in to the MOZ run. No observational information has been used to improve the tropospheric simulation of the C-IFS run. Another difference between MOZ and REAN is that the IFS diffusion and convection scheme, as used in C-IFS, controls the vertical transport in REAN whereas MOZART's generic schemes were used in the MOZ run.

MOZ, REAN and C-IFS used the same anthropogenic emissions (MACCity), biogenic emissions (MEGAN 2.1 Guenther et al., 2006, <http://acd.ucar.edu/~guenther/MEGAN/MEGAN.htm>) and natural emissions from the POET project. The biomass burning emissions for MOZ and REAN came from the Global Fire Emission Data version 3 inventory which was redistributed according to Fire Radiative Power observations used in GFAS. Hence, the average biomass burning emissions used by MOZART (MOZ and REAN) agree well with the GFAS emissions used by C-IFS, but they are not identical in temporal and spatial variability.

### 3.2 Observations

The runs (C-IFS, MOZ, REAN) were evaluated with O<sub>3</sub> observations from ozonesondes and O<sub>3</sub> and CO aircraft profiles from the Measurement of Ozone, Water Vapour, Carbon Monoxide and Nitrogen Oxides by Airbus in-service Aircraft (MOZAIC) program. Simulated surface O<sub>3</sub>, CO, NO<sub>2</sub> and SO<sub>2</sub> fields were compared against Global Atmospheric Watch (GAW) surface observations and additionally O<sub>3</sub> against observations from the of the European Monitoring and Evaluation Programme (EMEP) and the European air quality database (AirBase). The global distributions of tropospheric NO<sub>2</sub> and HCHO were evaluated with retrievals of tropospheric columns from Global Ozone Monitoring Experiment 2

(GOME-2). Measurements Of Pollution In The Troposphere (MOPITT) retrievals were used for the validation of the global CO total column fields.

### 3.2.1 In-situ observations

The ozonesondes were obtained from the World Ozone and Ultraviolet Radiation Data Centre (WOUDC) and from the ECWMF Meteorological Archive and Retrieval System. The observation error of the sondes is about  $\pm 5\%$  in the range between 200 and 10 hPa and -7 - 17% below 200 hPa (Beekmann et al., 1994, Komhyr et al., 1995 and Steinbrecht et al., 1996). The number of soundings varied for the different stations. Typically, the sondes are launched once a week but in certain periods such as during O<sub>3</sub> hole conditions soundings are more frequent. Sonde launches were carried out mostly between 9 and 12 hours local time. The global distribution of the launch sites is even enough to allow meaningful averages over larger areas such North-America, Europe, the Tropics, the Arctic and Antarctica. Table 2 contains a list of the ozonesondes used in this study. Tilmes et al. (2012) suggest a further refinement of the North-America region into Canada, Eastern and Western United States as well of the Tropics into Atlantic/Africa, equatorial Americas and Eastern Indian Ocean/Western Pacific based on the inter-comparison of ozone sonde observation for the 1994-2010 period. The results will be discussed also for the sub-regions and figures will be presented in the supplement.

The MOZAIC program (Marengo et al., 1998 and Nédélec et al., 2003) provides profiles of various trace gases taken during commercial aircraft ascents and descents at specific airports. MOZAIC CO data have an accuracy of  $\pm 5$  ppbv, a precision of  $\pm 5\%$ , and a detection limit of 10 ppbv (Nédélec et al., 2003). Since the aircraft carrying the MOZAIC unit were based in Frankfurt, the majority of the CO profiles (837 in 2008) were observed at this airport. A further 10 of the 28 airports with observations in 2008 had a sufficient number of profiles: Windhoek (323), Caracas (129), Hyderabad (125) and London-Gatwick (83) as well as the North-American airports Atlanta (104), Portland (69), Philadelphia (65), Vancouver (56), Toronto (46) and Dallas (43). The North-American airports were considered to be close enough to make a spatial average meaningful. Because of the varying data availability the North-American mean is dominated by the airports in the Eastern United States.

Apart from Frankfurt, typically 2 profiles (takeoff and landing) are taken within 2-3 hours or with a longer gap in the case of an overnight stay. At Frankfurt there were 2-6 profiles available each day, mostly in the morning and the later afternoon to the evening. At the other

Formatted: German (Germany)

airports the typical observation times were 6 & 18 UTC for Windhoek (+/- 0 h local time), 19 and 21 UTC for Hyderabad (+ 4 h local time), 20 and 22 UTC for Caracas (-6 h), 4 and 22 for London (+/- 0 h) and 19 and 22 (- 5/6 h) for the North American airports. This means that most of the observations were taken between the late evening and early morning hours, i.e. at a time of increased stability and large CO vertical gradients close to the surface. Only the observations at Caracas (afternoon) and to some extent in Frankfurt represent a more mixed day-time boundary layer. The modelled column profile was obtained at the middle between start and end time of the profile observation. The model columns were interpolated in time between two subsequent output time steps.

The global atmospheric watch (GAW) program of the World Meteorological Organization is a network for mainly surface based observations (WMO, 2007). The data were retrieved from the World Data Centre for Greenhouse Gases [http://ds.data.jma.go.jp/gmd/wdcgg/]. The GAW observations represent the global background away from the main polluted areas. Often, the GAW observation sites are located on mountains, which makes it necessary to select a model level different from the lowest model level for a sound comparison with the model. In this study the procedure described in Flemming et al. (2009b) is applied to determine the model level, which is based on the difference between a high resolution orography and the actual station height. The data coverage for CO and O<sub>3</sub> was global, whereas for SO<sub>2</sub> and NO<sub>2</sub> only a few observations in Europe were available at the data repository.

The Airbase and EMEP databases host operational air quality observations from different national European networks. All EMEP stations are located in rural areas, while Airbase stations are designed to monitor local pollution. Many AirBase observations may therefore not be representative of a global model with a horizontal resolution of 80 km. However, stations of rural regime may capture the larger scale signal in particular for O<sub>3</sub>, which is spatially well correlated (Flemming et al., 2005). The EMEP observations and the rural Airbase O<sub>3</sub> observations were used for the evaluation over Europe. Only the rural Airbase O<sub>3</sub> observations have been selected for the evaluation of the diurnal cycle.

### 3.2.2 Satellite retrievals

Satellite retrievals of atmospheric composition are more widely used to evaluate model results. Satellite data provide good horizontal coverage but have limitation with respect to the vertical resolution and signal from the lowest atmospheric levels. Further, satellite

Formatted: Subscript

640 observations are only possible at the specific overpass time, and they can be disturbed by the  
641 presence of clouds and surface properties. Depending on the instrument type global coverage  
642 is achieved in several days.

643 Day-time CO total column retrievals from MOPITT, version 6 (Deeter et al., 2013b) and  
644 retrievals of tropospheric columns of NO<sub>2</sub> (IUP-UB v0.7, Richter et al., 2005) and of HCHO  
645 (IUP-UB v1.0; Wittrock et al., 2006) from GOME-2 (Callies et al., 2000) have been used for  
646 the evaluation. The retrievals were averaged to monthly means values to reduce the random  
647 retrieval error.

648 MOPITT is a multispectral thermal infrared (TIR) / near infrared (NIR) instrument onboard  
649 the TERRA satellite with a pixel resolution of 22 km. TERRA's local equatorial crossing time  
650 is approximately 10:30 a.m. The MOPITT CO level 2 pixels were binned within 1x1° within  
651 each month. Deeter et al. (2013a) report a bias of about +0.08e<sup>18</sup> molec/cm<sup>2</sup> and a standard  
652 deviation (SD) of the error of 0.19e<sup>18</sup> molec/cm<sup>2</sup> for the TIR/NIR product version 5. This is  
653 equivalent to a bias of about 4 % and a SD of 10% respectively assuming typical observations  
654 of 2.0 e<sup>18</sup> molec/cm<sup>2</sup>. For the calculation of the simulated CO total column the a-priori profile  
655 in combination with the averaging kernels (AK) of the retrievals were applied. They have the  
656 largest values between 300 and 800 hPa. ~~At surface the sensitivity is reduced even though the~~  
657 ~~combined NIR/TIR product has been used, which has a higher sensitivity than the NIR and~~  
658 ~~TIR only products. The AK have been applied to ensure that the difference between retrieval~~  
659 ~~and AK-weighted model column is independent of the a-priori CO profiles used in the~~  
660 ~~retrieval. Applying the AK makes the difference between retrieval and AK weighted model~~  
661 ~~column independent of the a-priori CO profiles used in the retrieval. On the other hand, it~~  
662 ~~makes the total column calculation dependent on the modelled profile. One should note~~  
663 ~~however, that t~~The AK-weighted column is not equivalent to the modelled atmospheric CO  
664 ~~burden anymore, which needs to be considered for the interpretation of the results.~~

665  
666 GOME-2 is a ultra violet - visible (UV-VIS) and NIR sensor designed to provide global  
667 observations of atmospheric trace gases. GOME-2 flies in a sun-synchronous orbit with an  
668 equator crossing time of 09:30 LT in descending mode and has a footprint of 40 x 80 km.  
669 Here, tropospheric vertical columns of NO<sub>2</sub> and HCHO have been computed using a three  
670 step approach. First, the Differential Optical Absorption Spectroscopy (DOAS; Platt, 1994)  
671 method is applied to measured spectra which yields the total slant column. The DOAS

method is applied in a 425–497 nm wavelength window (Richter et al., 2011) for NO<sub>2</sub>. and between 337 and 353 nm for HCHO (Vrekoussis et al., 2010). Second, the reference sector approach is applied to total slant columns for stratospheric correction. In a last step, tropospheric slant columns are converted to tropospheric vertical columns by applying an air mass factor. Only data with cloud fractions smaller than 0.2 according to the FRESCO cloud data base (Wang et al., 2008) are used here. Furthermore, retrievals are limited to maximum solar zenith angles of 85° for NO<sub>2</sub> and 60° for HCHO. Uncertainties in NO<sub>2</sub> satellite retrievals are large and depend on the region and season. Winter values in mid and high latitudes are usually associated with larger error margins. As a rough estimate, systematic uncertainties in regions with significant pollution are of the order of 20% – 30%. As the HCHO retrieval is performed in the UV part of the spectrum where less light is available and the HCHO absorption signal is smaller than that of NO<sub>2</sub>, the uncertainty of monthly mean HCHO columns is relatively large (20% – 40%) and both noise and systematic offsets have an influence on the results. However, absolute values and seasonality are retrieved more accurately over HCHO hotspots.

For comparison to GOME-2 data, model data are vertically integrated without applying AK to tropospheric vertical columns of NO<sub>2</sub> and HCHO, interpolated to satellite observation time and then sampled to match the location of available cloud free satellite data, which has been gridded to match the model resolution. The resulting daily files are then averaged over months for both satellite and model data to reduce the noise.

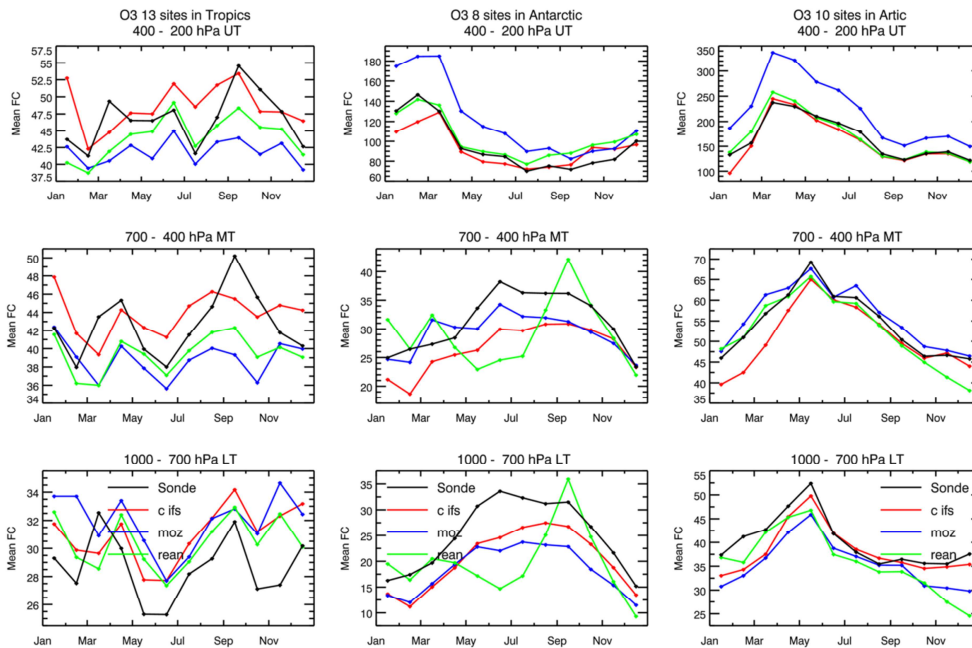
### 3.3 Tropospheric Ozone

Figure 2 shows the monthly means of O<sub>3</sub> volume mixing ratios in the pressure ranges surface to 700 hPa (lower troposphere, LT) 700-400 hPa (middle troposphere, MT) and 400-200 hPa (upper troposphere UT) observed by sondes and averaged over Europe, North

Formatted: Subscript



696 America and East Asia.

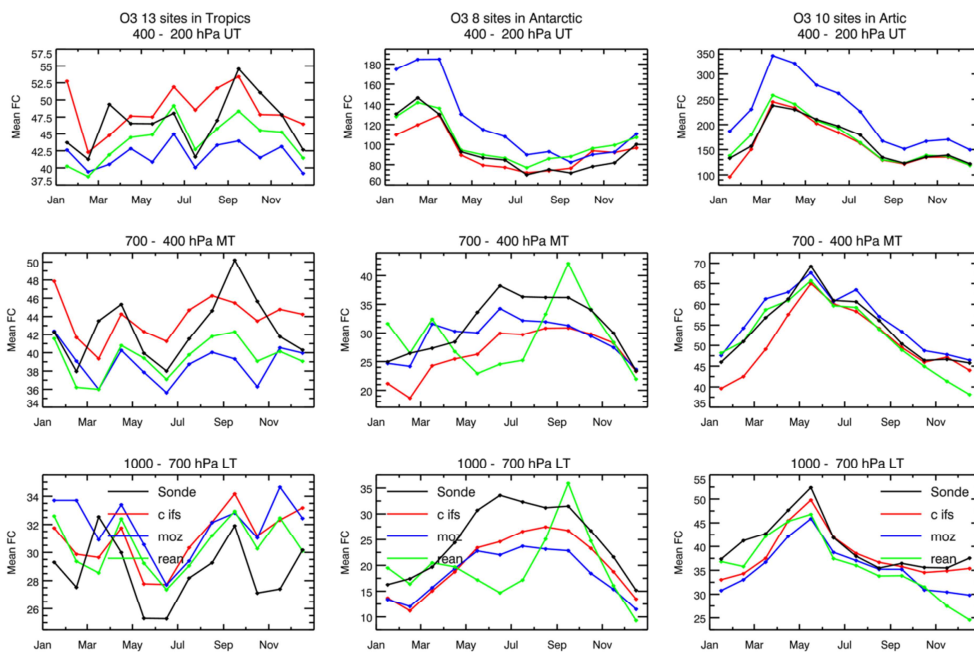


697  
698 Figure 3 shows the same as Figure 2 for the Tropics, Arctic and Antarctica.  
699 A more detailed breakdown of North America (Canada, Eastern and Western United States)  
700 and the Tropics (Atlantic/Africa, equatorial Americas and Eastern Indian Ocean/Western  
701 Pacific) following Times et al. (2012) is presented in the supplement. The observations have a  
702 pronounced spring maximum for UT O<sub>3</sub> over Europe, North America and East Asia and a  
703 more gradually developing maximum in late spring and summer in MT and LT. The LT  
704 seasonal cycle is well re-produced in all runs for the areas of the Northern Hemisphere (NH).  
705 In Europe, REAN tends to overestimate by about 5 ppb where the C-IFS and MOZ have  
706 almost no bias before the annual maximum in May apart from a small negative bias in spring.  
707 Later in the year, C-IFS tends to overestimate in autumn, whereas MOZ overestimates more  
708 in late summer. In MT over Europe C-IFS agrees slightly better with the observations than  
709 MOZ. MOZ overestimates in winter and spring and this overestimation is more prominent in  
710 the UT, where MOZ is biased high throughout the year. This overestimation in UT is highest  
711 in spring, where it can be 25% and more. These findings show that data assimilation in REAN  
712 improved UT O<sub>3</sub> considerably but had only little influence in LT and MT. The overestimation  
713 of MOZ in UT seems to be caused by increased stratospheric O<sub>3</sub> rather than a more efficient  
714 transport as lower stratospheric O<sub>3</sub> was overestimated in MOZ. The good agreement of C-IFS

715 with observation in UT in all three regions is also present in a run without nudging to  
 716 stratospheric O<sub>3</sub>. It is therefore not a consequence of the use of assimilated observations in C-  
 717 IFS (CB05).

718 Over North-America the spring time underestimation by C-IFS and MOZ is more pronounced  
 719 than over Europe. The underestimation occurs in all regions but was largest in early spring  
 720 over Canada. C-IFS also underestimates spring ozone throughout North America in MT. LT  
 721 summer time ozone was overestimated in North America by all models, in particular over the  
 722 Eastern United States. The bias of C-IFS was the smallest in LT but in contrast to MOZ and  
 723 REAN C-IFS underestimates summer time ozone in MT over the Eastern United States. The  
 724 overestimation of UT ozone by MOZ was most pronounced in Canada. C-IFS also  
 725 underestimated MT O<sub>3</sub> observations in this period, whereas MOZ and REAN slightly  
 726 overestimate.

727 In East Asia all runs overestimate by 5-10 ppb in LT and MT especially in autumn and winter.  
 728 In the northern high latitudes (



729 Figure 3 Figure 3) the negative spring bias appears in all runs in LT and only for C-IFS in MT.  
 730 As in the other regions, MOZ greatly overestimates UT O<sub>3</sub>.  
 731

732 | Averaged over the tropics, the annual variability is below 10 ppb with maxima in May and in  
733 | September caused by the dry season in South-America (May) and Africa (September). The  
734 | variability is well reproduced and biases are mostly below 5 ppb in the whole troposphere.  
735 | Note that the 400-200 hPa range (UT) in the tropics is less influenced by the stratosphere  
736 | because of the higher tropopause. C-IFS had smaller biases because of lower values in LT and  
737 | higher values in MT and UT than MOZ. A more detailed analysis for different tropical  
738 | regions shows that the seasonality is well captured by all models over Atlantic-Africa,  
739 | equatorial America and eastern Indian Ocean/Western Pacific in all three tropospheric levels.  
740 | However, the strong observed monthly anomalies (a observation glitch ? by one station) in  
741 | equatorial America in March and September were underestimated by up to 20 ppb in all  
742 | tropospheric levels.

743 | Over the Arctic C-IFS and MOZ reproduce the seasonal cycle, which peaks in late spring, but  
744 | generally underestimate the observations in LT. C-IFS had a smaller bias in LT than MOZ but  
745 | had a larger negative bias in MT. The biggest improvement of C-IFS w.r.t to MOZ occurred  
746 | at the surface in Antarctica as the biases compared to the GAW surface observations were  
747 | greatly reduced. Notably, the assimilation (REAN) led to increased biases for LT and MT O<sub>3</sub>,  
748 | in particular during polar night when UV satellite observations are not available as already  
749 | discussed in Flemming et al. (2011a).

750 | The ability of the models to simulate O<sub>3</sub> near the surface is tested with rural AirBase and  
751 | EMEP stations (see section 3.2).

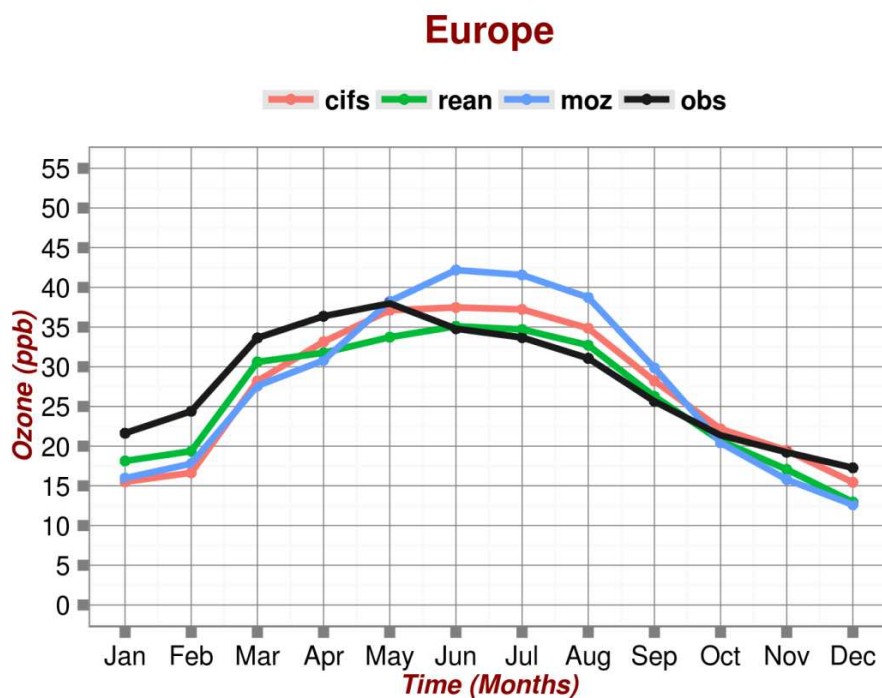


Figure 4 shows monthly means and Figure 5 the average diurnal cycle in different season in Europe. All runs underestimate monthly mean  $O_3$  in spring and winter and overestimate it in late summer and autumn. The overestimation in summer was largest in MOZ. The recently reported (Val Martin et al. 2014) missing coupling of the leaf area index to the leaf and stomatal vegetation resistance in the calculation of dry deposition velocities could be an explanation of the MOZ bias. While the overestimation appeared also with respect to the ozonesondes in LT (see Figure 2, left) the spring time underestimation was less pronounced in LT.

The comparison of the diurnal cycle with observations (Figure 5) shows that C-IFS produced a more realistic diurnal cycle than the MOZART model. The diurnal variability simulated by the MOZART model is much less pronounced than the observations suggest. The diurnal cycle of C-IFS and REAN were similar. This finding can be explained by the fact that C-IFS and REAN use the IFS diffusion scheme whereas MOZART applies the diffusion scheme of the MOZART CTM.

767 The negative bias of C-IFS in winter and spring seems mainly caused by an underestimation  
768 of the night time values whereas the overestimation of the summer and autumn average values  
769 in C-IFS were caused by an overestimation of the day time values. However, the  
770 overestimation of the summer night time values by MOZART seems to be a strong  
771 contribution to the average overestimation in this season.

### 772 3.4 Carbon Monoxide

773 The seasonality of CO is mainly driven by its chemical lifetime, which is lower in summer  
774 because of increased photochemical activity. The seasonal cycle of the CO emissions plays  
775 also an important role in the case of biomass burning and high anthropogenic emissions. The  
776 global distribution of total column CO retrieved from MOPITT and from AK weighted  
777 columns simulated by C-IFS, MOZ and REAN is shown for April 2008 in Figure 6 and for  
778 August in Figure 7. April and August have been selected because they are the months of the  
779 NH CO maximum and minimum. C-IFS reproduced well the [location of the](#) observed global  
780 maxima in North-America, Europe and China as well as the biomass burning signal in Central  
781 Africa. However, there was a widespread underestimation of the MOPITT values in the NH,  
782 which was strongest over European Russia and Northern China. Tropical CO was slightly  
783 overestimated but more strongly over Southeast Asia in April at the end of the biomass  
784 burning season in this region. The lower CO columns in mid- and high latitudes in the  
785 Southern Hemisphere (SH) were underestimated. The same global gradients of the bias were  
786 found in MOZ and REAN. The negative NH bias in April of MOZ is however more  
787 pronounced but the positive bias in the tropics is slightly reduced. The bias of MOZ seems  
788 stronger over the entire land surface in NH and not predominately in the areas with high  
789 emission. This is consistent with the finding of Stein et al. (2014) that dry deposition, besides  
790 underestimated emissions, contributes to the large negative biases in NH in MOZ.  
791 Assimilating MOPITT (V4) in REAN led to much reduced biases everywhere even though  
792 the sign of bias in NH, Tropics and SH remained. In August, the NH bias is reduced but the  
793 hemispheric pattern of the CO bias was similar as in April for all runs. The only regional  
794 exception from the general overestimation in the tropics is the strong underestimation of CO  
795 in the biomass burning maximum in Southern Africa, which points to an underestimation of  
796 the GFAS biomass burning emissions in that area.

797 More insight into the seasonal cycle and the vertical CO distribution can be obtained from  
798 MOZAIC aircraft profiles. CO profiles at Frankfurt (Figure 8, left) provide a continuous

799 record with about 2 - 6 observations per day. As already reported in Inness et al. (2013) and  
800 Stein et al. (2014), MOZ underestimates strongly LT CO with a negative bias of 40 - 60 ppb  
801 throughout the whole year. The highest underestimation occurred in April and May, i.e. at the  
802 time of the observed CO maximum. C-IFS CB05 also underestimates CO but with a smaller  
803 negative bias in the range of 20-40 ppb even though it used the same CO emission data as  
804 MOZ. REAN has the lowest bias throughout the year but the improvement is more important  
805 in winter and early spring. The comparison over London, which is representative for 4 and 22  
806 UTC, leads to similar results as for Frankfurt (Figure 8, middle). ~~The outcome of the~~  
807 ~~comparison with LT CO from MOZAIC is consistent with the model bias with respect to the~~  
808 ~~CAW surface observations in Europe, predominantly located in the Alpine region, shown in~~  
809 ~~Figure 10.~~ The seasonal variability of LT CO from MOZAIC and the model runs in North-  
810 America is very similar to the one in Europe (Figure 8, right). The late winter and spring bias  
811 is slightly increased whereas the summer time bias was lower for all models. The surface bias  
812 in winter and spring of MOZ, C-IFS and REAN is about -50, -40 and -20 ppb respectively. In  
813 the rest of the year REAN and C-IFS have a bias of about -15 ppb whereas the bias of MOZ is  
814 about twice as large.

815 MT CO was very well produced by REAN in Europe and North-America probably because  
816 MOPITT has the highest sensitivity at this level. The MT bias of C-IFS is about 75% of the  
817 bias of MOZ, which underestimates by about 30 ppb. In the UT the CO biases are for all  
818 models mostly below 10ppb, i.e. about 10 %. C-IFS has overall the smallest CO bias whereas  
819 REAN tends to overestimate and MOZ to underestimate CO over Europe and North America.

820 CO observed by MOZAIC over Windhoek (Figure 9, middle) has a pronounced maximum in  
821 September because of the seasonality of biomass burning in this region. Although all runs  
822 show increased CO in this period, the models without assimilation were less able to reproduce  
823 the high observed CO values and are biased low up to 40 ppb in LT and MT. Biases were  
824 much reduced, i.e. mostly within 10 ppb, during the rest of the year. The assimilation in  
825 REAN greatly reduces the bias in the biomass burning period. In UT C-IFS had slightly  
826 smaller biases of about 10 ppb than MOZ and REAN. A less complete record of the seasonal  
827 variability is available for Caracas (Figure 9, left). All models tend to underestimate UT and  
828 MT CO maxima in April by about 20% but in contrast to Windhoek the C-IFS and not REAN  
829 has the smallest bias in LT. Hyderabad (Figure 9, right) is the only observation site where a  
830 substantial overestimation of CO in LT and UT is present even though the observations are in

the range of 150 - 250 ppb, which is mostly higher than at any of the other airports discussed. All models overestimate the seasonality because of an underestimation in JJA and an overestimation during the rest of the year.

The outcome of the comparison with LT CO from MOZAIC is consistent with the model bias with respect to the GAW surface observations in Europe (Figure 10). The winter biases were larger than summer biases and MOZ showed the largest underestimation. -predominantly located in the Alpine region, shown in Figure 10. The GAW stations measuring CO are mostly located on mountains in the Alpine region and typical annual biases were about - 5, - 20 and -35 ppb for REAN, C-IFS and MOZ respectively. The negative biases of stations in flatter terrain such as Kollumerward tended to be larger.

### 3.5 Nitrogen dioxide

The global maxima of NO<sub>2</sub> are located in areas of high anthropogenic and biomass burning NO emissions. The global annual distribution of annual tropospheric columns retrieved from the GOME-2 instrument and simulated by the models is shown in

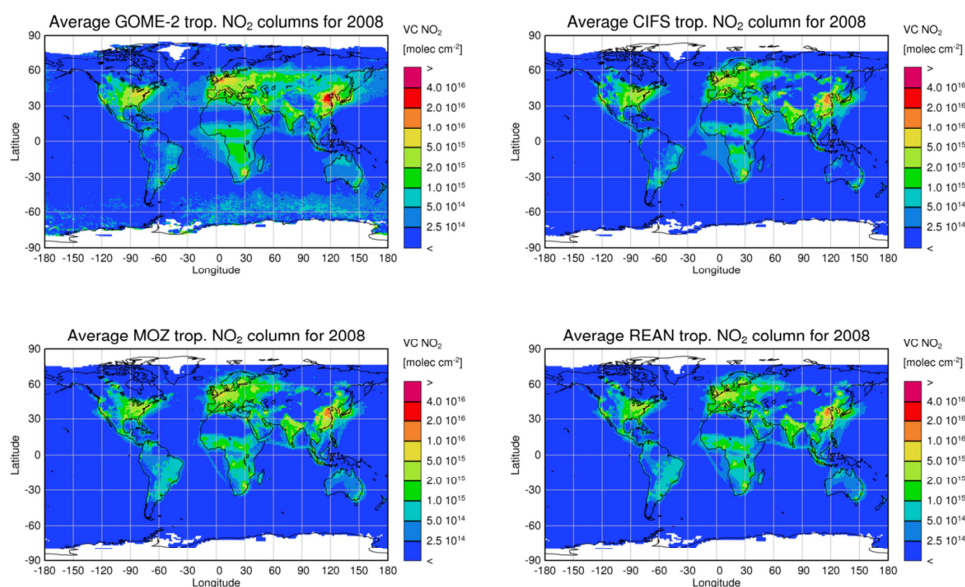


Figure 11Figure 11. C-IFS, MOZ and REAN showed a very similar distribution, which can be explained by that fact that the same NO emission data were used in all runs. The global



patterns of the modelled fields resemble the observed annual patterns to a large extent. But the models tend to underestimate the high observed values in East-Asia and Europe and also simulate too little NO<sub>2</sub> in larger areas of medium observed NO<sub>2</sub> levels in Asia and Central Africa as well as in the outflow areas over the West-Atlantic and West Pacific Ocean. This could mean that NO emissions in the most polluted areas are too low but also that the simulated lifetime of NO<sub>2</sub> is too short. Further, an insufficient simulation of NO<sub>x</sub> reservoir species such as PAN and the lack of alkyl nitrates in CB05 might be the reason for the underestimation.

The validation of the seasonality of NO<sub>2</sub> (

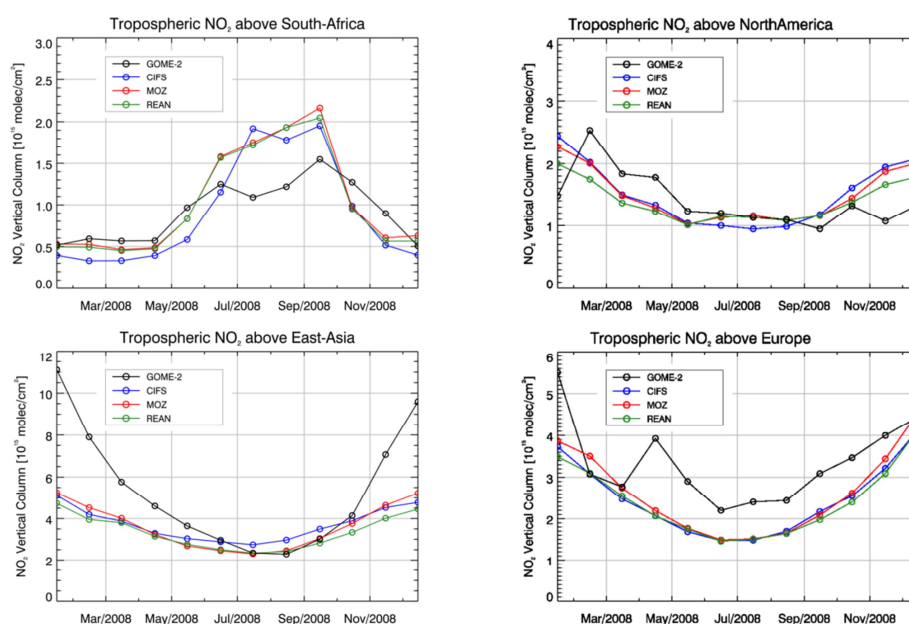


Figure 12) for different regions and months shows that tropospheric NO<sub>2</sub> columns over Europe, North America, South Africa and East-Asia are reasonably reproduced. The models tend to underestimate tropospheric columns over Europe in summer (see Table 2 for area descriptions). However, the evaluation with GAW surface stations mainly from Central and Eastern Europe (

Formatted: Font color: Red

Formatted: Subscript



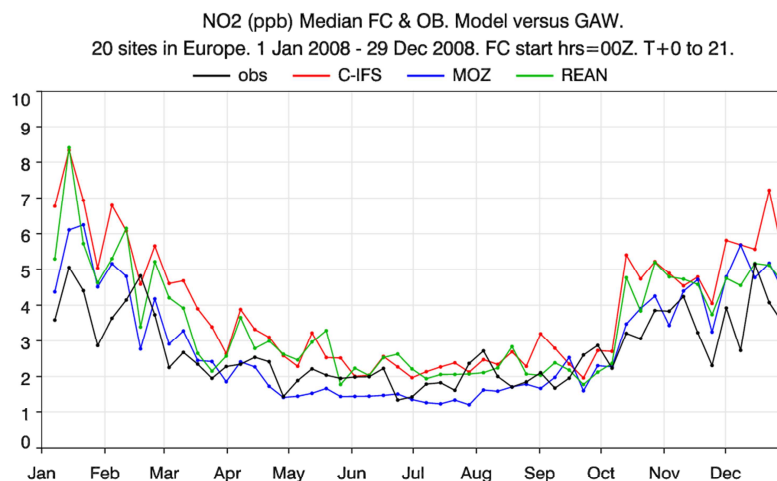
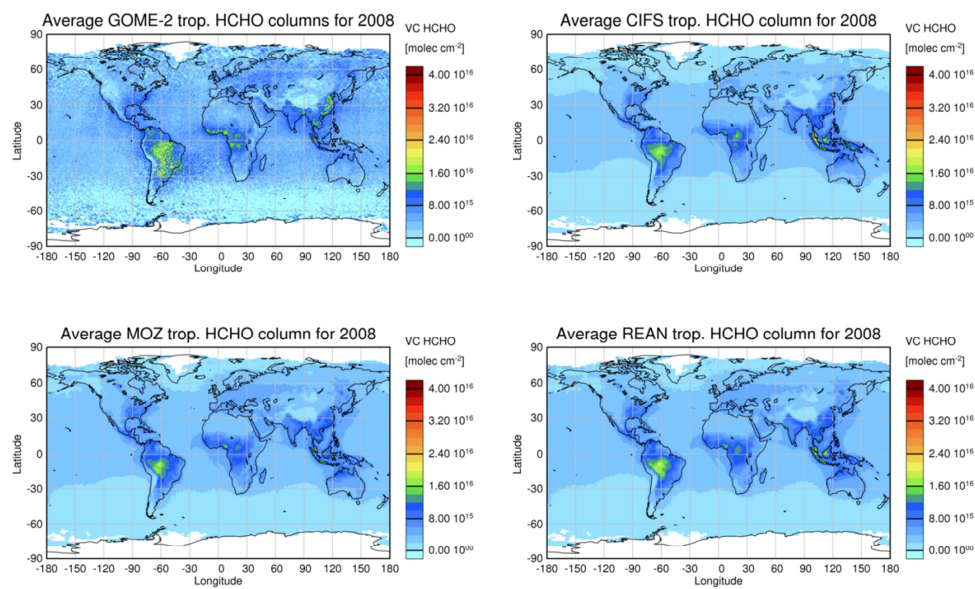


Figure 13 (Figure 13) revealed an overestimation by all models in winter and a small overestimation in summer for REAN and C-IFS. All runs significantly underestimate the annual cycle of the GOME-2 NO<sub>2</sub> tropospheric columns over East-Asia. The winter time values are only half of the observations whereas in summer models agree well with observations. In Southern Africa (20°S/0°S/15°E/15°W), the models overestimate the increased NO<sub>2</sub> values in the biomass burning season by a factor 2 but show good agreement with observations in the rest of the year. The overestimation during biomass burning events could be related to the assumed NO emission factor.

### 3.6 HCHO

On the global scale HCHO is mainly chemically produced by the oxidation of isoprene and CH<sub>4</sub>. Isoprene is emitted by vegetation. On the regional scale HCHO emissions from anthropogenic sources, vegetation and biomass burning also contribute to the HCHO burden.

877 The annual average of tropospheric HCHO retrieved from GOME-2 and from the model runs  
878 is shown in



879  
880 **Figure 14** ~~Figure 14~~. The observations show higher values in the tropics and the NH and  
881 maxima in the rain forest regions of South America and Central Africa and in South East  
882 Asia. The simulated fields of the three runs are very similar. C-IFS, MOZ and REAN  
883 reproduce the observed global patterns but show a small but widespread underestimation in  
884 the NH extra-Tropics and in industrialized East Asia. On the other hand HCHO is  
885 overestimated in Indonesia.

886

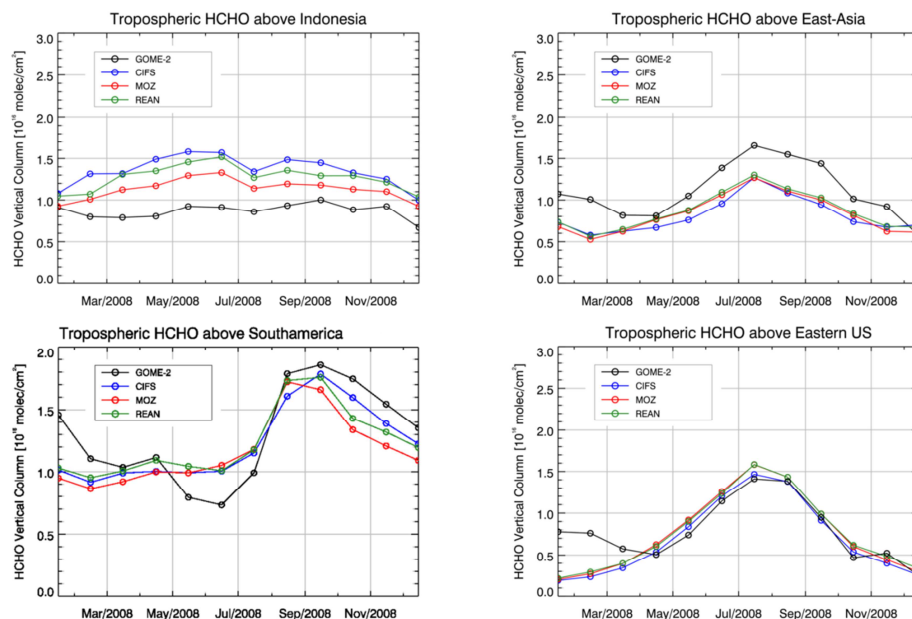
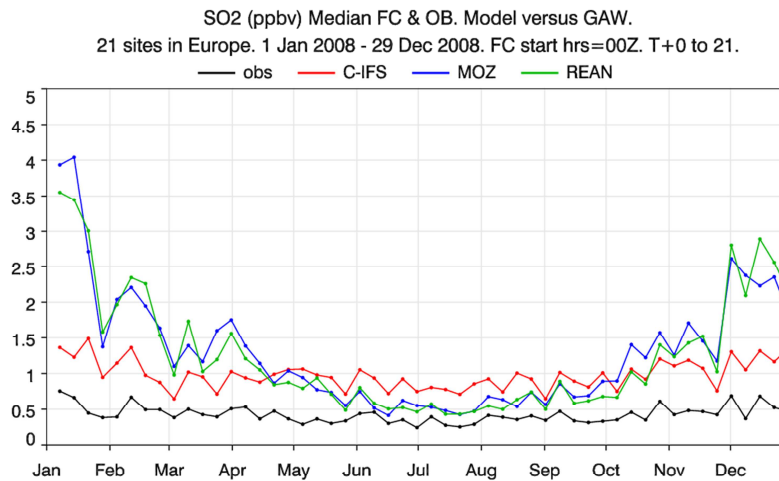


Figure 15 shows model time series of tropospheric HCHO against corresponding GOME-2 satellite retrievals for selected regions. The models underestimated satellite values over East-Asia especially in summer and overestimate HCHO columns for Indonesia (5°S/5°N/100°E/120°E) throughout the year. The seasonality in Southern Africa (not shown) and tropical South America (10°S/5°S/73°W/35°W) is well captured in particular by C-IFS. All models also reproduced the observations rather well for the Eastern United States (30°N/40°N/90°W/75°W), but tend to underestimate wintertime HCHO columns for this region.

### 3.7 Sulfur dioxide

SO<sub>2</sub> was evaluated with available GAW surface observations from Central and Eastern Europe. There were considerable differences in the performance for individual stations often

caused by local effects not resolved by the models. To summarize the evaluation for SO<sub>2</sub>



**Figure 16** Figure 16 shows the median of weekly observed and modelled time series. REAN and MOZ greatly exaggerated the seasonal cycle since the values in winter were up to eight times larger than the median of the observations. The summer values of the two runs were about 50% higher than the observations. C-IFS followed better the weak seasonality of the observations but suffered from a nearly constant bias of about 1 ppb (100%), which was much smaller than the bias of REAN and MOZ in winter but slightly higher in summer. Overall, the on-line integration of C-IFS showed lower SO<sub>2</sub> biases.

As no SO<sub>2</sub> observations were assimilated in REAN and identical SO<sub>2</sub> emission were used, the differences between the runs were caused by differences in the simulation of vertical mixing, sulphur chemistry and wet and dry deposition in C-IFS and MOZART. The winter time bias of REAN and MOZ could be introduced by the diffusion scheme in MOZART.

### 3.8 Computational cost

The computational cost is an important factor for the operational applications in CAMS. The computational cost of different configurations of IFS, C-IFS and IFS-MOZART are given in Table 3. Computational cost is expressed in billing units (BU) of the ECMWF IBM

917 Power 7 super-computer. BUs are proportional to the number of used Central Processing Unit  
918 (CPU) times the simulation time.

919 The increase of cost because of the simulation of the CB05 chemistry with respect to an NWP  
920 run is about a factor 4 at the resolutions T159 (110km), T255 (80 km) and T511 (40 km). C-  
921 IFS (CB05) is about 8 times more efficient than the coupled system IFS-MOZART at a T159  
922 resolution and about 15 times more at a T255 resolution. This strong relative increase in cost  
923 of IFS-MOZART is caused by the increasing memory requirements of the IFS at higher  
924 resolution, or also in data assimilation mode. However, there is insufficient parallelism in  
925 MOZART to exploit the larger number of CPU for speeding up the simulation of the coupled  
926 system. The additional resources allocated to the IFS are however mostly latent as the coupled  
927 MOZART model and the coupler software could not be made faster by using more resources.

928 C-IFS with the MOZART chemical mechanism, i.e. the same chemistry scheme as in IFS-  
929 MOZART, is about 2 times and C-IFS with RACMOBUS 7 times more costly than C-IFS  
930 (CB05) at a T159 resolution. Both the MOZART and the RACMOBUS schemes encompass a  
931 larger number of species and reactions and include a full stratospheric chemistry scheme,  
932 which is missing in CB05. The overhead because of the doubled number of advected species  
933 in C-IFS RACMOBUS and MOZART is however small because of the efficiency of the SL  
934 advection scheme.

#### 935 **4 Summary and outlook**

936 Modules for the simulation of atmospheric chemistry have been implemented on-line in the  
937 Integrated Forecasting System (IFS) of ECMWF. The chemistry scheme complements the  
938 already integrated modules for aerosol and greenhouse gases as part of the IFS for  
939 atmospheric composition (C-IFS). C-IFS for chemistry replaces the coupled system IFS-  
940 MOZART for forecast and assimilation of reactive gases within the pre-operational  
941 Copernicus Atmosphere Monitoring Service.

942 C-IFS applies the chemical mechanism CB05, which describes tropospheric chemistry with  
943 55 species and 126 reactions. C-IFS benefits from the detailed cloud and precipitation physics  
944 of the IFS for the calculation of wet deposition and lightning NO emission. Wet deposition  
945 modelling is based on Jacob (2000) and accounts for the sub-grid scale distribution of clouds  
946 and precipitation. Dry deposition is modelled using pre-calculated monthly-mean dry  
947 deposition velocities following (Wesely, 1989) with a superimposed diurnal cycle. Surface

emissions and dry deposition fluxes are applied as surface boundary conditions of the diffusion scheme. Lightning emissions of NO can be calculated either by cloud height (Price and Rind, 1993) or by convective precipitation (Meijer et al., 2010). The latter parameterization was used in this study. The anthropogenic emissions were taken from the MACCcity inventory and biomass burning emissions from the GFAS data set for 2008.

An evaluation for the troposphere of a simulation in 2008 with C-IFS (CB05) and the MOZART CTM (MOZ) as well as with the MACC re-analysis (REAN) was carried out. The model results were compared against ozonesondes, MOZAIC CO aircraft profiles, European surface observations of O<sub>3</sub>, CO, SO<sub>2</sub> and NO<sub>2</sub> and global satellite retrievals of CO, NO<sub>2</sub> and HCHO. The evaluation showed that C-IFS performs better or with similar accuracy as MOZART and mostly of similar quality as the MACC re-analysis. It should be noted that satellite retrievals of CO, O<sub>3</sub> and NO<sub>2</sub> were assimilated in the MACC re-analysis to improve the realism of the fields simulated by IFS-MOZART.

In comparison to MOZ, C-IFS (CB05) had smaller biases (i) for CO in the Northern Hemisphere, (ii) for O<sub>3</sub> in the upper troposphere and (iii) for winter-time SO<sub>2</sub> at the surface in Europe. Further, the diurnal cycle of surface O<sub>3</sub>, tested with rural European Air quality observations, showed greater realism in the C-IFS simulation. As both models used the same emission data, the improvements can be explained by the differences in the chemical mechanism and the simulation of wet and dry deposition. However, the improvements in SO<sub>2</sub> and the diurnal cycle of O<sub>3</sub> are most probably caused by the more consistent interplay of diffusion and sink and sources processes in the on-line integrated C-IFS.

There is still room for improvement of C-IFS (CB05). It underestimated surface O<sub>3</sub> over Europe and North America in spring and overestimated it in late summer and autumn. CO was still underestimated by C-IFS in particular in Europe and North America throughout the year but more in spring and winter, and in the biomass burning season in Africa. Winter time tropospheric NO<sub>2</sub> over China as retrieved from the GOME-2 instrument was two times higher than the fields modelled by C-IFS, MOZART and the MACC re-analysis.

Although only one chemical mechanism is described in the paper, C-IFS is a model that can apply multiple chemistry schemes. The implementation of the chemistry schemes of the CTMs MOCAGE and MOZART has technically been completed but further optimisation and evaluation is required. Both schemes offer a description of stratospheric chemistry, which is not included in the tropospheric scheme CB05. For this reason it is intended to combine the

CB05 mechanism with the BASCOE stratospheric mechanism. An inter-comparison of the performance of the different chemical mechanism is planned.

It is foreseen to further improve the link between the physics and chemistry packages in IFS. For example, the detailed information from the IFS surface scheme will be utilised for the calculation of dry deposition and biogenic emissions. A first important step is to replace the climatological dry deposition velocities with-online calculated values. Further, the impact of the simulated O<sub>3</sub> fields, once the stratospheric chemistry is fully implemented, on the IFS radiation scheme and the corresponding feedback on the temperature fields will be investigated.

Another ongoing development is to link more closely the greenhouse gas, aerosol and gas-phase chemistry modules of C-IFS. Relevant chemical conversion terms can already be fed to the GLOMAP aerosol (Mann et al, 2010) module for the simulation of secondary aerosols. The calculation of photolysis rates can account for the presence of aerosols, and HO<sub>2</sub> uptake on aerosols can be simulated (Huijnen et al., 2014).

In summary, C-IFS is a new global chemistry weather model for forecast and assimilation of atmospheric composition. C-IFS (CB05) has already been successfully applied in data assimilation mode and a paper on the subject is in preparation (Inness et al., 2014). C-IFS offers improvements over the coupled system IFS-MOZART because (i) it simulates several trace gas C-IFS (CB05)es with better accuracy, (ii) it is computational several times more efficient in particular at high resolution and (iii) it better facilitates the implementation of feedback processes between gas-phase and aerosol processes as well as between atmospheric composition and meteorology.

## Acknowledgments

MACC II is funded by the European Union's Seventh Framework Programme (FP7) under Grant Agreement no. 283576. The MOPITT data were obtained from the NASA Langley Research Atmospheric Science Data Center. We are grateful to the World Ozone and Ultraviolet Radiation Data Centre (WOUDC) for providing ozonesonde observations. We thank the Global Atmospheric Watch programme for the provision of NO<sub>2</sub>, CO and SO<sub>2</sub> surface observations. We thank the European Environmental Agency for providing access to European O<sub>3</sub> observations in the AirBase data base. We also thank the MOZAIC (Measurements of OZone, water vapour, carbon monoxide and nitrogen oxides by in-service

1011 Airbus aircraft) and IAGOS (In-Service Aircraft for a Global Observing System) programmes  
1012 for providing CO profile observations.  
1013



## 1014 **References**

- 1015 Archibald, A. T., Cooke, M. C., Utembe, S. R., Shallcross, D. E., Derwent, R. G., and Jenkin,  
1016 M. E.: Impacts of mechanistic changes on HOx formation and recycling in the oxidation of  
1017 isoprene, *Atmos. Chem. Phys.*, 10, 8097-8118, doi:10.5194/acp-10-8097-2010, 2010.
- 1018 Arnold, S. R., Emmons, L. K., Monks, S. A., Law, K. S., Ridley, D. A., Turquety, S., Tilmes,  
1019 S., Thomas, J. L., Bouarar, I., Flemming, J., Huijnen, V., Mao, J., Duncan, B. N., Steenrod,  
1020 S., Yoshida, Y., Langner, J., and Long, Y.: Biomass burning influence on high latitude  
1021 tropospheric ozone and reactive nitrogen in summer 2008: a multi-model analysis based on  
1022 POLMIP simulations, *Atmos. Chem. Phys. Discuss.*, 14, 24573-24621, doi:10.5194/acpd-14-  
1023 24573-2014, 2014.
- 1024 Atkinson, R., Baulch, D. L., Cox, R. A., Crowley, J. N., Hampson, R. F., Hynes, R. G.,  
1025 Jenkin, M. E., Rossi, M. J. and Troe, J.: Evaluated kinetic and photochemical data for  
1026 atmospheric chemistry: Volume I – gas phase reactions of Ox, HOx, NOx and SOx, species,  
1027 *Atmos. Chem. Phys.*, 4, 1461–1738, doi:10.5194/acp-4-1461-2004, 2004.
- 1028 Atkinson, R., Baulch, D. L., Cox, R. A., Crowley, J. N., Hampson, R. F., Hynes, R. G.,  
1029 Jenkin, M. E., Rossi, M. J., Troe, J., and IUPAC Subcommittee: Evaluated kinetic and  
1030 photochemical data for atmospheric chemistry: Volume II – gas phase reactions of organic  
1031 species, *Atmos. Chem. Phys.*, 6, 3625–4055, doi:10.5194/acp-6-3625-2006, 2006.
- 1032 Baklanov, A., Schlünzen, K., Suppan, P., Baldasano, J., Brunner, D., Aksoyoglu, S.,  
1033 Carmichael, G., Douros, J., Flemming, J., Forkel, R., Galmarini, S., Gauss, M., Grell, G.,  
1034 Hirtl, M., Joffre, S., Jorba, O., Kaas, E., Kaasik, M., Kallos, G., Kong, X., Korsholm, U.,  
1035 Kurganskiy, A., Kushta, J., Lohmann, U., Mahura, A., Manders-Groot, A., Maurizi, A.,  
1036 Moussiopoulos, N., Rao, S. T., Savage, N., Seigneur, C., Sokhi, R. S., Solazzo, E., Solomos,  
1037 S., Sørensen, B., Tsegas, G., Vignati, E., Vogel, B., and Zhang, Y.: Online coupled regional  
1038 meteorology chemistry models in Europe: current status and prospects, *Atmos. Chem. Phys.*,  
1039 14, 317-398, doi:10.5194/acp-14-317-2014, 2014.
- 1040
- 1041 [Banda, N., Krol, M., van Noije, T. , van Weele, M. , Williams, J. E., Le Sager, P. , Niemeier,](#)  
1042 [U., Thomason, L. and Röckmann, T. : The effect of stratospheric sulfur from Mount Pinatubo](#)  
1043 [on tropospheric oxidizing capacity and methane, \*J. Geophys. Res. Atmos.\*, 119,](#)  
1044 [doi:10.1002/2014JD022137, 2014.](#)

1045 |  
1046

1047 Barkley, M., Description of MEGAN biogenic VOC emissions in GEOS-Chem, 2010.  
1048 [http://acmg.seas.harvard.edu/geos/wiki\\_docs/emissions/megan.pdf](http://acmg.seas.harvard.edu/geos/wiki_docs/emissions/megan.pdf)

1049 Bechtold, P., Semane, N., Lopez, P., Chaboureaud, J-P, Beljaars, A., Bormann, N: 2014:  
1050 Representing Equilibrium and Nonequilibrium Convection in Large-Scale Models. *J. Atmos.*  
1051 *Sci.*, 71, 734–753. doi: <http://dx.doi.org/10.1175/JAS-D-13-0163.1>. 2014.

1052 Beekmann M., Ancellet G., Megie G., Smit H. G. J., and Kley D.: Intercomparison campaign  
1053 for vertical ozone profiles including electrochemical sondes of ECC and Brewer-Mast type  
1054 and aground based UV-differential absorption radar, *J. Atmos. Chem.*, 10, 259–288, 1994.

1055 Beljaars, A. and Viterbo, P.: The role of the boundary layer in a numerical weather prediction  
1056 model, in: *Clear and cloudy boundary layers*, A.A.M. Holtslag and P. Duynkerke (eds.),  
1057 Royal Netherlands Academy of Arts and Sciences, p. 287-304, Amsterdam, North Holland  
1058 Publishers, 1998.

1059 Beljaars, A., Bechtold, P., Kohler, M., Morcrette, J-J., Tompkins, A., Viterbo, P. and Wedi,  
1060 N.: The numerics of physical parameterization, Seminar on Recent developments in  
1061 numerical methods for atmospheric and ocean modelling, 6-10 September,  
1062 <http://www.ecmwf.int/publications/library/do/references/>, 2004.

1063 Benedetti, A., Morcrette, J.-J., Boucher, O., Dethof, A., Engelen, R. J., Fisher, M., Flentje, H.,  
1064 Huneus, N., Jones, L., Kaiser, J. W., Kinne, S., Mangold, A., Razinger, M., Simmons, A. J.,  
1065 Suttie, M., and the GEMS-AER team: Aerosol analysis and forecast in the European Centre  
1066 for Medium-Range Weather Forecasts Integrated Forecast System: 2. Data assimilation, *J.*  
1067 *Geophys. Res.*, 114, D13205, doi:10.1029/2008JD011115, 2009.

1068 Bousserez, N., Attié, J.-L., Peuch, V.-H., Michou, M., and Pfister, G.: Evaluation of the  
1069 MOCAGE chemistry and transport model during the ICARTT/ITOP experiment, *J. Geophys.*  
1070 *Res.*, 112, D10S42, doi:10.1029/2006JD007595, 2007.

1071 Callies, J., Corpacicioli, E., Eisinger, M., Hahne, A., and Lefebvre, A.: GOME-2 Metop's  
1072 Second Generation Sensor for Operational Ozone Monitoring, *ESA Bulletin*, 102, 2000.

1073 Cariolle, D. and Deque, M.: Southern hemisphere medium-scale waves and total ozone  
1074 disturbances in a spectral general circulation model, *J. Geophys. Res.*, 91D, 10825–10846,  
1075 1986.

1076 Cariolle, D. and Teyssède, H.: A revised linear ozone photochemistry parameterization for  
1077 use in transport and general circulation models: multi-annual simulations, *Atmos. Chem.*  
1078 *Phys.*, 7, 2183-2196, doi:10.5194/acp-7-2183-2007, 2007.

1079 Carslaw, K. S., Luo, B., Peter, T., and Clegg, S. L.: Vapour pressures of  
1080 H<sub>2</sub>SO<sub>4</sub>/HNO<sub>3</sub>/HBr/H<sub>2</sub>O solutions to low stratospheric temperatures, *Geophys. Res. Lett.*, 22,  
1081 247-250, 1995.

1082 Cecil, D.J., Buechler, D. E., Blakeslee, R. J. : Gridded lightning climatology from TRMM-  
1083 LIS and OTD: Dataset description, *Atmospheric Research*, 135–136, 404-414,  
1084 doi:10.1016/j.atmosres.2012.06.028, 2012.

1085 Chin, M., D. J. Jacob, G. M. Gardner, M. S. Foreman-Fowler, P. A. Spiro, and D. L. Savoie:  
1086 A global three-dimensional model of tropospheric sulfate, *J. Geophys. Res.*, 101, (D13),  
1087 18,667–18,690, 1996

1088 DeCaria, A. J., Pickering, K. E. , Stenchikov, G. L. and Ott, L. E.: Lightning-generated NO<sub>x</sub>  
1089 and its impact on tropospheric ozone production: A three-dimensional modeling study of a  
1090 Stratosphere-Troposphere Experiment: Radiation, Aerosols and Ozone (STERAO-A)  
1091 thunderstorm, *J. Geophys. Res.*, 110, D14303, doi:10.1029/2004JD005556, 2005.

1092 Dee, D.P., Uppala, S.M., Simmons, A.J., Berrisford, P., Poli, P., Kobayashi, S., Andrae, U.,  
1093 Balmaseda, M.A., Balsamo, G., Bauer, P., Bechtold, P., Beljaars, A.C.M., van de Berg, L.,  
1094 Bidlot, J., Bormann, N., Delsol, C., Dragani, R., Fuentes, M., Geer, A.J., Haimberger, L.,  
1095 Healy, S.B., Hersbach, H., Hólm, E.V., Isaksen, I., Kållberg, P., Köhler, M., Matricardi, M.,  
1096 McNally, A.P., Monge-Sanz, B.M., Morcrette, J.-J., Park, B.-K., Peubey, C., de Rosnay, P.,  
1097 Tavolato, C., Thépaut, J.-N., Vitart, F.: The ERA-Interim reanalysis: Configuration and  
1098 performance of the data assimilation system, *Quarterly Journal of the Royal Meteorological*  
1099 *Society*, 2011.

1100 Deeter, M. N., S. Martínez-Alonso, D. P. Edwards, L. K. Emmons, J. C. Gille, H. M. Worden,  
1101 J. V. Pittman, B. C. Daube, and S. C. Wofsy: Validation of MOPITT Version 5 thermal-  
1102 infrared, near-infrared, and multispectral carbon monoxide profile retrievals for 2000–2011, *J.*  
1103 *Geophys. Res. Atmos.*, 118, 6710–6725, doi:10.1002/jgrd.50272, 2013a.

1104 Deeter, M.N., MOPITT Version 6 Product User's Guide, Technical Report, NCAR, Boulder,  
 1105 USA, 2013.137 (656), pp. 553-597, 2013b.

1106 [Dentener, F. J. and Crutzen, P. J.: Reaction of N<sub>2</sub>O<sub>5</sub> on tropospheric aerosols: Impact on the](#)  
 1107 [global distributions of NO<sub>x</sub>, O<sub>3</sub> and OH, J. Geophys. Res., 98\(D4\), 7149–7163, 1993.](#)

1108 Diamantakis, M. and Flemming, J.: Global mass fixer algorithms for conservative tracer  
 1109 transport in the ECMWF model, Geosci. Model Dev., 7, 965-979, doi:10.5194/gmd-7-965-  
 1110 2014, 2014.

1111 Elguindi, N., Clark, H., Ordóñez, C., Thouret, V., Flemming, J., Stein, O., Huijnen, V.,  
 1112 Moinat, P., Inness, A., Peuch, V.-H., Stohl, A., Turquety, S., Athier, G., Cammas, J.-P., and  
 1113 Schultz, M.: Current status of the ability of the GEMS/MACC models to reproduce the  
 1114 tropospheric CO vertical distribution as measured by MOZAIC, Geosci. Model Dev., 3, 501-  
 1115 518, doi:10.5194/gmd-3-501-2010, 2010.

1116 Emmons, L. K., Walters, S., Hess, P. G., Lamarque, J.-F., Pfister, G. G., Fillmore, D.,  
 1117 Granier, C., Guenther, A., Kinnison, D., Laepple, T., Orlando, J., Tie, X., Tyndall, G.,  
 1118 Wiedinmyer, C., Baughcum, S. L., and Kloster, S.: Description and evaluation of the Model  
 1119 for Ozone and Related chemical Tracers, version 4 (MOZART-4), Geosci. Model Dev., 3, 43-  
 1120 67, doi:10.5194/gmd-3-43-2010, 2010.

1121 Emmons, L.K., Arnold, S., Monks, S., Huijnen, V., Tilmes, S., Law, K., Thomas, J.L., Raut,  
 1122 J.-C., Bouarar, I., Turquety, S., Long, Y., Duncan, B., Steenrod, S., Strode, S., Flemming, J.  
 1123 Mao, J., Langner, J., Thompson, A., Tarasick, D., Apel, E., Blake, D., Brune, W., Cohen, R.,  
 1124 Dibb, J., Diskin, G. S., Fried, A., Hall, S., Huey, G., Weinheimer, ennberg, P., Wisthaler, A.,  
 1125 de Gouw, J., Holloway, J., Montzka, S., Nowak, J., Roberts, J. and Ryerson, J.: The  
 1126 POLARCAT Model Intercomparison Project (POLMIP): Overview and evaluation with  
 1127 observations, Atmospheric Chemistry and Physics, to be submitted, 2014.

1128 Engelen, R. J., Serrar, S., and Chevallier, F.: Four-dimensional data assimilation of  
 1129 atmospheric CO<sub>2</sub> using AIRS observations, J. Geophys. Res., 114, D03303,  
 1130 doi:10.1029/2008JD010739, 2009.

1131 Errera, Q., Daerden, F., Chabrilat, S., Lambert, J. C., Lahoz, W. A., Viscardy, S., Bonjean,  
 1132 S., and Fonteyn, D.: 4D-Var assimilation of MIPAS chemical observations: ozone and  
 1133 nitrogen dioxide analyses, Atmos. Chem. Phys., 8, 6169-6187, doi:10.5194/acp-8-6169-2008,  
 1134 2008.

1135 [Evans, M. J., and Jacob, D. J.: Impact of new laboratory studies of N<sub>2</sub>O<sub>5</sub> hydrolysis on global](#)  
 1136 [model budgets of tropospheric nitrogen oxides, ozone, and OH. Geophys. Res. Lett., 32,](#)  
 1137 [L09813, doi:10.1029/2005GL022469, 2005.](#)

1138 ~~Evans, M.J., and Daniel J. J.: Impact of new laboratory studies of N<sub>2</sub>O<sub>5</sub> hydrolysis on global~~  
 1139 ~~model budgets of tropospheric nitrogen oxides, ozone, and OH. Geophysical Research Letters~~  
 1140 ~~32(L09813): 1-4., 2005.~~

1141 Fiore, A.M., Naik, V., Spracklen, D.V., Steiner, A., Unger, N., Prather, M., Bergmann, D.,  
 1142 Cameron-Smith, P.J., Cionni, I., Collins, W.J., Dalsoren, S., Eyring, V., Folberth, G.A.,  
 1143 Ginoux, P., Horowitz, L.W., Josse, B., Lamarque, J.-F., MacKenzie, I.A., Nagashima, T.,  
 1144 O'Connor, F.M., Righi, M., Rumbold, S.T., Shindell, D.T., Skeie, R.B., Sudo, K., Szopa, S.,  
 1145 Takemura, T., Zeng, G., Global air quality and climate, Chemical Society Reviews, 41 (19),  
 1146 pp. 6663-6683, 2012.

1147 Flemming, J., Stern, R., and Yamartino, R. J.: A new air quality regime classification scheme  
 1148 for O<sub>3</sub>, NO<sub>2</sub>, SO<sub>2</sub> and PM<sub>10</sub> observations sites, Atmos. Environ., 39, 6121–6129, 2005

1149 Flemming, J., Inness, A., Flentje, H., Huijnen, V., Moinat, P., Schultz, M. G., and Stein, O.:  
 1150 Coupling global chemistry transport models to ECMWF's integrated forecast system, Geosci.  
 1151 Model Dev., 2, 253-265, doi:10.5194/gmd-2-253-2009, 2009a.

1152 Flemming, J., Inness, A., Flentje, H., Huijnen, V., Moinat, P., Schultz, M. G., and Stein, O.:  
 1153 Coupling global chemistry transport models to ECMWF's integrated forecast system  
 1154 ECMWF technical memorandum 590  
 1155 [[http://old.ecmwf.int/publications/library/ecpublications/\\_pdf/tm/501-600/tm590.pdf](http://old.ecmwf.int/publications/library/ecpublications/_pdf/tm/501-600/tm590.pdf)]  
 1156 tm590.pdf, 2009 b.

1157 Flemming, J., Inness, A., Jones, L., Eskes, H. J., Huijnen, V., Schultz, M. G., Stein, O.,  
 1158 Cariolle, D., Kinnison, D., and Brasseur, G.: Forecasts and assimilation experiments of the  
 1159 Antarctic ozone hole 2008, Atmos. Chem. Phys., 11, 1961–1977, doi:10.5194/acp-11-1961-  
 1160 2011, 2011 a.

1161 Flemming, J. and Huijnen, V.: IFS Tracer Transport Study, MACC Deliverable G-  
 1162 RG 4.2, Tech. rep., ECMWF, [http://www.gmes-atmosphere.eu/documents/deliverables/g-](http://www.gmes-atmosphere.eu/documents/deliverables/g-rg/ifs_transport_study.pdf)  
 1163 [rg/ifs\\_transport\\_study.pdf](http://www.gmes-atmosphere.eu/documents/deliverables/g-rg/ifs_transport_study.pdf), 2011 b.

1164 Flemming, J.; Peuch, V.-H.; Engelen, R.; Kaiser, J.W. A European Global-to-Regional Air  
 1165 Pollution Forecasting System that Combines Modeling with Satellite Observations; EM  
 1166 Magazine of A&WMA, November 2013, pp. 6-10.

1167 [https://www.researchgate.net/publication/259535688\\_A\\_European\\_Global-to-](https://www.researchgate.net/publication/259535688_A_European_Global-to-)  
1168 [Regional\\_Air\\_Pollution\\_Forecasting\\_System\\_that\\_Combines\\_Modeling\\_with\\_Satellite\\_Obse-](https://www.researchgate.net/publication/259535688_A_European_Global-to-)  
1169 [rvations](https://www.researchgate.net/publication/259535688_A_European_Global-to-), 2013

1170 Forbes, R.M., A.M. Tompkins & A. Untch, A new prognostic bulk-microphysics scheme for  
1171 the IFS. ECMWF Tech. Memo. No. 649, 2011.

1172 Fu, Q., Yang, P. and Sun, W. B.: An accurate parametrization of the infrared radiative  
1173 properties of cirrus clouds of climate models. *J. Climate*, 11, 2223–2237, 1998

1174 Gauss, M., Isaksen, I. S. A., Lee, D. S., and Søvde, O. A.: Impact of aircraft NO<sub>x</sub> emissions  
1175 on the atmosphere – tradeoffs to reduce the impact, *Atmos. Chem. Phys.*, 6, 1529-1548,  
1176 doi:10.5194/acp-6-1529-2006, 2006.

1177 Gery, M., Whitten, G. Z., Killus, J. P., and Dodge, M. C.: A photochemical kinetics  
1178 mechanism for urban and regional scale computer modelling, *J. Geophys. Res.*, 94, 18925–  
1179 18956, 1989.

1180 Granier, C., J.F. Lamarque, A. Mieville, J.F. Muller, J. Olivier, J. Orlando, J. Peters, G.  
1181 Petron, G. Tyndall, S. Wallens, POET, a database of surface emissions of ozone precursors,  
1182 available on internet at <http://www.aero.jussieu.fr/projet/ACCENT/POET.php> , 2005.

1183 Granier, C., B. Bessagnet, T. Bond, A. D'Angiola, H.D.v.d. Gon, G.J. Frost, A. Heil, J.W.  
1184 Kaiser, S. Kinne, Z. Klimont, S. Kloster, J.-F. Lamarque, C. Lioussé, T. Masui, F. Meleux, A.  
1185 Mieville, T. Ohara, J.-C. Raut, K. Riahi, M.G. Schultz, S.J. Smith, A. Thomson, J.v.  
1186 Aardenne, G.R.v.d. Werf, and D.P.v. Vuuren, Evolution of anthropogenic and biomass  
1187 burning emissions of air pollutants at global and regional scales during the 1980-2010 period,  
1188 *Climatic Change*, 109(1-2), 163-190, doi:10.1007/s10584-011-0154-1, 2011.

1189 Grell, G. A., Peckham, S. E. , Schmitz, R , McKeen, S. A., Frost, G. J, Skamarock, W. and  
1190 Eder B.: Fully coupled online chemistry within the WRF model, *Atmospheric Environment* ,  
1191 39, 37, 6957-6975, 2005.

1192 Groö, J.-U. and Russell III, J. M.: Technical note: A stratospheric climatology for O<sub>3</sub>, H<sub>2</sub>O,  
1193 CH<sub>4</sub>, NO<sub>x</sub>, HCl and HF derived from HALOE measurements, *Atmos. Chem. Phys.*, 5, 2797–  
1194 2807, doi:10.5194/acp-5-2797-2005, 2005

1195 Guenther, A. B., Karl, T., Harley, P., Wiedinmyer, C., Palmer, P. I., and Geron, C.: Estimates  
1196 of global terrestrial isoprene emissions using MEGAN (Model of Emissions of Gases and

1197 Aerosols from Nature), *Atmos. Chem. Phys.*, 6, 3181–3210, doi:10.5194/acp-6-3181-2006,  
1198 2006.

1199 Haywood, J. M., Roberts, D. L., Slingo, A., Edwards, J. M., and Shine, K. P.: General  
1200 circulation model calculations of the direct radiative forcing by anthropogenic sulfate and  
1201 fossil-fuel soot aerosol, *Journal of Climate*, 10, 1562–1577, 1997.

1202 Hertel, O., Berkowicz, R., Christensen, J. and Hov Ø: Test of two numerical schemes for use  
1203 in atmospheric transport-chemistry models *Atmos. Environ.*, 27A(16), 2591–2611, 1993.

1204 Hollingsworth, A., Engelen, R.J., Textor, C., Benedetti, A., Boucher, O. , Chevallier, F.,  
1205 Dethof, A., Elbern, H., Eskes, H., Flemming, J., Granier, C., Kaiser, J.W. , Morcrette, J.-J.,  
1206 Rayner, P., Peuch, V.H., Rouil, L., Schultz, M.G., Simmons, A.J and The GEMS  
1207 Consortium: Toward a Monitoring and Forecasting System For Atmospheric Composition:  
1208 The GEMS Project. *Bull. Amer. Meteor. Soc.*, 89, 1147-1164, 2008.

1209 Holtslag, A.A. and B. Boville: Local versus nonlocal boundary-layer diffusion in a global  
1210 climate model, *J. Clim.*, 6, 1825-1842, 1993.

1211 Horowitz, L. W., Walters, S., Mauzerall, D. L., Emmons, L. K., Rasch, P. J., Granier, C., Tie,  
1212 X., Lamarque, J.-F., Schultz, M. G., Tyndall, G. S., Orlando, J. J., and Brasseur, G. P.: A  
1213 global simulation of tropospheric ozone and related tracers, Description and Evaluation of  
1214 MOZART version 2, *J. Geophys. Res.*, 108, 4784, doi:10.1029/2002JD002853, 2003.

1215 Hortal, M. and Simmons, A. J.: Use of reduced Gaussian grids in spectral models, *Mon.*  
1216 *Weather Rev.*, 119, 1057-1074, 1991.

1217 Hortal, M.: The development and testing of a new two-time-level semi-Lagrangian scheme  
1218 (SETTLS) in the ECMWF forecast model, 128, 1671–1687, DOI: 10.1002/qj.200212858314,  
1219 2002.

1220 Houweling, S., Dentener, F. J., and Lelieveld, J.: The impact of nonmethane hydrocarbon  
1221 compounds on tropospheric photochemistry, *J. Geophys. Res.*, 103(D9), 10673–10696, 1998.

1222 Huijnen, V., Williams, J., van Weele, M., van Noije, T., Krol, M., Dentener, F., Segers, A.,  
1223 Houweling, S., Peters, W., de Laat, J., Boersma, F., Bergamaschi, P., van Velthoven, P., Le  
1224 Sager, P., Eskes, H., Alkemade, F., Scheele, R., Nédélec, P., and Pätz, H.-W.: The global  
1225 chemistry transport model TM5: description and evaluation of the tropospheric chemistry  
1226 version 3.0, *Geosci. Model Dev.*, 3, 445-473, doi:10.5194/gmd-3-445-2010.

1227 Huijnen, V., Flemming, J., Kaiser, J. W., Inness, A., Leitão, J., Heil, A., Eskes, H. J., Schultz,  
 1228 M. G., Benedetti, A., Hadji-Lazaro, J., Dufour, G., and Eremenko, M.: Hindcast experiments  
 1229 of tropospheric composition during the summer 2010 fires over western Russia, *Atmos.*  
 1230 *Chem. Phys.*, 12, 4341-4364, doi:10.5194/acp-12-4341-2012, 2012.

1231 Huijnen, V., Williams, J. E., and Flemming, J.: Modeling global impacts of heterogeneous  
 1232 loss of HO<sub>2</sub> on cloud droplets, ice particles and aerosols, *Atmos. Chem. Phys. Discuss.*, 14,  
 1233 8575-8632, doi:10.5194/acpd-14-8575-2014, 2014.

1234 Im, U., Bianconi, R., Solazzo, E., Kioutsioukis, I., Badia, A., Balzarini, A., Baró, R., Bellasio,  
 1235 R., Brunner, D., Chemel, C., Curci, G., Flemming, J., Forkel, R., Giordano, L., Jiménez-  
 1236 Guerrero, P., Hirtl, M., Hodzic, A., Honzak, L., Jorba, O., Knote, C., Kuenen, J.J.P., Makar,  
 1237 P.A., Manders-Groot, A., Neal, L., Pérez, J.L., Pirovano, G., Pouliot, G., San Jose, R.,  
 1238 Savage, N., Schroder, W., Sokhi, R.S., Syrakov, D., Torian, A., Tuccella, P., Werhahn, J.,  
 1239 Wolke, R., Yahya, K., Zabkar, R., Zhang, Y., Zhang, J., Hogrefe, C., Galmarini, S.:  
 1240 Evaluation of operational on-line-coupled regional air quality models over Europe and North  
 1241 America in the context of AQMEII phase 2. Part I: Ozone, *Atmospheric Environment*, doi:  
 1242 10.1016/j.atmosenv.2014.09.042, 2014.

1243 Inness, A., Baier, F., Benedetti, A., Bouarar, I., Chabrilat, S., Clark, H., Clerbaux, C.,  
 1244 Coheur, P., Engelen, R. J., Errera, Q., Flemming, J., George, M., Granier, C., Hadji-Lazaro,  
 1245 J., Huijnen, V., Hurtmans, D., Jones, L., Kaiser, J. W., Kapsomenakis, J., Lefever, K., Leitão,  
 1246 J., Razinger, M., Richter, A., Schultz, M. G., Simmons, A. J., Suttie, M., Stein, O., Thépaut,  
 1247 J.-N., Thouret, V., Vrekoussis, M., Zerefos, C., and the MACC team: The MACC reanalysis:  
 1248 an 8 yr data set of atmospheric composition, *Atmos. Chem. Phys.*, 13, 4073-4109,  
 1249 doi:10.5194/acp-13-4073-2013, 2013.

1250 Inness, A., Blechschmidt, A., Bouarar, I., Chabrilat, S., Crepulja, M., Engelen, R. J., Errera,  
 1251 Q., Flemming, J., Gaudel, A., Huijnen, V., Jones, L., Kapsomenakis, J., Keppens A.,  
 1252 Lambert, J.-C., Langerock, B., Peuch, V.H., Razinger, M., Richter, A., Schultz, M. G., Suttie,  
 1253 M., Thouret, V., Vrekoussis, M., Wagner, A. and Zerefos, C.: Data assimilation experiments  
 1254 of satellite retrievals of O<sub>3</sub>, CO and NO<sub>2</sub> with Composition IFS, in preparation for Geosci.  
 1255 Model Dev, 2014.

1256 Jacob, D.J. H. Liu, C.Mari, and R.M. Yantosca, Harvard wet deposition scheme for GMI,  
 1257 Harvard University Atmospheric Chemistry Modeling Group, revised March 2000.  
 1258 [http://acmg.seas.harvard.edu/geos/wiki\\_docs/deposition/wetdep.jacob\\_etal\\_2000.pdf](http://acmg.seas.harvard.edu/geos/wiki_docs/deposition/wetdep.jacob_etal_2000.pdf)



1259 Jakob, C. and Klein, S.: A parameterization of the effects of cloud and precipitation overlap  
1260 for use in general-circulation models, *Q. J. Roy. Meteor. Soc.*, 126, 2525–2544, 2000.

1261 Jung, T., T. N. Palmer, M. J. Rodwell, and S. Serrar, 2008: Diagnosing forecast error using  
1262 relaxation experiments. ECMWF Newsletter 82, ECMWF, Shinfield Park, Reading, Berkshire  
1263 RG2 9AX, UK.

1264 Kaiser, J. W., Heil, A., Andreae, M. O., Benedetti, A., Chubarova, N., Jones, L., Morcrette,  
1265 J.-J., Razinger, M., Schultz, M. G., Suttie, M., and van der Werf, G. R.: Biomass burning  
1266 emissions estimated with a global fire assimilation system based on observed fire radiative  
1267 power, *Biogeosciences*, 9, 527-554, doi:10.5194/bg-9-527-2012, 2012.

1268 Kaminski, J. W., Neary, L., Struzewska, J., McConnell, J. C., Lupu, A., Jarosz, J., Toyota, K.,  
1269 Gong, S. L., Côté, J., Liu, X., Chance, K., and Richter, A.: GEM-AQ, an on-line global  
1270 multiscale chemical weather modelling system: model description and evaluation of gas phase  
1271 chemistry processes, *Atmos. Chem. Phys.*, 8, 3255-3281, 2008.

1272 Kinnison, D. E., Brasseur, G. P., Walters, S. , Garcia, R. R., Marsh, D. R , Sassi, F., Harvey,  
1273 V. L., Randall, C. E., Emmons, L., Lamarque, J. F., Hess, P. , Orlando, J. J., Tie, X. X. ,  
1274 Randel, W. , Pan, L. L., Gettelman, A. , Granier, C., Diehl, T., Niemeier, U. and Simmons, A.  
1275 J.: Sensitivity of Chemical Tracers to Meteorological Parameters in the MOZART-3  
1276 Chemical Transport Model. *J. Geophys. Res.*, 112, D03303, doi:10.1029/2008JD010739, 2007.

1277 Komhyr, W. D., Barnes, R. A., Borthers, G. B., Lathrop, J. A., Kerr, J. B., and Opperman, D.  
1278 P.: Electrochemical concentration cell ozonesonde performance evaluation during STOIC  
1279 1989, *J. Geophys. Res.*, 100, 9231–9244, 1995

1280 Lamarque, J.-F., Emmons, L. K., Hess, P. G., Kinnison, D. E., Tilmes, S., Vitt, F., Heald, C.  
1281 L., Holland, E. A., Lauritzen, P. H., Neu, J., Orlando, J. J., Rasch, P. J., and Tyndall, G. K.:  
1282 CAM-chem: description and evaluation of interactive atmospheric chemistry in the  
1283 Community Earth System Model, *Geosci. Model Dev.*, 5, 369-411, doi:10.5194/gmd-5-369-  
1284 2012, 2012.

1285 Lamarque, J.-F., Shindell, D. T., Josse, B., Young, P. J., Cionni, I., Eyring, V., Bergmann, D.,  
1286 Cameron-Smith, P., Collins, W. J., Doherty, R., Dalsoren, S., Faluvegi, G., Folberth, G.,  
1287 Ghan, S. J., Horowitz, L. W., Lee, Y. H., MacKenzie, I. A., Nagashima, T., Naik, V.,  
1288 Plummer, D., Righi, M., Rumbold, S. T., Schulz, M., Skeie, R. B., Stevenson, D. S., Strode,  
1289 S., Sudo, K., Szopa, S., Voulgarakis, A., and Zeng, G.: The Atmospheric Chemistry and

1290 Climate Model Intercomparison Project (ACCMIP): overview and description of models,  
 1291 simulations and climate diagnostics, *Geosci. Model Dev.*, 6, 179-206, doi:10.5194/gmd-6-  
 1292 179-2013, 2013.

1293 Landgraf, J. and Crutzen, P. J.: An efficient method for online calculations of photolysis and  
 1294 heating rates, *J. Atmos. Sci.*, 55, 863–878, 1998.

1295 Lawrence, M.G. and Crutzen, P. J.: The impact of cloud particle gravitational settling on  
 1296 soluble trace gas distributions. *Tellus B*, 50: 263–289. doi: 10.1034/j.1600-0889.1998.

1297 Lefever, K., van der A, R., Baier, F., Christophe, Y., Errera, Q., Eskes, H., Flemming, J.,  
 1298 Inness, A., Jones, L., Lambert, J.-C., Langerock, B., Schultz, M. G., Stein, O., Wagner, A.,  
 1299 and Chabrillat, S.: Copernicus atmospheric service for stratospheric ozone: validation and  
 1300 intercomparison of four near real-time analyses, 2009–2012, *Atmos. Chem. Phys. Discuss.*,  
 1301 14, 12461-12523, doi:10.5194/acpd-14-12461-2014, 2014.

1302 Levine, S. Z. and Schwartz, S. E.: In-cloud and below-cloud scavenging of nitric acid vapor.  
 1303 *Atmos. Environ.* doi:10.1016/0004-6981(82)90266-9, 1982.

1304 Lin, J.-T., McElroy, M. B., and Boersma, K. F.: Constraint of anthropogenic NO<sub>x</sub> emissions  
 1305 in China from different sectors: a new methodology using multiple satellite retrievals, *Atmos.*  
 1306 *Chem. Phys.*, 10, 63-78, doi:10.5194/acp-10-63-2010, 2010.

1307 Liu, H., Jacob, D.J., Bey, I., Yantosca, R.M., 2001. Constraints from <sup>210</sup>Pb and <sup>7</sup>Be on wet  
 1308 deposition and transport in a global three-dimensional chemical tracer model driven by  
 1309 assimilated meteorological fields. *Journal of Geophysical Research* 106, 12109e12128.

1310 McGregor, J. L.: C-CAM Geometric Aspects and Dynamical Formulation, Tech. Rep. 70,  
 1311 CSIRO Atmospheric Research, Aspendale, Victoria, 2005.

1312 MACC VAL report, Validation report of the MACC reanalysis of global atmospheric  
 1313 composition Period, 2003-  
 1314 2011.[http://www.copernicusatmosphere.eu/documents/maccii/deliverables/val/MACCII\\_VAL](http://www.copernicusatmosphere.eu/documents/maccii/deliverables/val/MACCII_VAL_DEL_D_83.4_REAreport02_20130207.pdf)  
 1315 [L\\_DEL\\_D\\_83.4\\_REAreport02\\_20130207.pdf](http://www.copernicusatmosphere.eu/documents/maccii/deliverables/val/MACCII_VAL_DEL_D_83.4_REAreport02_20130207.pdf), 2013

1316 Mann, G. W., Carslaw, K. S., Spracklen, D. V., Ridley, D. A., Manktelow, P. T.,  
 1317 Chipperfield, M. P., Pickering, S. J., and Johnson, C. E.: Description and evaluation of  
 1318 GLOMAP-mode: a modal global aerosol microphysics model for the UKCA composition-

1319 climate model, *Geosci. Model Dev.*, 3, 519-551, doi:10.5194/gmd-3-519-2010, 20103-651-  
1320 2010, 2010.

1321 Marengo, A., Thouret, V., Nédélec, P., Smit, H. G., Helten, M., Kley, D., Karcher, F., Simon,  
1322 P., Law, K., Pyle, J., Poschmann, G., Von Wrede, R., Hume, C., and Cook, T.: Measurement  
1323 of ozone and water vapour by Airbus in-service air-craft: The MOZAIC airborne programme,  
1324 an overview, *J. Geophys. Res.*, 103, 25631–25642, 1998.

1325 Mari, C., Jacob, D. J., and Bechtold, P.: Transport and scavenging of soluble gases in a deep  
1326 convective cloud, *J. Geophys. Res.*, 105, 22 255-22 267, 2000.

1327 Matsumi, Y., Comes, F. J., Hancock, G., Hofzumahus, A., Hynes, A. J., Kawasaki, M., and  
1328 Ravishankara, A. R.: Quantum yields for the production of O(1D) in the ultraviolet photolysis  
1329 of ozone: recommendation based on evaluation of laboratory data, *J. Geophys. Res.*, 107,  
1330 4024, doi:10.1029/2001JD000510, 2002.

1331 Meijer, E.W., P. F. J. van Velthoven, D. W. Brunner, H. Huntrieser and H. Kelder:  
1332 Improvement and evaluation of the parameterization of nitrogen oxide production by  
1333 lightning, *Physics and Chemistry of the Earth, Part C, Volume 26, Issue 8, Pages 577-583*,  
1334 2001.

1335 Ménard , R. et al. ,Coupled chemical-dynamical data assimilation, Final Report, ESA/ESTEC.  
1336 2007.

1337 Metzger, S., F. Dentener, S. Pandis, and J. Lelieveld, Gas/aerosol partitioning, 1, A  
1338 computationally efficient model, *J. Geophys. Res.*, 107(D16), doi:10.1029/2001JD001102,  
1339 2002a.

1340 Metzger, S., Dentener, F., Krol, M. C., Jeuken, A., and Lelieveld, J.: Gas/aerosol partitioning  
1341 2. Global modeling results, *J. Geophys. Res.*, 107(D16), 4313, doi:10.1029/2001JD001103,  
1342 2002b.

1343 Michou M., P. Laville, D. Serça, A. Fotiadis, P. Bouchou and V.-H. Peuch, Measured and  
1344 modeled dry deposition velocities over the ESCOMPTE area, *Atmos. Res.*, 74 (1-4), 89-116,  
1345 2004.

1346 Monks, S. A., Arnold, S. R., Emmons, L. K., Law, K. S., Turquety, S., Duncan, B. N.,  
1347 Flemming, J., Huijnen, V., Tilmes, S., Langner, J., Mao, J., Long, Y., Thomas, J. L.,  
1348 Steenrod, S. D., Raut, J. C., Wilson, C., Chipperfield, M. P., Schlager, H., and Ancellet, G.:

1349 Multi-model study of chemical and physical controls on transport of anthropogenic and  
 1350 biomass burning pollution to the Arctic, *Atmos. Chem. Phys. Discuss.*, 14, 25281-25350,  
 1351 doi:10.5194/acpd-14-25281-2014, 2014.

1352 Morcrette, J.-J., Boucher, O., Jones, L., Salmond, D. , Bechtold, P., Beljaars, A., Benedetti,  
 1353 A., Bonet, A., Kaiser, J. W., Razinger, M., Schulz, M. , Serrar, S. , Simmons, A. J., Sofiev,  
 1354 M., Suttie, M., Tompkins, A. M. and Untch, A.: Aerosol analysis and forecast in the ECMWF  
 1355 Integrated Forecast System. Part I: Forward modelling, *J. Geophys. Res.*, 2009.

1356 Morgenstern, O., Braesicke, P., O'Connor, F. M., Bushell, A. C., Johnson, C. E., Osprey, S.  
 1357 M., and Pyle, J. A.: Evaluation of the new UKCA climate-composition model – Part 1: The  
 1358 stratosphere, *Geosci. Model Dev.*, 2, 43–57, doi:10.5194/gmd-2-43-2009, 2009.

1359 Nedelec, P., Cammas, J.-P., Thouret, V., Athier, G., Cousin, J.-M., Legrand, C., Abonnel, C.,  
 1360 Lecoeur, F., Cayez, G., and Marizy, C.: An improved infrared carbon monoxide analyser for  
 1361 routine measurements aboard commercial Airbus aircraft: technical validation and first  
 1362 scientific results of the MOZAIC III programme, *Atmos. Chem. Phys.*, 3, 1551–1564,  
 1363 doi:10.5194/acp-3-1551-2003, 2003.

1364 Neu, J. L. and Prather, M. J.: Toward a more physical representation of precipitation  
 1365 scavenging in global chemistry models: cloud overlap and ice physics and their impact on  
 1366 tropospheric ozone, *Atmos. Chem. Phys.*, 12, 3289-3310, doi:10.5194/acp-12-3289-2012,  
 1367 2012.

1368 O'Connor, F. M., Johnson, C. E., Morgenstern, O., Abraham, N. L., Braesicke, P., Dalvi, M.,  
 1369 Folberth, G. A., Sanderson, M. G., Telford, P. J., Voulgarakis, A., Young, P. J., Zeng, G.,  
 1370 Collins, W. J., and Pyle, J. A.: Evaluation of the new UKCA climate-composition model –  
 1371 Part 2: The Troposphere, *Geosci. Model Dev.*, 7, 41-91, doi:10.5194/gmd-7-41-2014, 2014.

1372 Olivier J., J. Peters, C. Granier, G. Petron, J.F. Muller, and S. Wallens: Present and future  
 1373 surface emissions of atmospheric compounds, POET report #2, EU project EVK2-1999-  
 1374 00011, 2003

1375 Ordóñez, C., Elguindi, N., Stein, O., Huijnen, V., Flemming, J., Inness, A., Flentje, H.,  
 1376 Katragkou, E., Moinat, P., Peuch, V.-H., Segers, A., Thouret, V., Athier, G., van Weele, M.,  
 1377 Zerefos, C. S., Cammas, J.-P., and Schultz, M. G.: Global model simulations of air pollution  
 1378 during the 2003 European heat wave, *Atmos. Chem. Phys.*, 10, 789-815, doi:10.5194/acp-10-  
 1379 789-2010, 2010.

1380 Ott, L. E., K. E. Pickering, G. L. Stenchikov, D. J. Allen, A. J. DeCaria, B. Ridley, R.-F. Lin,  
 1381 S. Lang, and W.-K. Tao (2010), Production of lightning NO<sub>x</sub> and its vertical distribution  
 1382 calculated from three-dimensional cloud-scale chemical transport model simulations, *J.*  
 1383 *Geophys. Res.*, 115, D04301, doi:10.1029/2009JD011880.

1384 Pickering, K. E., Y. Wang, W.-K. Tao, C. Price, and J.-F. Müller: Vertical distributions of  
 1385 lightning NO<sub>x</sub> for use in regional and global chemical transport models, *J. Geophys. Res.*,  
 1386 103, 31,203 – 31,216, doi:10.1029/98JD0265. 1998.

1387 Pozzoli L., Bey, I., Rast, J. S., Schultz, M. G., Stier, P., and Feichter, J.: Trace gas and aerosol  
 1388 interactions in the fully coupled model of aerosol-chemistry-climate ECHAM5-HAMMOZ,  
 1389 PART I: Model description and insights from the spring 2001 TRACE-P experiment, *J.*  
 1390 *Geophys. Res.*, 113 , 2008.

1391 Prather, M., Ehhalt, D., et al.: Atmospheric chemistry and greenhouse gases, in: *Climate*  
 1392 *Change 2001: The Scientific Basis*, edited by: Houghton, J. T., Ding, Y., Griggs, D. J., et al.,  
 1393 239–287, Cambridge University Press, Cambridge, UK, 2001.

1394 Prather, M. J., Holmes, C. D., and Hsu, J.: Reactive greenhouse gas scenarios: Systematic  
 1395 exploration of uncertainties and the role of atmospheric chemistry, *Geophys. Res. Lett.*, 39,  
 1396 L09803,doi:10.1029/2012GL051440, 2012.

1397 Price, C., and Rind, D.: A simple lightning parameterization for calculating global lightning  
 1398 distributions, *J. Geophys. Res.*, 97, 9919-9933, 1992.

1399 Price, C., and Rind, D.: What determinest he cloud-to-ground fraction in thunderstorms?  
 1400 *Geophys Res. Lett.*, 20, 463-466, 1993.

1401 Price, C., J. Penner, and M. Prather: NO<sub>x</sub> from lightning 1. Global distributions based on  
 1402 lightning physics, *J. Geophys. Res.*, 102, 5929–5941, doi:10.1029/96JD03504, 1997.

1403 Rast, S., Schultz, M.G. , Bey, I., van Noije, T. , Aghedo, A.M. , Brasseur, G.P., Diehl, T.,  
 1404 Esch, M., Ganzeveld, L., Kirchner, I., Kornblueh, L., Rhodin, A. , Röckner, E. , Schmidt, H. ,  
 1405 Schröder, S., Schulzweida, U., Stier, P., Thomas, K., Walters, S.: Evaluation of the  
 1406 tropospheric chemistry general circulation model ECHAM5–MOZ and its application to the  
 1407 analysis of the chemical composition of the troposphere with an emphasis on the late RETRO  
 1408 period 1990–2000, *Reports on Earth-System Science*, 114, Max-Planck Institut fuer  
 1409 Meteorologie, Hamburg, 2014.

1410 Redler, R., Valcke, S. and Ritzdorf, H.: OASIS4 - A Coupling Software for Next Generation  
 1411 Earth System Modelling, *Geoscience Model Development*, 3, 87 - 104, DOI:10.5194/gmd-3-  
 1412 87-2010.

1413 Richter, A., Burrows, J. P., Nüß, H., Granier, C., Niemeier, U., Increase in tropospheric  
 1414 nitrogen dioxide over China observed from space, *Nature*, 437, 129-132, doi:  
 1415 10.1038/nature04092, 2005.

1416 Sander, R., Compilation of Henry's Law Constants for Inorganic and Organic Species of  
 1417 Potential Importance in Environmental Chemistry, MPI for Chemistry Mainz, Germany,  
 1418 1999, <http://www.henrys-law.org/henry.pdf>

1419 Sander, S. P., Friedl, R. R., Golden, D. M., Kurylo, M. J., Moortgat, G. K., Keller-Rudek, H.,  
 1420 Wine, P. H., Ravishankara, A. R., Kolb, C. E., Molina, M. J., Finlayson-Pitts, B. J., Huie, R.  
 1421 E., and Orkin, V. L.: Chemical Kinetics and Photochemical Data for Use in Atmospheric  
 1422 Studies, Evaluation Number 15, JPL Publication 06-02, Jet Propulsion Laboratory, Pasadena,  
 1423 Calif., 2006.

1424 Sander, S. P., Abbatt, J. R., Burkholder, J. B., Friedl, R. R., Golden, D. M., Huie, R. E., Kolb,  
 1425 C. E., Kurylo, G., Moortgat, K., Orkin, V. L. and Wine, P. H.: Chemical kinetics and  
 1426 Photochemical Data for Use in Atmospheric studies, Evaluation No.17, JPL Publication 10-6,  
 1427 Jet Propulsion Laboratory, Pasadena, 2011.

1428 Savage, N. H., Agnew, P., Davis, L. S., Ordóñez, C., Thorpe, R., Johnson, C. E., O'Connor, F.  
 1429 M., and Dalvi, M.: Air quality modelling using the Met Office Unified Model (AQUUM OS24-  
 1430 26): model description and initial evaluation, *Geosci. Model Dev.*, 6, 353-372,  
 1431 doi:10.5194/gmd-6-353-2013, 2013.

1432 Schumann, U., and H. Huntrieser: The global lightning-induced nitrogen oxides source,  
 1433 *Atmos. Chem. Phys.*, 7, 3823–3907, 2007.

1434 Seinfeld J. H. and Pandis S. N., *Atmospheric Chemistry and Physics: From Air Pollution to*  
 1435 *Climate Change*, 1st edition, J. Wiley, New York, 1998.

1436 Shindell, D.T., G. Faluvegi, D.S. Stevenson, M.C. Krol, L.K. Emmons, J.-F. Lamarque, G.  
 1437 Pétron, F.J. Dentener, K. Ellingsen, M.G. Schultz, O. Wild, M. Amann, C.S. Atherton, D.J.  
 1438 Bergmann, I. Bey, T. Butler, J. Cofala, W.J. Collins, R.G. Derwent, R.M. Doherty, J. Drevet,  
 1439 H.J. Eskes, A.M. Fiore, M. Gauss, D.A. Hauglustaine, L.W. Horowitz, I.S.A. Isaksen, M.G.  
 1440 Lawrence, V. Montanaro, J.-F. Müller, G. Pitari, M.J. Prather, J.A. Pyle, S. Rast, J.M.

1441 Rodriguez, M.G. Sanderson, N.H. Savage, S.E. Strahan, K. Sudo, S. Szopa, N. Unger, T.P.C.  
 1442 van Noije, and G. Zeng: Multi-model simulations of carbon monoxide: Comparison with  
 1443 observations and projected near-future changes. *J. Geophys. Res.*, 111, D19306,  
 1444 doi:10.1029/2006JD007100, 2006.

1445 Slingo, A.: A GCM parameterization for the shortwave radiative properties of water clouds. *J.*  
 1446 *Atmos. Sci.*, 46, 1419–1427, 1989.

1447 Smithson, P. A., IPCC, 2001: climate change 2001: the scientific basis. Contribution of  
 1448 Working Group 1 to the Third Assessment Report of the Intergovernmental Panel on Climate  
 1449 Change, edited by J. T. Houghton, Y. Ding, D. J. Griggs, M. Noguer, P. J. van der Linden, X.  
 1450 Dai, K. Maskell and C. A. Johnson (eds). Cambridge University Press, Cambridge, UK, and  
 1451 New York, USA, *Int. J. Climatol.*, 22: 1144. doi: 10.1002/joc.763, 2002.

1452 Steil, B., Dameris, M., Brühl, C., Crutzen, P. J., Grewe, V., Ponater, M., and Sausen, R.:  
 1453 Development of a chemistry module for GCMs: first results of a multiannual integration,  
 1454 *Ann. Geophys.*, 16, 205-228, doi:10.1007/s00585-998-0205-8, 1998.

1455 Stein, O., Flemming, J., Inness, A., Kaiser, J.W., Schultz, M.G. , Global reactive gases  
 1456 forecasts and reanalysis in the MACC project, *Journal of Integrative Environmental Sciences*,  
 1457 9, Iss. sup1, 57-70, doi:10.1080/1943815X.2012.696545, 2012.

1458 Stein, O., Schultz, M. G., Bouarar, I., Clark, H., Huijnen, V., Gaudel, A., George, M., and  
 1459 Clerbaux, C.: On the wintertime low bias of Northern Hemisphere carbon monoxide in global  
 1460 model studies, *Atmos. Chem. Phys. Discuss.*, 14, 245-301, doi:10.5194/acpd-14-245-2014,  
 1461 2014.

1462 Steinbrecht, W., Shwartz, R., and Claude, H.: New pump correction for the Brewer-Mast  
 1463 ozonesonde: Determination from experiment and instrument intercomparisons, *J. Atmos.*  
 1464 *Ocean. Tech.*15, 144–156, 1998.

1465 Stevenson, D. S., et al. (2006), Multimodel ensemble simulations of present-day and near-  
 1466 future tropospheric ozone, *J. Geophys. Res.*, 111, D08301, doi:10.1029/2005JD006338.

1467 Temperton, C., Hortal, M. and Simmons, A.: A two-time-level semi-Lagrangian global  
 1468 spectral model, *QJR*, 127, 111-127, 2001.

1469 Tiedtke, M. A: comprehensive mass flux scheme for cumulus parameterization in large-scale  
 1470 models. *Mon. Weather. Rev.*, 117(8):1779-1800, 1989.

1471 [Tilmes, S., Lamarque, J.-F., Emmons, L. K., Conley, A., Schultz, M. G., Saunois, M.,](#)  
 1472 [Thouret, V., Thompson, A. M., Oltmans, S. J., Johnson, B., and Tarasick, D.: Technical Note:](#)  
 1473 [Ozonesonde climatology between 1995 and 2011: description, evaluation and applications,](#)  
 1474 [Atmos. Chem. Phys., 12, 7475-7497, doi:10.5194/acp-12-7475-2012, 2012.](#)

1475 Wesely, M.L.: Parameterization of Surface Resistances to Gaseous Dry Deposition in  
 1476 Regional-Scale Numerical Models. Atmos. Environ., 23, 1293-1304, 1989.

1477 ~~[von Blohn, N., Diehl, K., Mitra, S. K., and Borrmann, S.: Wind tunnel experiments on the](#)~~  
 1478 ~~[retention of trace gases during riming: nitric acid, hydrochloric acid, and hydrogen peroxide,](#)~~  
 1479 ~~[Atmos. Chem. Phys., 11, 11569-11579, doi:10.5194/acp-11-11569-2011, 2011.](#)~~ [Val Martin,](#)  
 1480 [M., Heald, C. L. and Arnold, S. R.: Coupling dry deposition to vegetation phenology in the](#)  
 1481 [Community Earth System Model: Implications for the simulation of surface O<sub>3</sub>,](#)  
 1482 [Geophys. Res. Lett., 41, 2988-2996, doi:10.1002/2014GL059651., 2014](#)

1483 van Noije, T. P. C., Le Sager, P., Segers, A. J., van Velthoven, P. F. J., Krol, M. C.,  
 1484 Hazeleger, W., Williams, A. G., and Chambers, S. D.: Simulation of tropospheric chemistry  
 1485 and aerosols with the climate model EC-Earth, Geosci. Model Dev., 7, 2435-2475,  
 1486 doi:10.5194/gmd-7-2435-2014, 2014.

1487 ~~[von Blohn, N., Diehl, K., Mitra, S. K., and Borrmann, S.: Wind tunnel experiments on the](#)~~  
 1488 ~~[retention of trace gases during riming: nitric acid, hydrochloric acid, and hydrogen peroxide,](#)~~  
 1489 ~~[Atmos. Chem. Phys., 11, 11569-11579, doi:10.5194/acp-11-11569-2011, 2011.](#)~~

1490

1491 Voulgarakis, A., Naik, V., Lamarque, J.-F., Shindell, D. T., Young, P. J., Prather, M. J., Wild,  
 1492 O., Field, R. D., Bergmann, D., Cameron-Smith, P., Cionni, I., Collins, W. J., Dalsøren, S. B.,  
 1493 Doherty, R. M., Eyring, V., Faluvegi, G., Folberth, G. A., Horowitz, L. W., Josse, B.,  
 1494 MacKenzie, I. A., Nagashima, T., Plummer, D. A., Righi, M., Rumbold, S. T., Stevenson, D.  
 1495 S., Strode, S. A., Sudo, K., Szopa, S., and Zeng, G.: Analysis of present day and future OH  
 1496 and methane lifetime in the ACCMIP simulations, Atmos. Chem. Phys., 13, 2563-2587,  
 1497 doi:10.5194/acp-13-2563-2013, 2013.

1498 [Vrekoussis, M., Wittrock, F., Richter, A., and Burrows, J. P.: GOME-2 observations of](#)  
 1499 [oxygenated VOCs: what can we learn from the ratio glyoxal to formaldehyde on a global](#)  
 1500 [scale?, Atmos. Chem. Phys., 10, 10145-10160, doi:10.5194/acp-10-10145-2010, 2010.](#)

1501 Williams, J. E., Strunk, A., Huijnen, V., and van Weele, M.: The application of the Modified  
 1502 Band Approach for the calculation of on-line photodissociation rate constants in TM5:



1503 implications for oxidative capacity, *Geosci. Model Dev.*, 5, 15-35, doi:10.5194/gmd-5-15-  
1504 2012, 2012.

1505 Williams, J. E., van Velthoven, P. F. J., and Brenninkmeijer, C. A. M.: Quantifying the  
1506 uncertainty in simulating global tropospheric composition due to the variability in global  
1507 emission estimates of Biogenic Volatile Organic 2857-2013, 2013.

1508 Wittrock, F., A. Richter, H. Oetjen, J. P. Burrows, M. Kanakidou, S. Myriokefalitakis, R.  
1509 Volkamer, S. Beirle, U. Platt, and T. Wagner, Simultaneous global observations of glyoxal  
1510 and formaldehyde from space, *Geophys. Res. Lett.*, 33, L16804, doi:10.1029/2006GL026310,  
1511 2006Compounds, *Atmos. Chem. Phys.*, 13, 2857-2891, doi:10.5194/acp-13-2857-2013, 2013.

1512 Yarwood, G., Rao, S., Yocke, M., and Whitten, G.: Updates to the carbon bond chemical  
1513 mechanism: CB05. Final report to the US EPA, EPA Report Number: RT-0400675, available  
1514 at: [www.camx.com](http://www.camx.com), last access: 1 July 2014, 2005.

1515 WMO (2007), WMO Global Atmosphere Watch (GAW) Strategic Plan: 2008 – 2015. World  
1516 Meteorological Organization, Geneva, Switzerland, 2007.

1517 Young, P. J., Archibald, A. T., Bowman, K. W., Lamarque, J.-F., Naik, V., Stevenson, D. S.,  
1518 Tilmes, S., Voulgarakis, A., Wild, O., Bergmann, D., Cameron-Smith, P., Cionni, I., Collins,  
1519 W. J., Dalsøren, S. B., Doherty, R. M., Eyring, V., Faluvegi, G., Horowitz, L. W., Josse, B.,  
1520 Lee, Y. H., MacKenzie, I. A., Nagashima, T., Plummer, D. A., Righi, M., Rumbold, S. T.,  
1521 Skeie, R. B., Shindell, D. T., Strode, S. A., Sudo, K., Szopa, S., and Zeng, G.: Pre-industrial  
1522 to end 21st century projections of tropospheric ozone from the Atmospheric Chemistry and  
1523 Climate Model Intercomparison Project (ACCMIP), *Atmos. Chem. Phys.*, 13, 2063-2090,  
1524 doi:10.5194/acp-13-2063-2013, 2013.

1525 Zaveri, R. A. and Peters, L. K.: A new lumped structure photochemical mechanism for large-  
1526 scale applications, *J. Geophys. Res.*, 104, 30387–30415, doi:10.1029/1999JD900876, 1999.

1527 Zdunkowski, W. G., Welsch, R. M., and Kord, G. J.: An investigation of the structure of  
1528 typical 2-stream methods for the calculation of solar fluxes and heating rates in clouds,  
1529 *Contrib. Atmos. Phys.*, 53, 215–238, 1980.

1530 Zhang, L., Brook, J. R., and Vet, R.: A revised parameterization for gaseous dry deposition in  
1531 air-quality models, *Atmos. Chem. Phys.*, 3, 2067-2082, doi:10.5194/acp-3-2067-2003, 2003.

1532 Zhang, Y.: On-line coupled meteorology and chemistry models: history, current status, and  
1533 outlook, *Atmos. Chem. Phys.*, 8, 2895-2032, 2008.

1534 [Zhang, Y., Karamchandani, P., Glotfelty, T., Streets, D. G., Grell, G., Nenes, A., Yu, F. and](#)  
1535 [Bennartz, R.: Development and initial application of the global-through-urban weather](#)

1536 | [research and forecasting model with chemistry \(GU-WRF/Chem\), J. Geophys. Res., 117,](#)  
1537 [D20206, doi:10.1029/2012JD017966, 2012.](#)

1538 Table 1 Annual emissions from anthropogenic, biogenic and natural sources and biomass  
 1539 burning for 2008 in Tg for a C-IFS (CB05) run at T255 resolution. Anthropogenic NO  
 1540 emissions contain a contribution of 1.8 Tg aircraft emissions and 12.3 Tg (5.7 Tg N) lightning  
 1541 emissions (LiNO) is added in the biomass burning columns.

| Species                           | Anthropogenic | Biogenic<br>natural | and Biomass burning |
|-----------------------------------|---------------|---------------------|---------------------|
| CO                                | 584           | 96                  | 328                 |
| NO                                | 70 + 1.8      | 10                  | 9.2 + 12.3 (LiNO)   |
| HCHO                              | 3.4           | 4.0                 | 4.9                 |
| CH <sub>3</sub> OH                | 2.2           | 159                 | 8.5                 |
| C <sub>2</sub> H <sub>6</sub>     | 3.4           | 1.1                 | 2.3                 |
| C <sub>2</sub> H <sub>5</sub> OH  | 3.1           | 0                   | 0                   |
| C <sub>2</sub> H <sub>4</sub>     | 7.7           | 18                  | 4.3                 |
| C <sub>3</sub> H <sub>8</sub>     | 4.0           | 1.3                 | 1.2                 |
| C <sub>3</sub> H <sub>6</sub>     | 3.5           | 7.6                 | 2.5                 |
| Parafins (Tg C)                   | 31            | 18                  | 1.7                 |
| Olefines (Tg C)                   | 2.4           | 0                   | 0.7                 |
| Aldehydes (Tg C)                  | 1.1           | 6.1                 | 2.1                 |
| CH <sub>3</sub> COCH <sub>3</sub> | 1.3           | 28                  | 2.4                 |
| Isoprene                          | 0             | 523                 | 0                   |
| Terpenes                          | 0             | 97                  | 0                   |
| SO <sub>2</sub>                   | 98            | 9                   | 2.2                 |
| DMS                               | 0             | 38                  | 0.2                 |
| NH <sub>3</sub>                   | 40            | 11                  | 6.2                 |

1542

1543

1544 Table 2 Ozone sondes sites used in the evaluation for different regions

| Region         | Area S/W/N/E          | Stations (Number of observations)  |
|----------------|-----------------------|--|
| Europe         | 35°N/20°W/60°N/40°E   | Barajas (52), DeBilt (57), Hohenpeissenberg (126), Legionowo (48), Lindenberg (52), Observatoire de Haute-Provence (46), Payerne (158), Prague (49), Uccle (142 ) and Valentia Observatory (49)                  |
| North America: | 30°N/135°W/60°N/60°W  | Boulder (65), Bratts Lake (61), Churchill (61), Egbert (29), Goose Bay (47), Kelowna (72), Stony Plain (77), Wallops (51), Yarmouth (60), Narragansett (7) and Trinidad Head (35)                                |
| Arctic:        | 60°N/180°W/90°N/180°E | Alert (52), Eureka (83), Keflavik (8), Lerwick (49), Ny-Aalesund (77), Resolute (63), Scoresbysund (54), Sodankyla (63), Summit (81) and Thule(15)   |
| Tropics        | 20°S/180°W/20°N/180°E | Alajuela (47), Ascension Island (32), Hilo (47), Kuala Lumpur (24), Nairobi (39), Natal (48), Paramaribo (35), Poona (13), Samoa (33), San Cristobal (28), Suva (28), Thiruvananthapuram (12) and Watukosek (19) |
| East Asia      | 15°N/100°E/45°N/142°E | Hong Kong Observatory (49), Naha (37), Sapporo (42) and Tateno Tsukuba (49)  |
| Antarctic      | 90°S/180°W/60°S/180°E | Davis (24), Dumont d'Urville (38), Maitri (9), Marambio (66), Neumayer (72), South Pole (63), Syowa( 41) and McMurdo (18)  |

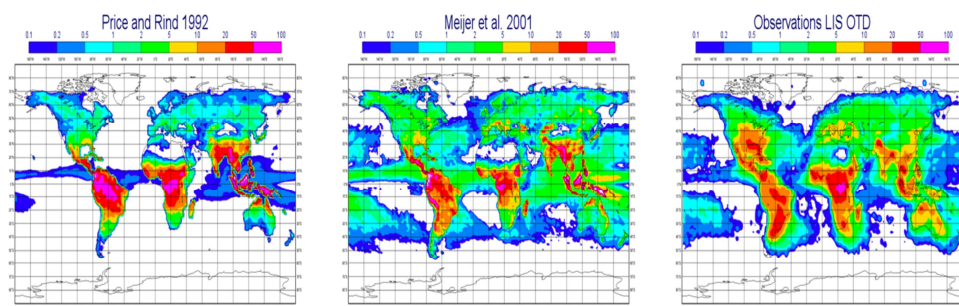
1545

1546 Table 3 Computational cost (BU) of a 24 h forecasts of different horizontal model resolutions  
1547 (60 levels) and chemistry schemes of C-IFS, IFS-MOZART and IFS, \*not fully optimised.

| Resolution | IFS-MOZART | C-IFS<br>(MOZART)* | C-IFS<br>(MOCAGE)* | C-IFS<br>(CB05) | IFS |
|------------|------------|--------------------|--------------------|-----------------|-----|
| T159       | 205        | 56                 | 147                | 20              | 6   |
| T255       | 1200       | -                  | -                  | 55              | 12  |
| T511       | -          | -                  | -                  | 700             | 125 |

1548

1549



1550  
 1551 Figure 1 Flash density in flashes/(km<sup>2</sup> yr) from the IFS input data using the parameterization  
 1552 by Price and Rind (1992) (left), Meijer et al. (2001) (middle) and observations from the LIS  
 1553 OTD data base (right). All fields were scaled to an annual flash density of 46 fl/s.  
 1554

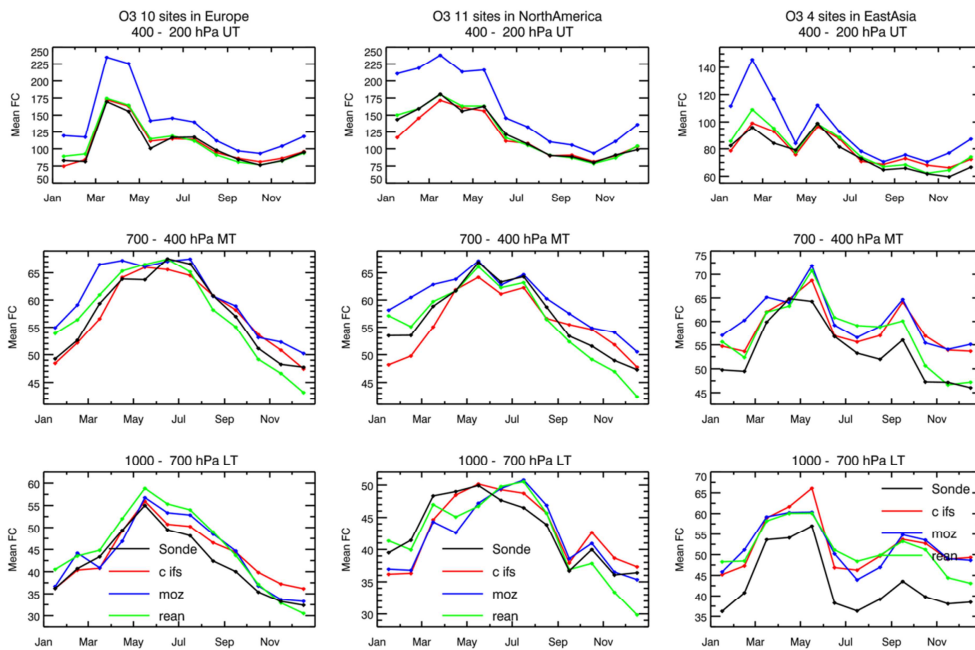


Figure 2 Tropospheric ozone volume mixing ratios (ppb) over Europe (left) and North-  
 America (middle) and East Asia (right) averaged in the pressure range 1000-700 hPa  
 (bottom), 700-400 hPa (middle) and 400-200 hPa (top) observed by ozonesondes (black) and  
 simulated by C-IFS (red), MOZ (blue) and REAN (green) in 2008.

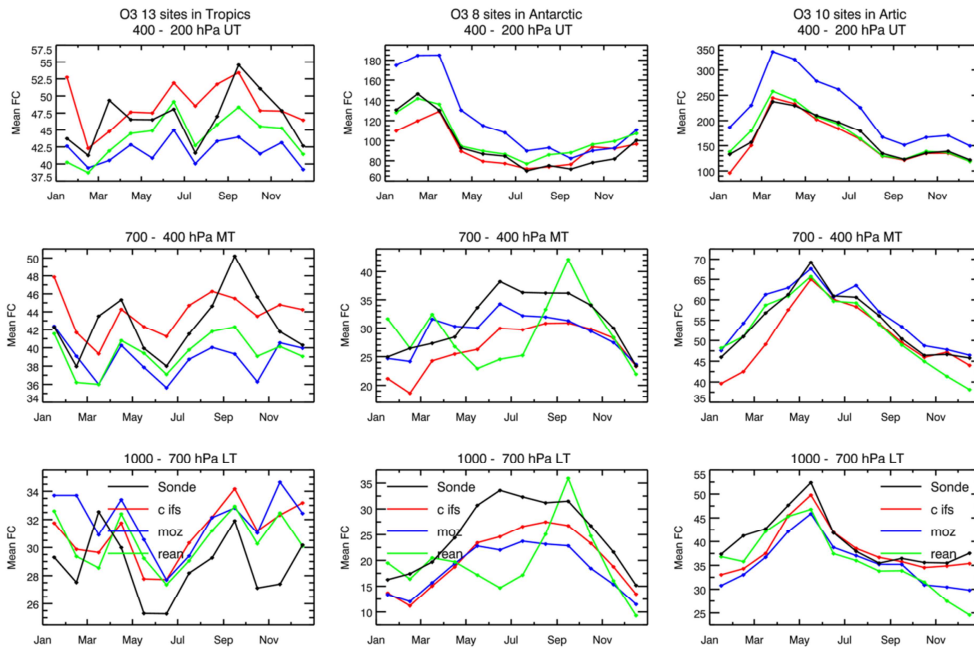
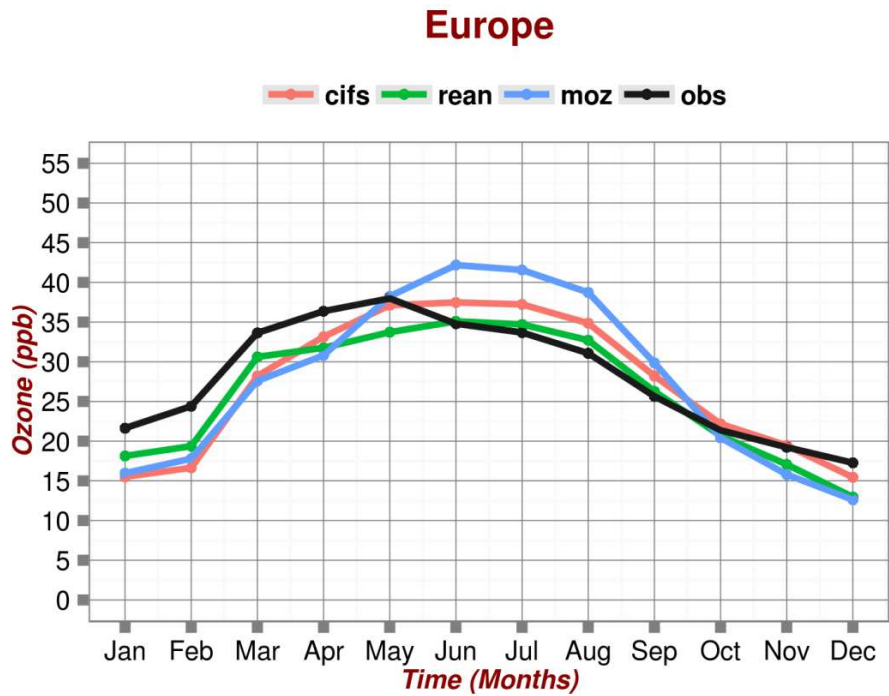


Figure 3 Tropospheric ozone volume mixing ratios (ppb) over the Tropics (left) Antarctica ~~Arctic~~ (middle) and Arctic ~~Antarctica~~ (right) averaged in the pressure bands 1000-700 hPa (bottom), 700-400 hPa (middle) and 400-200 hPa (top) observed by ozonesondes and simulated by C-IFS (red), MOZ (blue) and REAN (green) in 2008.

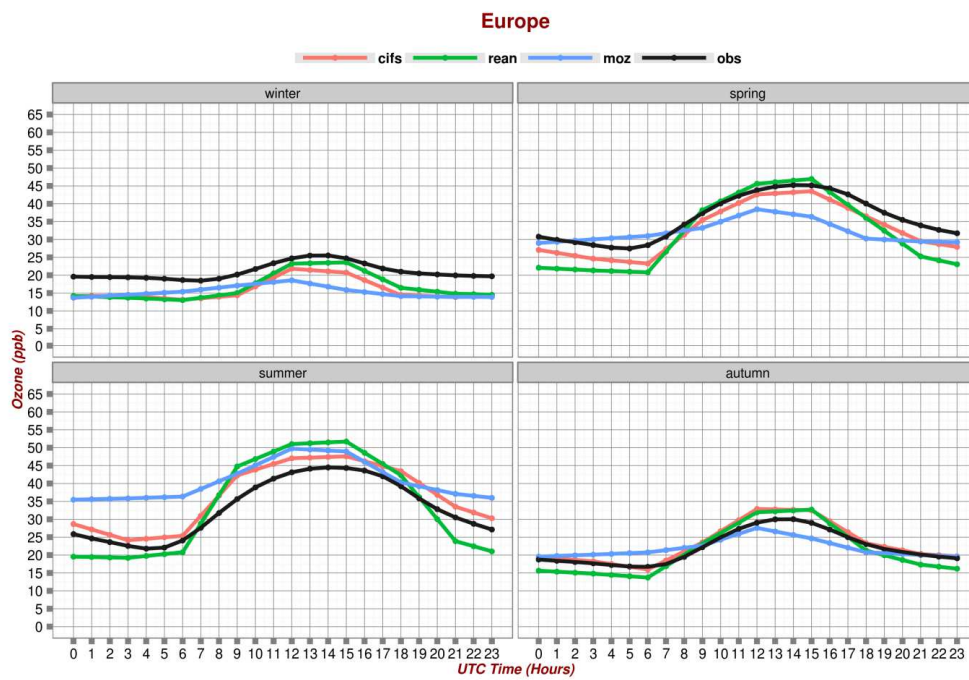


1567

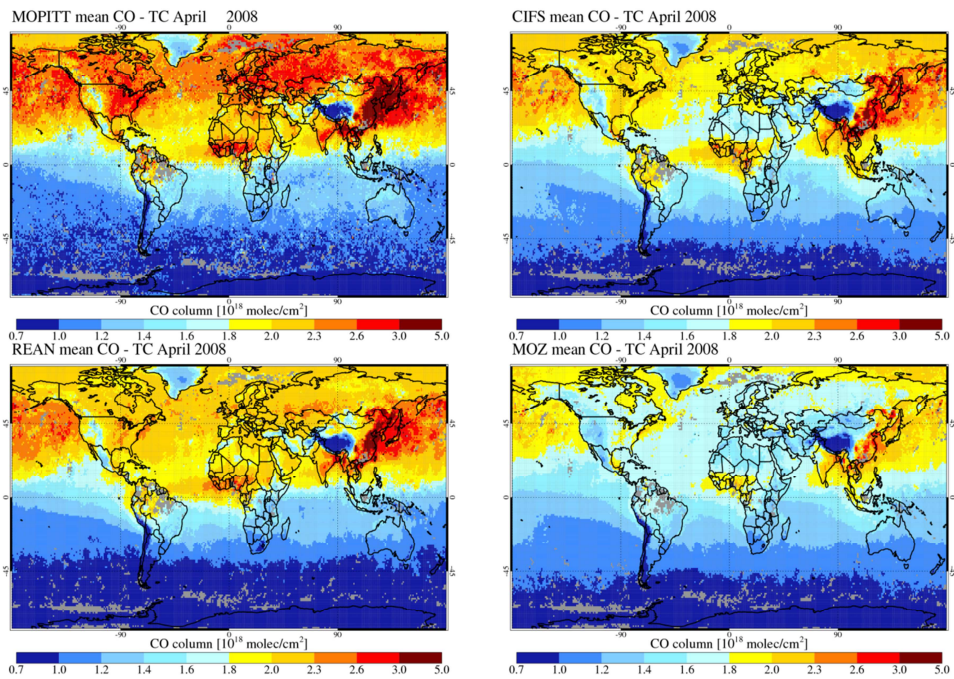


1568

1569 Figure 4 Annual cycle of the mean ozone volume mixing ratios (ppb) at rural sites of the  
1570 EMEP and AirBase data base and simulated by C-IFS (red), MOZ (blue) and REAN (green).



1571  
 1572 Figure 5 Diurnal cycle of surface ozone volume mixing ratios (ppb) over Europe in winter  
 1573 (top, left), spring (top, right), summer (bottom, left) and autumn (bottom, right) at rural site of  
 1574 the EMEP and AirBase data base and simulated by C-IFS (red), MOZ (blue) and REAN  
 1575 (green).  
 1576



1577  
 1578 Figure 6 CO total column retrieval (MOPITT V6) for April 2008 (top left) and simulated by  
 1579 C-IFS (top right), MOZ (bottom left) and REAN (bottom right), AK are applied.

1580

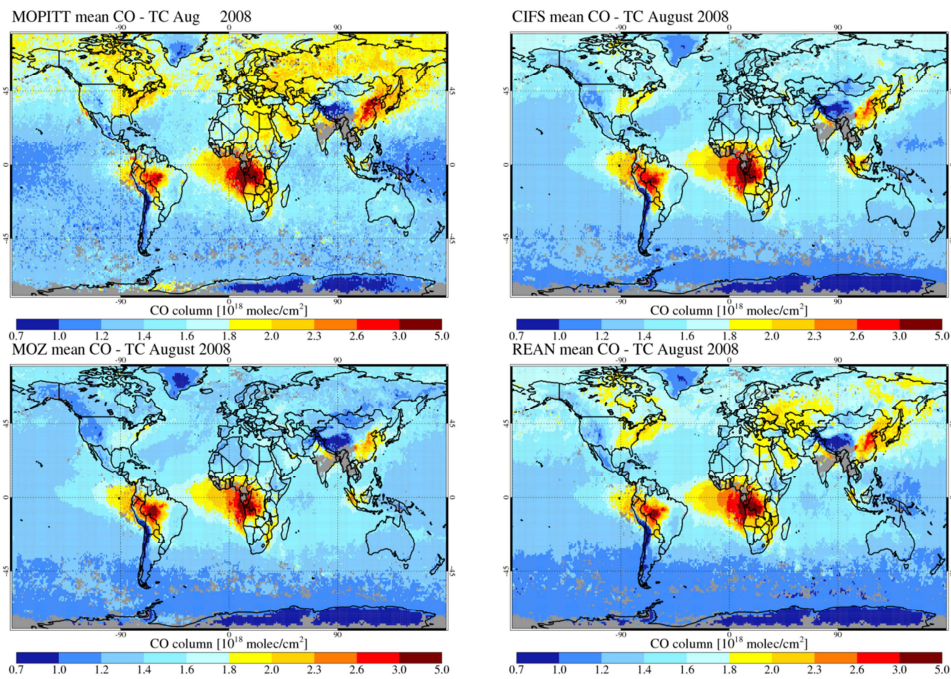


Figure 7 CO total column retrieval (MOPITT V6) for August 2008 (top left) and simulated by C-IFS (top right), MOZ (bottom right) and REAN (bottom left), AK are applied.

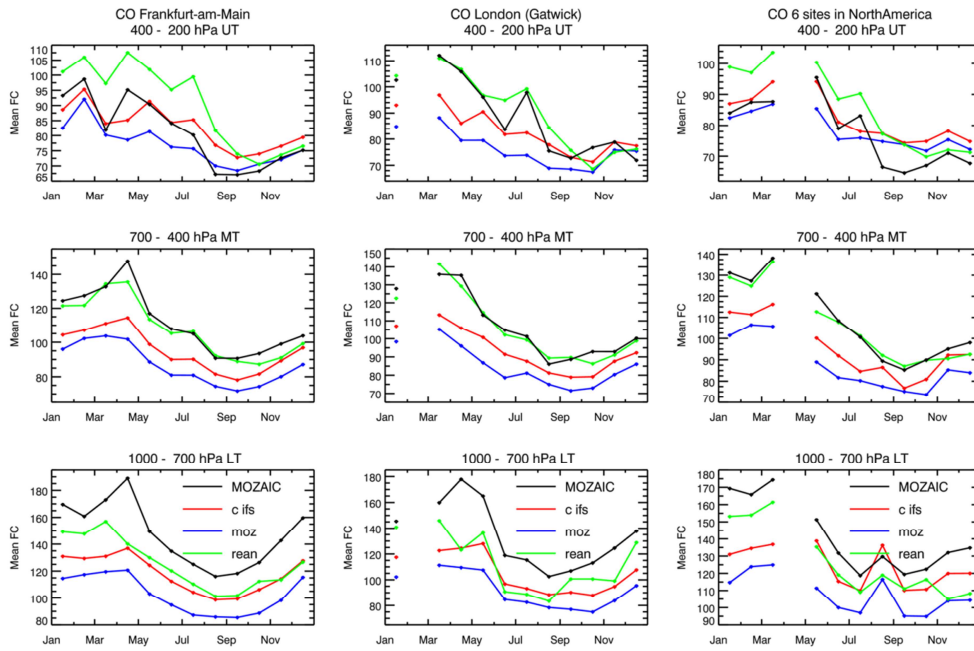
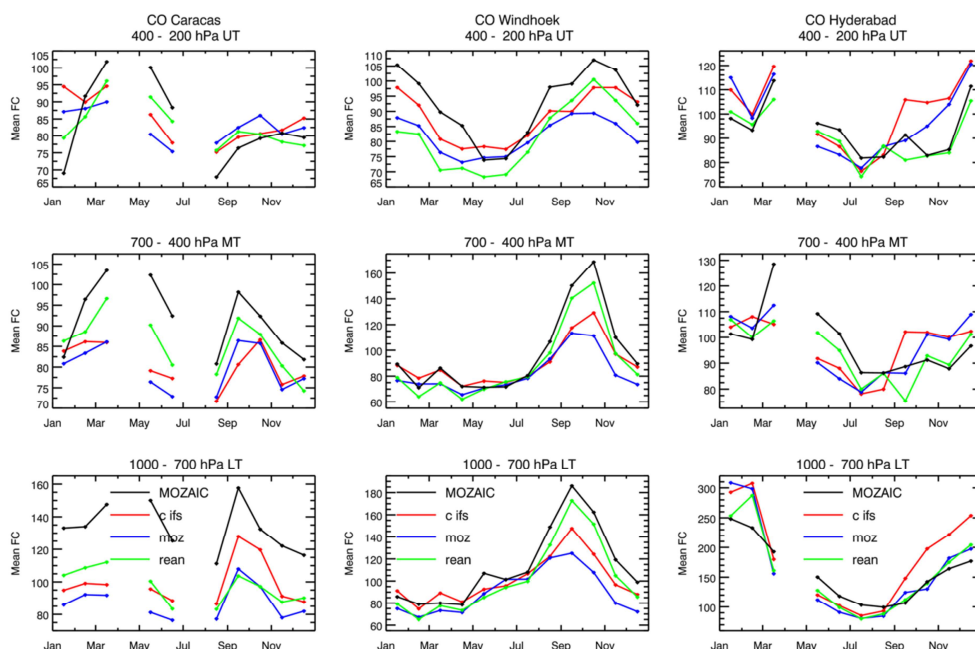


Figure 8 CO volume mixing ratios (ppb) over Frankfurt (left), London (middle) and North America (left, averaged over 86 airports) averaged in the pressure bands 1000-700 hPa (bottom), 700-400 hPa (middle) and 400-200 hPa (top) observed by MOZAIC and simulated by C-IFS (red), MOZ (blue) and REAN (green) in 2008.

1591



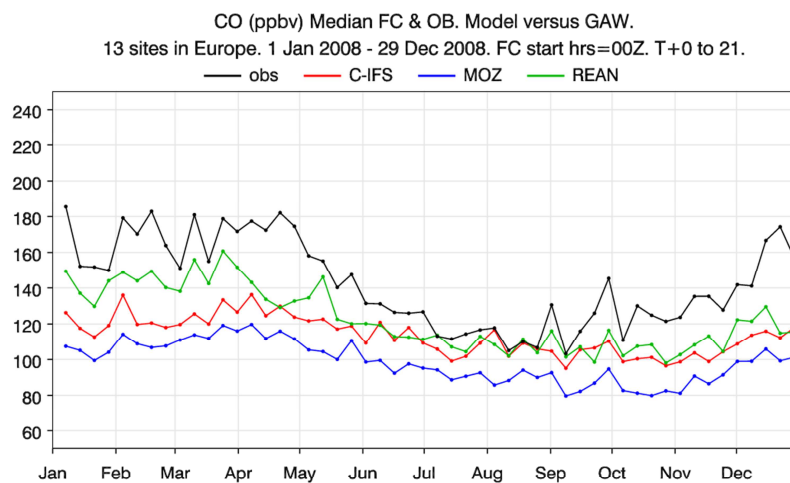
1592

1593 Figure 9 CO volume mixing ratios (ppb) over Caracas (left) Windhoek (middle) and  
 1594 Hyderabad (right) averaged in the pressure bands 1000-700 hPa (bottom), 700-400 hPa  
 1595 (middle) and 400-200 hPa (top) observed by MOZAIC, and simulated by C-IFS (red), MOZ  
 1596 (blue) and REAN (green) in 2008.

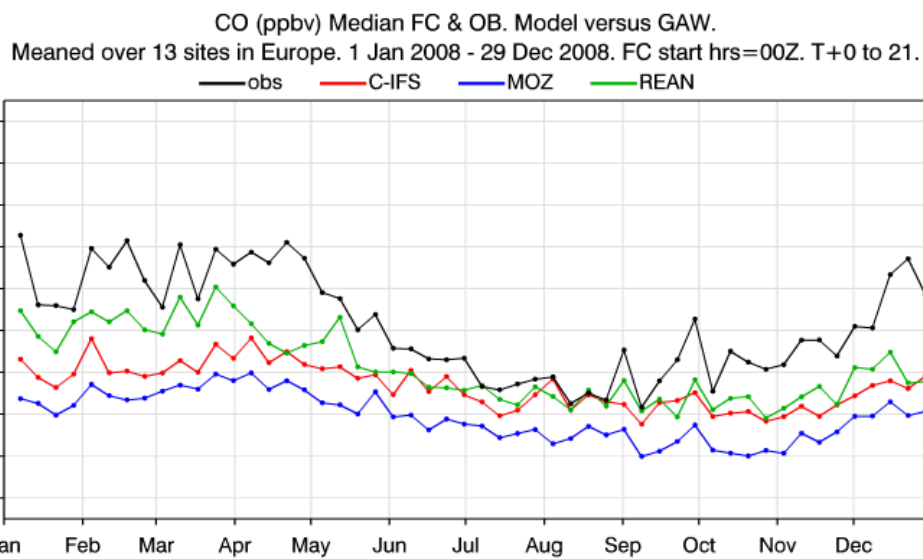
1597



1598



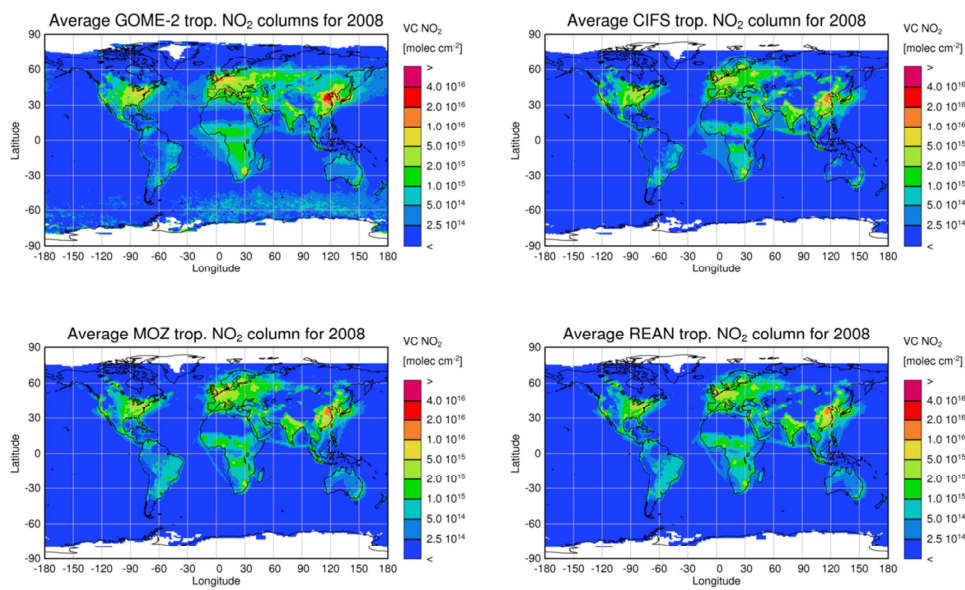
1599



1600

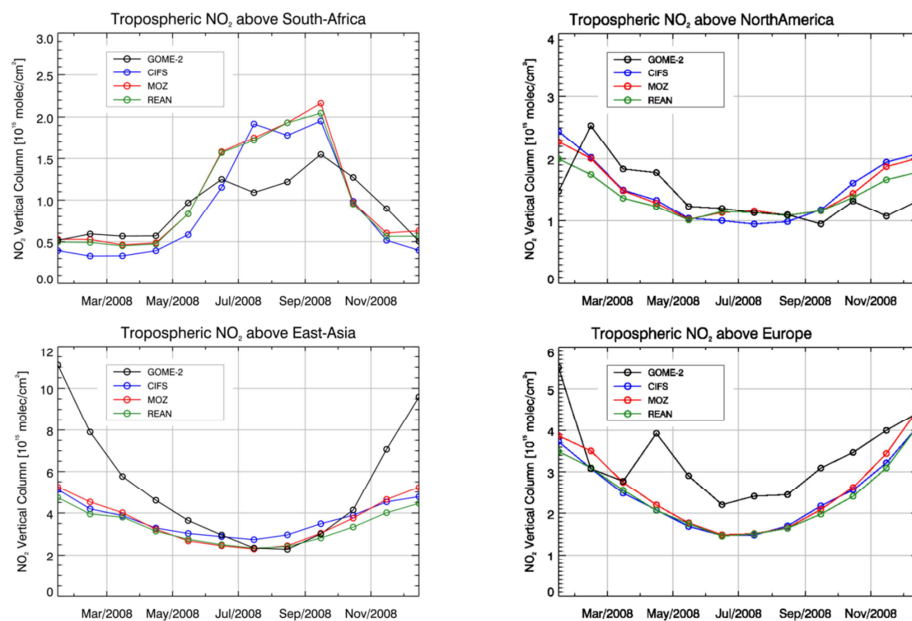
1601 Figure 10 Time series of median of weekly CO surface volume mixing ratios (ppb) in Europe  
1602 (13 GAW sites) and model results of C-IFS, MOZ and REAN.

1603



1604  
 1605  
 1606 Figure 11 NO<sub>2</sub> tropospheric column retrieval (GOME-2) for 2008 (top left) and by C-IFS (top  
 1607 right), REAN (bottom right) and MOZ (bottom left)  
 1608



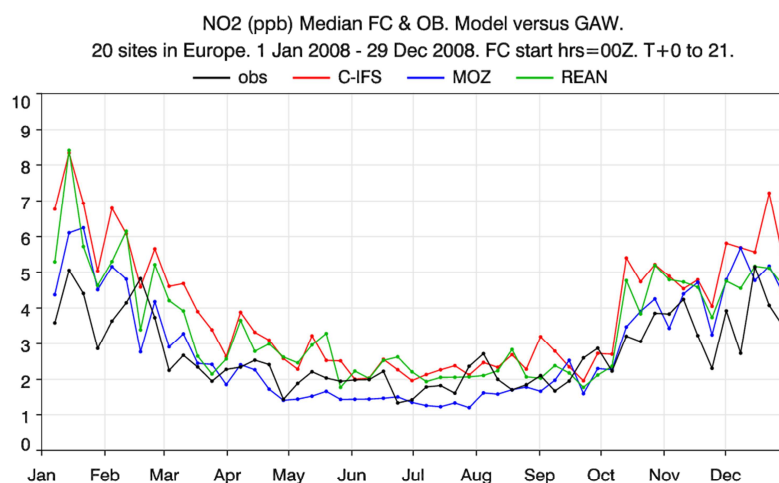


1609  
 1610 Figure 12 Time series of area-averaged tropospheric NO<sub>2</sub> columns [10<sup>15</sup> molec cm<sup>-2</sup>] from  
 1611 GOME-2 compared to model results of C-IFS (CB05) (blue), MOZ (red) and REAN (green)  
 1612 for different regions.

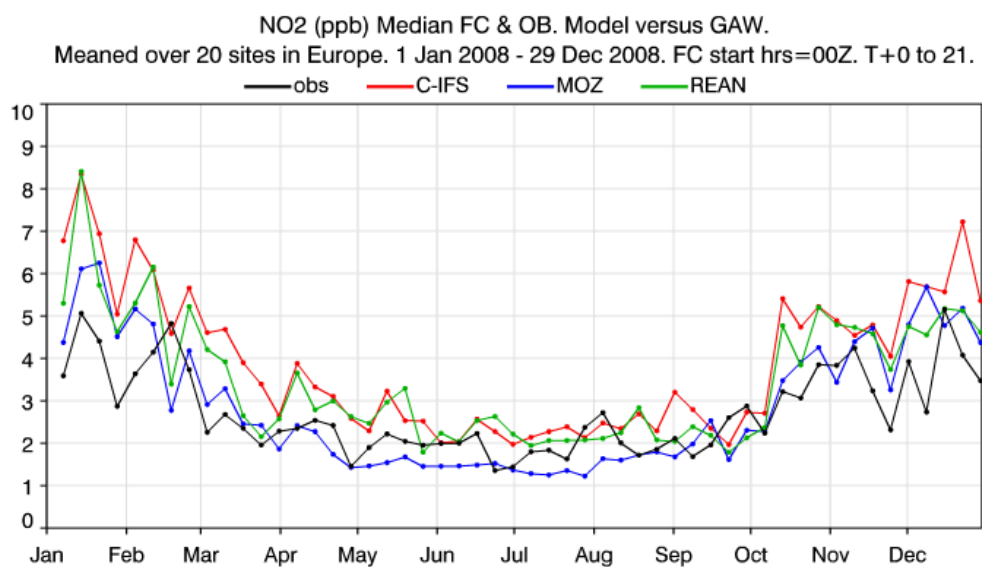
1613

1614

1615



1616



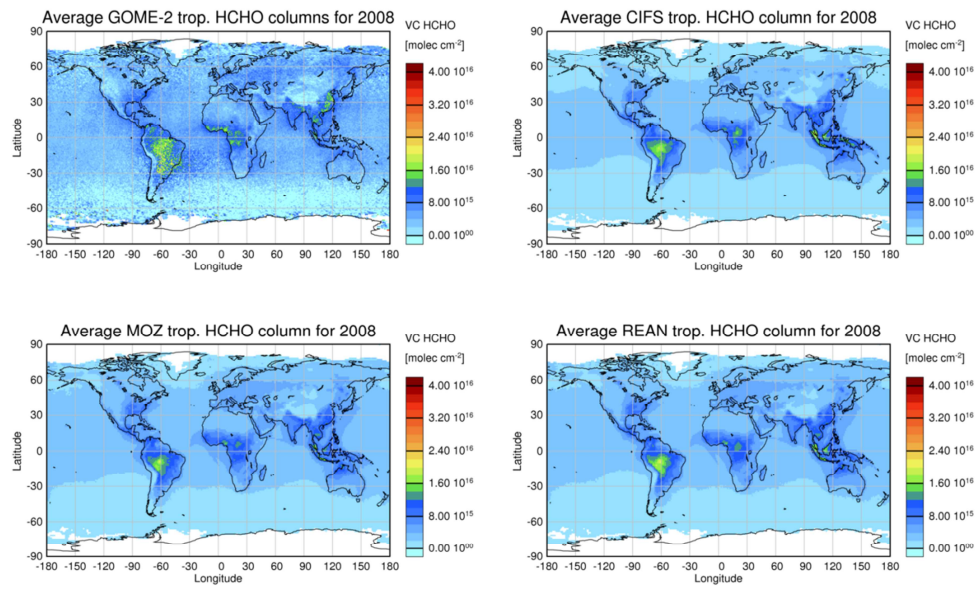
1617

1618 Figure 13 Time series of median of weekly surface NO<sub>2</sub> volume mixing ratios (ppb) in  
1619 Europe (20 GAW sites) and model results of C-IFS, MOZ and REAN.

1620



1622



1623

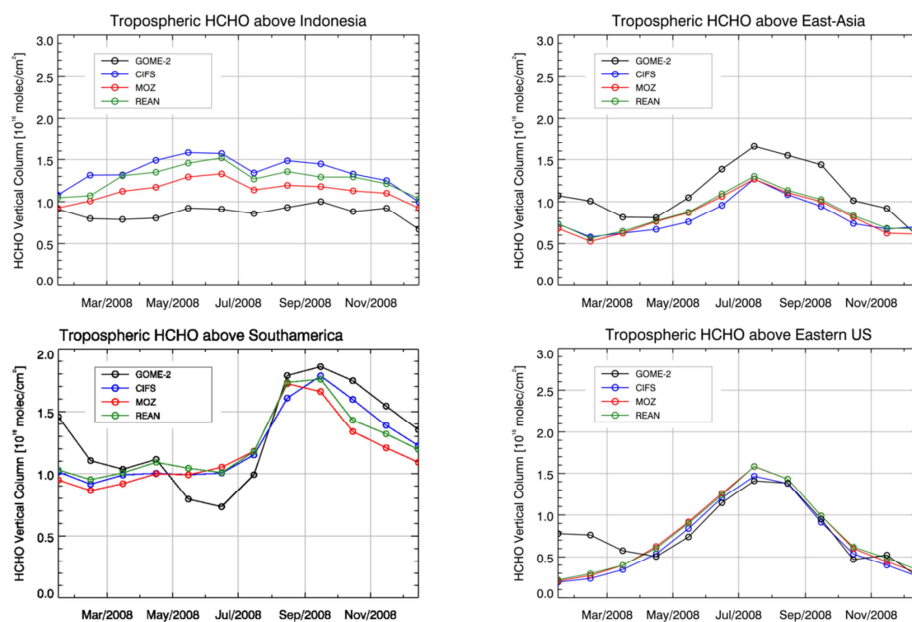
1624

1625

1626

Figure 14 HCHO tropospheric column retrieval (GOME-2) for 2008 (top left) and by C-IFS (top right), REAN (bottom right) and MOZ (bottom left)

1627



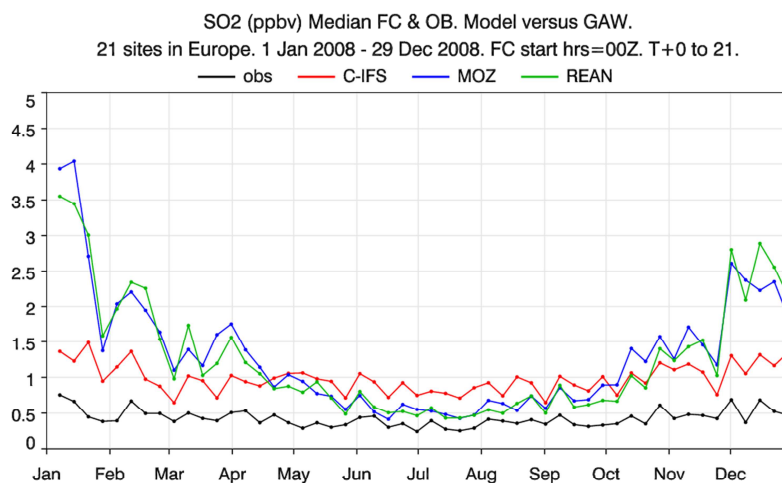
1628

1629

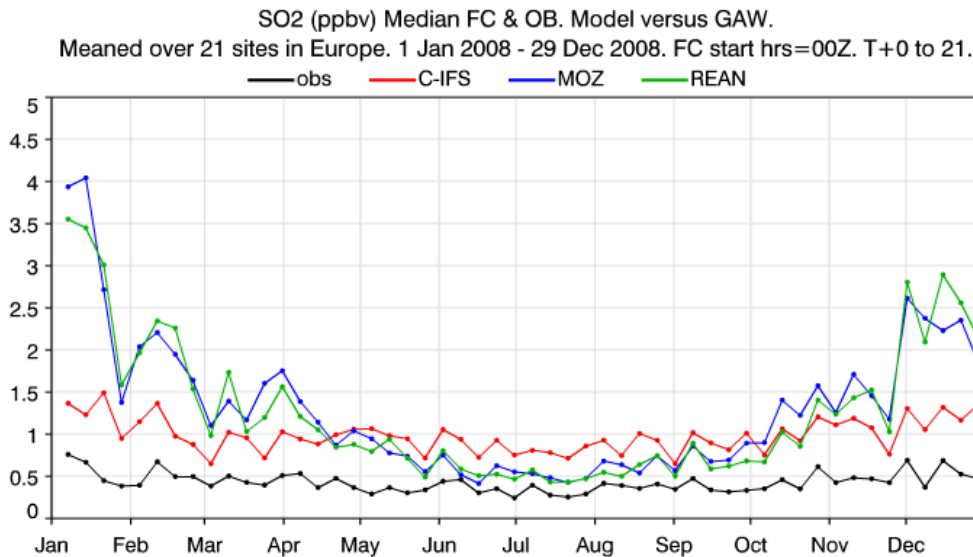
1630 Figure 15 Time series of area-averaged tropospheric HCHO columns [ $10^{16}$  molec cm<sup>-2</sup>] from  
 1631 GOME-2 compared to model results of C-IFS, MOZ and REAN for different regions.

1632

1633  
1634  
1635



1636



1637  
1638  
1639

Figure 16 Time series of median of weekly surface SO<sub>2</sub> volume mixing ratios (ppb) in Europe (21 GAW sites) and model results of C-IFS, MOZ and REAN